The Development of Nanostructured Calcium Phosphate Biomaterials for Bone Tissue Regeneration

Caroline Joanne Wilcock

A thesis submitted towards the degree of

Doctor of Philosophy

The University Of Sheffield.

Faculty of Medicine, Dentistry and Health

University of Sheffield

June 2015

Abstract

Relatively little progress has been made in the preparation of new nanoscale calcium phosphates that have been modified to introduce improved properties when used as injectable bone graft substitutes. The aim of this research was therefore to investigate the preparation and properties of injectable nanoscale hydroxyapatite (nHA) materials that were modified by either substitution of calcium for strontium, or doping with silver. Wet precipitation and sol-gel fabrication of nHA were investigated in order to select and further optimise the methods which may be most suitable for the production of nanoscale hydroxyapatite pastes and gels, whilst also considering which methods would be most suited for the production of chemically modified nHA. Materials characterisation results using X-ray diffraction, transmission electron microscopy and X-ray fluorescence demonstrated the successful formation of a range of strontium-substituted nHA (0 – 100 at. % strontium content), and a range of silver-doped nHA (0 – 10 at. % silver content). *In vitro* biocompatibility results suggested that the majority of strontium-substituted nHA pastes and gels had no detrimental effects on cellular viability. Silver-doped nHA pastes were shown to have potent antibacterial activity against two microorganisms associated with bone infection, *Staphylococcus aureus* and *Pseudomonas aeruginosa.* In conclusion, this research has optimised manufacturing processes for the preparation of nHA, described new methods for the preparation of substituted and doped nHA, and shown that these modifications introduce additional properties including antimicrobial activity. The further commercial translation of these new materials with superior performance has the potential to benefit millions of patients worldwide.

Acknowledgements

I would like to thank all of my supervisors, both academic and industrial, for their help, support and guidance throughout my PhD. Firstly, thanks to my primary supervisor Professor Paul Hatton for his enthusiasm, motivation, encouragement for self-improvement and for providing the opportunity for a PhD with such strong industrial links. I would also like to give my great thanks to Dr Cheryl Miller and Dr Piergiorgio Gentile for their academic input and advice. Many thanks to my industrial supervisors, Mr Wayne Austin and Dr Rebecca Goodchild, for providing close industrial collaboration throughout my PhD and for my warm welcome during my industrial placements.

I would like to give great thanks to other staff in the School of Clinical Dentistry who helped me with enthusiasm; I greatly appreciate the input and advice from Dr Abigail Pinnock, Dr Yulia Ryabenkova, Dr Aileen Crawford, Dr Carolina Herranz, Dr Graham Stafford, Dr Jill Callaghan and Dr Martin Santocildes Romero. I would also like to thank the approachable and friendly technical staff who always offer a helping hand including Dr Rob Moorehead, Jason Heath, Kirsty Franklin, David Thompson, Ian Brock, Nik Reeves-McLaren and Chris Hill. I would like to extend my thanks to the group of Professor Steve Armes group for access to their FTIR-ATR machine and Dr Robert Burton from Sheffield Hallam University for XRF analysis.

My great thanks go to all inhabitants of the D22 office (D22 crew) over the years for lots of excellent and unforgettable memories – from CFCs to chad-gate; Harriet Drouin, Eleanor Ashworth, Sarah Lindsay, Saima Ahmed, Dr Richard Senior, Dr Katie Bardsley and Dr Dalal Alatobi. Thanks to all the other PhD students from the University who have helped me including Altair Contreras and the Materials, Tissue Culture and Microbiology lab students from the Dental School.

Muito obrigada and muito prazer to all the team at the University of São Paulo, Ribeirão Preto campus who carried out *in vivo* work and offered such a warm and friendly welcome to Brazil; Dr Evandro Carneiro, Dr Paulo Faria and Professor Luiz Salata.

I would like to thank all my friends for welcome distractions from thesis writing and my family for supporting my education, especially my Mum and Sister for always showing a keen interest in my research. Finally, I send my love and thanks to Brett for always being there to listen and offer sound advice, and for all his house husband duties whilst this thesis was being written.

PhD by numbers

162 batches of HA made

46 TEM sessions

44 atoms in a unit cell of HA

38 twilight XRD sessions (over 324 patterns analysed)

25 (+ 1) age at submission

5 rating of apatite on the Mohs hardness scale

4 years

3 BDs / CFCs (at least)

2 pH probes smashed

1 thesis

Contents

Abbreviations

α-MEM: Minimum Essential Medium Eagles (α-modification)

α-TCP: α-tricalcium phosphate

Ag-nHA: Silver-doped nanoscale hydroxyapatite

ALP: Alkaline phosphatase

at. %: Atomic percentage

β-TCP: β-tricalcium phosphate

Ca/P: Calcium: phosphorus molar ratio

(Ca+Sr)/P: (Calcium and strontium): phosphorus molar ratio

CaO: Calcium oxide

Cbfa1: Core binding factor alpha 1

CDHA: Calcium-deficient hydroxyapatite

COL1A1: Alpha 1 chain of type 1 collagen

DBM: Demineralised bone matrix

FCS: Foetal calf serum

FTIR-ATR: Fourier transform infrared spectroscopy in attenuated total reflectance mode

HA: Hydroxyapatite

ICP-AES: Inductively coupled plasma-atomic emission spectroscopy

MIC: Minimum inhibition concentration

MSC: Mesenchymal stromal cell

NFATc: Nuclear factors of activated T-cells

nHA: Nanoscale hydroxyapatite

OCP: Octacalcium phosphate

O.D.: Optical density

OPG: Osteoprotegerin

PBS: Phosphate buffered saline

PGA: Poly(glycolic acid)

PLA: Poly(lactic acid)

PLGA: Poly(lactic-co-glycolic acid)

ppm: Parts per million

PVA: Poly(vinyl alcohol)

RANK: Receptor activator of nuclear factor kappa-B

RANKL: Receptor activator of nuclear factor kappa-B ligand

rpm: Revolutions per minute

Sol^{n}: Solution

Sr nHA: Strontium-substituted nanoscale hydroxyapatite

Sr/P: Strontium: phosphorus molar ratio

TEM: Transmission electron microscopy

VEGF-A: Vascular endothelial growth factor A

v/v %: Volume percentage

wt. %: Weight percentage

XRD: X-ray diffraction

XRF: X-ray fluorescence

List of Figures

List of Tables

1. Introduction

Annually, millions of patients worldwide require bone augmentation materials to fill defects caused by trauma or congenital deformities. When bone healing is compromised, there can be a great impact on a patient's quality of life as well as increased treatment costs. The current gold standard bone augmentation material is an autologous bone graft typically taken from the iliac crest of the patient. However, harvesting of the bone has significant disadvantages in terms of donor site morbidity, pain suffered by the patient and graft availability. The most commonly used bone augmentation material is allograft bone, which carries the risk of viral infections and undergoes deterioration in its osteoconductive and mechanical properties due to its processing [1]. Therefore, there is a great interest in the use of synthetic biomaterials for bone tissue regeneration. The ideal bone augmentation material should be osteoconductive to aid the regrowth of bone tissue, and be available in a suitable form to allow for the surgeon to easily implant it into the defect site. Synthetic bone augmentation materials have the potential to overcome the disadvantages of naturally derived bone graft substitutes summarised above.

Synthetic calcium phosphates such as hydroxyapatite (HA) have been widely used in medicine and dentistry, in part due to their similarity to the mineral found naturally in bone and tooth enamel. Calcium phosphates have typically been used in the form of powders, granules or as coatings on the surface of implants. However, the development of nanoscale HA has encouraged alternative forms of bone graft substitute to be investigated. One promising technology that has been developed relatively recently is a paste based upon the combination of nanoscale calcium phosphate with water. Preliminary clinical data for the first generation of nanoscale calcium phosphate paste products is encouraging, suggesting that they are capable of promoting bone tissue regeneration [2, 3]. The reasons underpinning their good clinical performance are not known, but this may be due in part to the extremely high

surface area to volume ratio and biomimetic nature of nanoscale calcium phosphates. The improvement and wider clinical use of nanoscale calcium phosphate pastes may be worthy of greater consideration for a number of reasons. Firstly, these systems are injectable thereby facilitating minimally invasive surgeries. Secondly, nanoscale calcium phosphate may be chemically modified to enhance their clinical performance. For example, the production of a paste with enhanced bioactivity may beneficially decrease the time for successful bone tissue regeneration. Additionally, the use of an antibacterial calcium phosphate paste has the potential to reduce the incidence of bone infection.

Despite this potential, modified nanoscale calcium phosphates have had little impact on the market or clinically. There is also a lack of laboratory studies that have considered the substitution of other chemical elements into injectable nanoscale calcium phosphate systems. Due to the vast array of elements that may be substituted into HA, there are many substitutions which might beneficially affect the bone healing response. Hence it is of great importance to investigate chemical substitutions, particularly those which are likely to have a potent effect on bone tissue regeneration.

Furthermore, although there are an increasing number of publications regarding the production of nHA, it is often difficult to draw conclusions due to the mixed quality of the papers and the wide variety of process parameters described. Therefore there is a need for a more systematic review of the nHA production methods, ideally combined with laboratory study, in order to select the processes that are best suited to the production of chemically modified nanoscale calcium phosphate pastes. Given the potential improvement in versatility and clinical usefulness, the aim of this research was therefore to investigate and develop methods which could be used for the production of injectable substituted nHA products, with enhanced biological properties. The specific focus of this project was to develop nanoscale ceramics due

to the potential increase of bioactivity with the use of nanoscale over microscale hydroxyapatite, and because nanoscale mineral may form a cohesive pastes or gels to a better degree than microscale powders. These aims and objectives are outlined in more detail in Chapter 3, but before this it is important to review the literature to consider current progress and future potential.

2. Literature Review

2.1 Bone Function and Structure

In order to design and optimise biomaterials to encourage bone tissue healing, it is first necessary to understand the function and structure of bone tissue to comprehend how biomaterials may interact *in vivo*. Throughout the body, bone has a variety of functions including providing support and protection of vital organs as well as allowing for movement and hearing. Bone tissue is also responsible for mineral and growth factor storage and blood cell formation [4]. All these functions contribute significantly to a person's quality of life. Therefore, considerable suffering can occur when bone healing is compromised.

Bone tissue contains a highly organised structure which is in the constant process of being remodelled to repair frequently occurring microfractures. Wolff's law states that the form which bone takes is a result of the biomechanical loads which are applied to it [4]. As a consequence, bone is found in different forms throughout the body which are highly specialised to achieve their required function; bone tissue is generally classified as cortical or cancellous (see Figure 2.1 A). Cortical or compact bone is found on all external layers of bones throughout the body, and is densely packed with structural units known as osteons (Figure 2.1 B). Osteons are made of hollow tubes of bone matrix called lamellae and surround blood vessels and nerve fibres in an arrangement known as the Haversian system. Within the osteons, osteocytes reside in lacunae at junctions between lamellae, and are connected to other osteocytes via narrow canals called canaliculi. The embedded osteocytes arise from osteoblasts which have become entrapped during the process of bone mineralisation. Cancellous bone is otherwise known as spongy bone and is located around the central cavity of most bones. It is made up of small struts called trabeculae, between which red or yellow marrow may reside. The trabeculae are aligned in response to external stresses exerted on the bones, in accordance with Wolff's law [4].

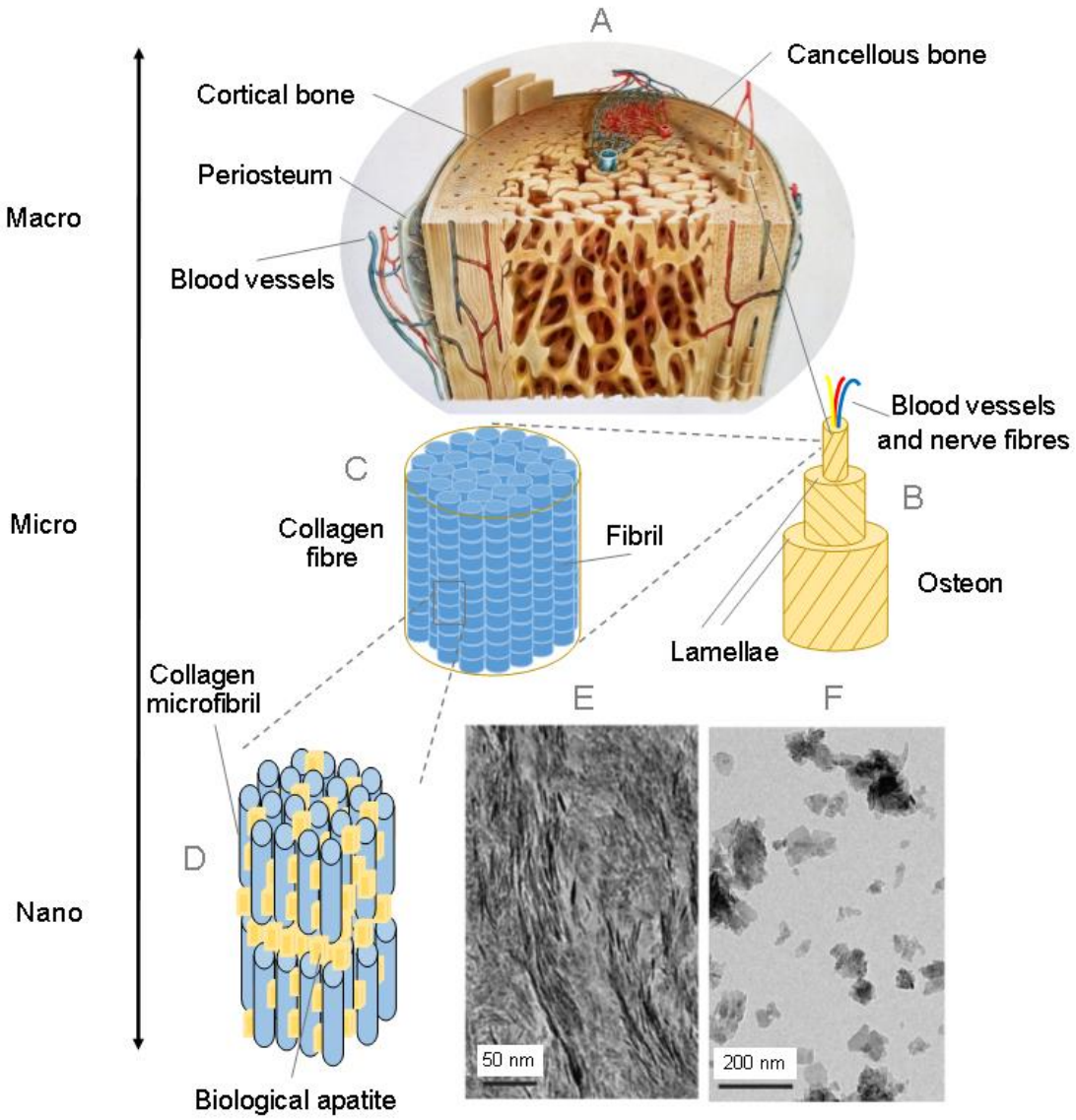

Figure 2.1. Hierarchical structure of bone tissue. (A) Schematic representation of a long bone cross section displaying the macroscopic organisation of the outer cortical bone layer and inner cancellous bone (Image from Wellcome Library, London). Cortical bone contains osteons (B) which are composed of layers of lamellae with collagen fibres (C) alternating direction between adjacent layers. Fibres contain collagen fibrils which have smaller structural units named microfibrils (D). Biological apatite crystals reside in between the collagen microfibrils. (E) TEM micrograph displaying arrangement of biological apatite crystals in sheep bone. (F) TEM micrograph of isolated biological apatite crystals. TEM imaged reproduced with permission from [5].

Bone tissue contains four main types of cells. Firstly, osteogenic cells residing in the periosteum and endosteum are the stem-like cells which provide a population of osteoblasts. Osteoblasts are responsible for secreting osteoid, which in turn is mineralised to provide structural strength to the bone tissue. Osteoclasts are responsible for the resorption of damaged bone. Lastly, osteocytes are responsible for monitoring the stresses exerted on the bone and communicate with other osteocytes through cellular extensions. When microfractures occur, a bone multicellular unit (BMU) is formed. A BMU is made up of osteoclasts which resorb the damaged bone, followed by osteoblasts which deposit osteoid. When the osteoid is mineralised and remodelled the bone once again possesses the necessary strength to withstand the applied loads. The combined activity of osteoblasts and osteoclasts therefore allow bone to maintain its structural strength by the removal of old, damaged bone and the formation of new bone tissue.

Bone is generally considered to have capacity for self-regeneration, providing that the injury site is not too large and that the defect site remains relatively free of soft tissue invasion. Conventional fracture healing generally follows these stages: haematoma formation, fibrocartilagenous callus formation, bony callus formation and remodelling. Briefly, blood vessels which are torn by the fracture cause local bleeding which is stabilised by the formation of a haematoma. After a few days new blood vessels grow into the fracture site and fibroblasts and chondrocytes produce collagen and cartilage matrix respectively. Bone trabeculae begin to grow into the fibrocartilagenous callus over a period which can last up to 2 months. Finally the bony callus is remodelled to achieve bone tissue which has appropriate mechanical properties [4]. This type of fracture healing is based on the endochondral ossification of bone tissue which uses a hypertrophic cartilaginous template to form the bone as observed during the embryonic development of long bones. The other type of embryonic bone tissue formation is termed intramembranous ossification, which occurs in flat bones such as

the cranium and sternum. The process begins in the fibrous connective tissue membranes where an ossification centre is formed, consisting of mesenchymal stem cells differentiating into osteoblasts. In turn the osteoblasts secrete osteoid which is mineralised within a few days. The formation of osteoid around the blood vessels results in woven bone trabeculae and the periosteum surrounding the bone forms from condensing mesenchyme. The thickening of the trabeculae close to the periosteum results in a structure with a compact bone collar, with red marrow residing in trabecular spaces [4].

The extracellular constituents of bone tissue can be divided into organic and inorganic categories. The organic component is termed osteoid and is comprised of proteoglycans, glycoproteins and type I collagen fibres, all of which are produced by osteoblasts. The inorganic phase of bone consists mainly of non-stoichiometric carbonated hydroxyapatite crystals that are in the form of nanoscale platelets residing between collagen microfibrils (see Figure 2.1 D and E). Apatite crystals have been reported to nucleate and grow in two different environments in the collagen network; the plate-like crystals grow in larger holes between the ends of collagen microfibrils and in smaller pores lateral to collagen microfibrils. The apatite crystals tend to be aligned with the c-axis parallel to the microfibril long axis. [6]. There is evidence that the mineralisation of developing bone occurs at the nanoscale, with 30 – 40 nm sized mineral in found in neonatal mouse bone [7]. Estimates for the size of mature biological apatite crystals include 50 x 30 x 2 nm [6] and 50 x 25 x 3 nm [8].

Natural apatite is composed of non-stoichiometric carbonated hydroxyapatite, which has the general formula $Ca_{10-x-y}[(HPO_4)(PO_4)]_{6-x}(CO_3)_y(OH)_{2-x}$. A variety of different elements are also present in bone (Table 2.1) as well as a variety of trace elements including silicon (500 ppm), zinc (39 ppm) and smaller amounts of chromium, cobalt and manganese [9]. The elements present in bone mineral may either be absorbed onto the crystal surface or substituted into the calcium phosphate lattice [9].

Therefore, there are a variety of biomimetic elemental substitutions which can be considered including carbonate, sodium, potassium and strontium. It should be noted that considerable variations in apatite composition can be found between individuals. For example the carbonate content in bone has been reported to be between 2.3 and 8 wt. % [10, 11]. There are conflicting reports regarding the nature of the carbonate substitution. Some reviews claim that the carbonate groups are generally accepted to substitute for the phosphate groups, termed a B-type carbonate substitution [12]. Whilst it was reported by Tampieri *et al.* that B-type substitution was predominant in young bones, substitution of hydroxyl groups for carbonate groups (A-type) was increasingly present in bones belonging to older individuals [10]. The presence of carbonate groups decreases the crystallinity and thermal stability of the nHA compared to stoichiometric HA, whilst increasing the solubility. These changes in material behaviour may be partly attributed to the weakness of the calcium-carbonate bond when compared to the calcium-phosphate bond [12].

Table 2.1. Elemental composition of the inorganic components of bone, enamel and dentine in weight percent [13].

Wt. %	**Bone**	**Enamel**	**Dentine**
Ca	36.6	37.6	40.3
P	17.1	18.3	18.6
CO_2	4.8	3.0	4.8
Na	1.0	0.7	0.1
K	0.07	0.05	0.07
Mg	0.6	0.2	1.1
Sr	0.05	0.03	0.04
Cl	0.1	0.4	0.27
F	0.1	0.01	0.07
Ca/P molar ratio	1.65	1.59	1.67

It has been reported that biological apatite has a low degree of hydroxylation. A mechanistic model to explain this has been reported by Wopenka *et al.* [12]; the smaller the crystallite size and the greater degree of atomic disorder progressively cause a less energetically favourable state for the incorporation of hydroxyl ions. Therefore the nanoscale nature of biological apatite leads to a large number of distorted bonds at the edges of the crystal, which inhibits the occupation of the channel sites by the hydroxyl groups. It has also been hypothesised that the hydroxyl site vacancies exist to accommodate the charge vacancy caused by the carbonate substitution for phosphate [6]. Indeed it may be a combination of these two effects that results in relatively low levels of hydroxyl groups in biological apatite.

The combination of collagen fibres and the mineral phase provides bone with its structural strength alongside its flexibility and durability [14]. In terms of material

structure, the complex organisation of bone tissue is inhomogeneous and anisotropic. It has been reported that cortical bone has a remarkable tensile strength between 90-230 MPa [15] which is comparable to steel, whereas the compressive strength of healthy bone is half as strong as steel [4]. The strength of bone is highly dependent on the volume of bone matrix present and its microarchitectural distribution, as well as the degree of mineralisation of the bone tissue. The mineralisation of bone begins to occur 5-10 days after the osteoid is deposited by osteoblasts, and can be described in two stages. Primary mineralisation progresses at a linear rate, followed by a slow gradual secondary mineralisation. It is believed that during primary mineralisation, matrix vesicles containing crystals or high concentrations of ions are delivered to the mineralisation front by osteoblasts. The matrix vesicles contain a number of proteins which allow for initial mineralisation to occur such as alkaline phosphatase and pyrophosphates. These proteins may allow for initial crystal nucleation to commence inside the vesicle before the mineral and protein contents are delivered via exocytosis to the extracellular matrix. Heterogeneous mineralisation can then occur with the presence of a nucleating substance allowing for crystal formation and growth. Gap zones at the end of collagen molecules are known sites of initial mineralisation. They are first filled with proteoglycans which bind calcium ions. The proteoglycans are then enzymatically degraded whilst phosphoproteins bind to the collagen. Alkaline phosphatase then dephosphorylates these molecules to make phosphate ions available for crystal growth. This whole process is highly regulated and controlled. For example, non-collagenous proteins can control the dimensions of the crystals by inhibiting crystal growth on particular faces [16]. During secondary mineralisation there may be an increase in the amount of crystals, or an increase in crystal size, or an improvement in the perfection of the crystal arrangement or any combination of the above [17].

The mineralisation of bone tissue also requires a degree of water content to allow for the diffusion of ions required during crystal growth. The surface of the hydroxyapatite crystal is surrounded by a layer of water known as the hydration shell. For the crystals to mature and grow, ions are required to diffuse from the surrounding fluid into the hydration shell. The ions can then either become deposited on the surface of the crystal or can flow into the crystal structure where substitution into the apatite structure can occur. As a result of this situation, biological apatite permits a variety of ionic substitution, exchange or absorption which is highly dependent upon its surrounding environment [16]. It has also been hypothesised that water is an essential component of bone mineral due to the stabilising effect of water molecules in the apatite channels. As discussed previously, biological apatite contains hydroxyl site vacancies, possibly to compensate for the charge imbalance arising from carbonate group (CO_3^{2-}) substitution into phosphate group (PO_4^{3-}) sites. It has been proposed that the structurally incorporated water molecules support the hydroxyl vacancies in order to stabilise biological apatite [6].

2.2 Clinical Need for Bone Augmentation Materials

Every year hundreds of thousands of patients in the US and millions of patients worldwide undergo bone graft procedures [18], with bone being the second most transplanted tissue after blood. The most recent estimate found for the number of bone grafting procedures performed worldwide is 2.2 million in 2006 [19, 20], however this number is likely to have increased considerably due to the aging population. Common procedures that require the use of bone grafts include treatment of fracture non-union, spinal fusions, filling voids left from the sites of bone tumour resection, or correction of congenital deformities. As well as in orthopaedics surgeries, bone graft materials are commonly used in maxillofacial surgery to repair areas of bone loss.

Bone has some capacity to heal itself as described in section 2.1 *Bone Function and Structure*. However, if the space in the bone tissue is above a particular size then it will not heal without surgical intervention; these are known as 'critical size defects'. In particular, non-union fractures present a challenge to surgeons, as well as incurring considerable costs due to the long lasting therapies frequently required. For example, it has been estimated that a 'best-case scenario' humeral non-union fracture may cost over £15,000. Furthermore in the same study it was reported that the results of these long term treatments are often unrewarding [21]. This certainly highlights a need to produce materials which can rapidly and effectively aid bone healing.

Another application which can require bone augmentation materials is to repair lesions left from the resection of cancerous bone tumours. Although primary bone cancer originating from the bone itself is rare, most commonly these osteosarcomas arise in young people, which often have devastating consequences on their quality of life. Furthermore, bone is a very common site for the metastasis of tumours. 65-80 % of patients with metastatic bone tumours have developed these as a result of breast or prostate cancer [22, 23], which are among the most prevalent cancers for women and men respectively. Bone metastases often greatly reduce the chance that a patient can be cured of cancer [24]. The current standard care for bone tumours are drugs which promote the activity of osteoclasts. Since 30-50 % of patients using these therapies develop further bone metastases more effective therapies are clearly required [24]. Promisingly, it has been reported that nanoscale hydroxyapatite exhibits inhibitory effects on osteosarcoma cells, whilst stimulating mesenchymal stromal cells [25]. Although no extensive research has been carried out into this area, this may present an alternative therapy which could be used in conjunction with current methods to potentially improve the prognosis for cancer patients.

Another large segment of the bone biomaterial market consists of spinal fusion products. In the US, fusion was reported to be the 19th most common inpatient

procedure in 2003 and had experienced a sharp rise from being the 41st most common inpatient procedure in 1997 [26]. Spinal fusions are often required to treat trauma cases and degenerative disc disease. During the last century, autogenous bone grafting has been employed to enhance the success of spinal fusion procedures. The osteoconductivity of hydroxyapatite has also resulted in the use of this material in these operations. However concerns regarding the suitability of current hydroxyapatite materials have been raised, particularly due to their brittle nature and low shear strength for solid formations of HA used in load bearing applications [27].

2.2.1 Materials used for Repair and Regeneration of Bone Defects

As described in the previous section, bone augmentation materials are required for a variety of applications. The ideal bone augmentation material should possess osteoconductive and osteoinductive properties as well as being biocompatible and bioresorbable. Osteoconductivity refers to the capability of the material to assist the growth of new bone; importantly the material should allow the ingrowth of blood vessels and support the growth of osteoprogenitor cells. Osteoinduction describes the ability of a material to recruit pluripotent mesenchymal stem cells and to allow the differentiation of these cells into osteoblasts [28]. For the surgeon the material must be easy to use, and for society it is beneficial if the material is cost-effective, in terms of reducing the socio-economic costs associated with these types of injuries, diseases and deformities.

The current gold standard bone augmentation material is autologous bone typically taken from the iliac crest of the patient. The living cells present on the resorbable bone matrix provides a bone substitute with no risk of rejection. It has been described to have the greatest osteogenic capacity of all bone augmentation materials. However the harvesting of autologous bone has major disadvantages such as donor site morbidity and graft availability [1]. The most common patient complaint is pain at the donor site, with less frequent complications including nerve injury, infection and

fracture at the donor site caused by the removal of bone [28]. Considerable costs are also amounted for the requirement of extra surgical time. Due to these disadvantages, allograft bone transplants are the most often used bone graft, but these materials have reduced osteoinduction and osteogenesis when compared to autograft transplantations. Also, allografts carry the risk of infections such as HIV and hepatitis B and C. The processing of allograft bone to reduce its immunogenicity has detrimental effects on the properties of the bone, particularly its mechanical strength and osteoinductive properties [1]. Similarly, xenogenic bone from animals must be processed before implantation to remove cells and proteins which would trigger an immune response. Human, bovine or equine bone can also be used to produce demineralised bone matrix (DBM), which is a sponge-like collagen scaffold, is prepared by decalcification and sterilisation of bone samples. DBM is mainly used as a bone graft extender due to its poor mechanical properties. As well as promoting revascularisation this material has been found to have osteoconductive and osteoinductive properties.

The considerable disadvantages associated with the use of natural bone have encouraged the development of synthetic bone augmentation materials (see Table 2.2). Although synthetic materials have a lower osteoconductivity than autografts and allografts, they can be prepared to be readily available ‘off the shelf’ products with no risk of disease transmission or immune rejection. Even though a wide variety of materials have been investigated for use in bone augmentation, the properties of a single material tend to be insufficient to recapitulate the natural composite material properties of bone. Indeed many composite materials based on combinations of the materials listed in Table 2.2 have been investigated in order to optimise material properties and characteristics.

Table 2.2. Classes of synthetic bone augmentation materials [29-31].

Class of material	Examples
Ceramics	Hydroxyapatite β-tricalcium phosphate Bioactive glasses (Glass-ceramic)
Metal	Titanium
Polymers	Poly(lactic acid) Poly(glycolic acid) Poly(lactide-co-glycolide)
Cements	Calcium phosphate Glass ionomer Calcium sulphate Poly(methyl methacrylate)

For example, polymers are generally combined with other materials such as ceramics or bioglasses in order to better match the mechanical properties of natural bone. For instance, the biomimetic use of collagen in bone graft substitutes imparts ductility to improve the mechanical properties. Problems associated with the use of natural collagen include ethical and disease transmission regarding the collagen source which is commonly derived from animals. Synthetic polymers such as PLA and PGA have also been extensively researched for use as composite bone augmentation materials. Advantages include the ability to control the degradation rate by altering the co-polymer ratio. However the acidity of the degradation products has to be considered to ensure a biocompatible response [29].

Table 2.3. Advantages and disadvantages of synthetic bone augmentation materials in clinical use.

Material	**Form**	**Advantages**	**Disadvantages**	**References**
Bioactive glass	Granules Blocks Paste	-Ability to form chemical bond with bone and osteoconductive properties -Degradation rate can be controlled by varying proportions of the reactants	-Not osteoinductive -Poor mechanical properties	[19, 32]
Calcium phosphates (generally HA and β-TCP)	Powder Granules Blocks Cements Pastes	-Inherently biocompatible due to similarity to mineral phase of bone -Osteoconductive -Degradation rate can be controlled by altering the HA:β-TCP ratio	-Not osteoinductive -Poor mechanical properties	[19, 30]
Calcium sulphate	Pre-set beads Cements	-Rapid resorption rate -Good biocompatibility -Provides scaffold for bone growth -Readily provides calcium ions to promote bone cell activity -Relatively inexpensive	-Not osteoinductive -Properties dependent of preparation technique -Blood may interfere with setting time -Poor mechanical properties	[33]

In contrast to resorbable polymers and ceramics, metals such as titanium have been used for bone tissue augmentation due to its good biocompatibility. The high strength of titanium has promoted its widespread use for joint replacement implants which are required to bear load. However, titanium is not resorbable and stress shielding effects

can cause the detrimental resorption of natural bone surrounding a titanium implant [34].

Popular bone augmentation materials are listed in Table 2.3. For example, calcium sulphate was one of the earliest materials used for bone augmentation which was first used for the filling of bony defects reported in 1892 (reported by Peltier [35]). Calcium sulphate is a well-tolerated biocompatible bone augmentation material *in vivo* which undergoes complete and rapid resorption, generally with no significant inflammatory response encountered. However, the rapid resorption rate can be a disadvantage if it does not match the bone regeneration rate [33].

Bioactive glasses were developed by Larry Hench in the 1960s and were the first material developed specifically for use in bone augmentation. When in contact with physiological aqueous solutions, a silica-rich gel layer forms on the surface which allows the material to form a direct bond with bone tissue [36]. Despite its' apparent ability to stimulate a greater amount of bone regeneration than the other bioactive ceramics (e.g. HA and β-TCP), bioactive glass is not as widely used in bone tissue regeneration as calcium phosphate. One proposed reason for this was the difficulty of producing a porous form of bioactive glass from the original formulation (45S5). However, recent advancements have allowed this challenge to be overcome [32].

Hydroxyapatite has been used widely in medical ceramic applications for decades. Due to its similarity to the mineral found naturally in tooth enamel and bone tissue, this calcium phosphate is inherently biocompatible and also displays good osteoconductive properties. Even though this material has been extensively studied over the last 40 years, there are an increasing number of publications focussed on improving the bioactivity of this material, potentially due to its' lack of osteoinductive and osteogenic potential [1]. Improvements in these properties may be possible with use of bone morphogenetic proteins or other bioactive factors. However, these

biological additions contribute to increased costs. Ceramic bone substitutes have recently been considered as the best alternative for autologous bone in orthopaedics surgery due to their safety, efficacy and low cost [30].

A recent review by Kolk specified that autologous bone grafts were still the optimal material for the repair of craniofacial defects [29] despite the limited availability and significant disadvantages for the patient and surgeon associated with the harvesting of autologous bone. Similarly, for orthopaedic bone augmentation procedures the use of autologous and allogeneic bone are considered to be suitable materials for use [30] despite the risk of disease and prion transmission associated with allogeneic material [29]. This clearly highlights the need for superior synthetic bone augmentation materials to be developed.

Future perspectives for bone augmentation materials highlight the need for improved materials which can allow for minimally invasive surgical intervention [37]. There is much interest in the use of growth factors to stimulate an optimal biological response. However, the high costs associated with these and other biological factors raise concerns that these developments are unsuitable for wide scale use. Alternatively, a more biomimetic mineral approach may impart beneficial biological properties, whilst providing a cost effective product. For instance, nanoscale calcium phosphate materials mimic the mineral found in bone tissue and therefore have attracted considerable interest for the development of superior biomaterials.

2.3 Clinical Challenge of Deep Bone Infection

In addition to the clinical need for the regeneration of bone tissue discussed in section 2.2 *Clinical Need for Bone Augmentation Materials*, the treatment of deep bone infection remains a significant unmet clinical need. Osteomyelitis is a bone disease which may present as an infection of the medullary cavity, cortex or periosteum. The infection leads to the destruction and necrosis of bone tissue [38]. As well as causing

significant morbidity to bone tissue, the recurrence rate of osteomyelitis is particularly high [39]. There are three recognised routes for an organism to cause infection in bone. Firstly, the organism may be directly introduced to the site of infection which may occur at the time of injury or during surgery [40]. Alternatively, infection may spread from a local source, for example from a skin ulcer, which is known as a contiguous route of infection. Lastly, it is possible for organisms to travel through the blood to infect the bone which is known as the haematogenous route [40]. Osteomyelitis can be caused by a variety of pathogens; although pyogenic (pus forming) bacteria are usually present [38], mycobacteria and fungi may also be found at the site of bone infections. The *Staphylococcus* species account for most osteomyelitis cases, followed by Enterobacteriaceae and *Pseudomonas* species [41]. Staphylococcal infections are considered one of the most difficult infections to treat with problematic factors including antibiotic resistance [38]. Specifically, *Staphylococcus aureus* and *Staphylococcus epidermidis* are the cause of over 50 % of osteomyelitis cases [39].

The management of bone infections remains a major challenge in orthopaedics and dentistry. The socio-economic costs associated with bone infections are particularly high due to increased lengths of hospitalisation and often the need for revision surgeries. The introduction of a biomaterial into the body unfortunately presents an opportunity for bacterial colonisation. For example, it was found that the minimum infection dose of *S. aureus* was reduced 100,000-fold for implant associated infections [42]. Indeed, it was suggested by Tavakoli *et al.* that the increased rates of bone infections are largely due to the increased use of prosthetic devices [38]. This may be caused by a decreased ability to kill phagocytosed bacteria in the presence of an orthopaedic implant due to a local polymorphonuclear cell defect [41]. Once bacteria have colonised an implant surface, the formation of a biofilm protects the bacteria from host defences and antibiotics. A biofilm is usually composed of

exopolysaccharides that are secreted by adhered microorganisms which act to protect the microbial community [43].

Once bone has become infected, rapid and thorough treatment is required to prevent the death of bone tissue (chronic osteomyelitis) caused by the devascularisation of a large area of bone [39]. If chronic osteomyelitis occurs, a three step treatment program is used which consists of surgical debridement, systemic antibiotic treatment and local antibiotic delivery. The administration of high doses of oral and intravenous antibiotics are often required when treating osteomyelitis usually with a 6 week treatment period. Considerable costs are associated with these treatments; intravenous delivery of antibiotics often requires a long period of hospitalisation and infectious relapses are not uncommon [39]. For instance, systemic antibiotic treatment can costs hundreds of US dollars per day for outpatients and considerably more when a hospital stay is required [44]. As well as the protective biofilm, it is particularly problematic to treat bone infections using oral or intravenous antibiotics due to the difficulty of achieving an effective antibiotic concentration in the infected site. This problem is often compounded by low blood supply [45].

2.3.1 Materials used to Treat Deep Bone Infections

Local antibiotic delivery systems which are used to treat osteomyelitis can be classified into two classes: non-biodegradable and biodegradable. The main advantage of a local delivery system is the maintenance of a high concentration of antibiotics at the infected site for a long period of time [46]. Furthermore, the local administration of antibiotics actually reduces costs and avoids systemic toxicity issues associated with the intravenous administration of antibiotics. Non-degradable PMMA cement beads have been widely used for the treatment of chronic osteomyelitis. For example, gentamycin loaded PMMA beads Septopal® have been available for over 35 years [47]. However, the requirement to remove the beads after treatment is a major drawback. Furthermore, this approach can lead to the undesirable colonisation

of the carrier surface by resistant bacteria during the later stages of low level antibiotic release [46]. The use of antibiotic impregnated PMMA beads is considered as the gold standard treatment despite their poor biocompatibility and cytotoxic effects [39]. Biodegradable systems provide the major advantage of not requiring removal. Collagen sponges, lactic acid polymers, calcium sulphate and calcium phosphate ceramics have all been investigated as biodegradable antibiotic delivery systems. The similarity of calcium phosphates to the mineral component of bone and their osteoconductive properties are advantages to their use. As such there are several reports of antibiotic loaded hydroxyapatite composites, typically involving the use of antibiotic loaded porous hydroxyapatite blocks [48] or tricalcium phosphate beads [49]. However, due to the rise of antibiotic resistant bacteria, it is becoming ever more important to seek alternative treatment options. As highlighted in a recent review, the increasing prevalence of antibiotic-resistant bacteria is considered a global health crisis. Furthermore the genes for antibiotic resistance are able to transfer between bacteria [50]. If a vancomycin-resistant *Staphylococcus aureus* were to evolve, this could cause infections that are resistant to all currently available antibacterial treatment [38].

2.4 Nanoscale Hydroxyapatite Bone Augmentation Pastes

There are currently three nanoscale hydroxyapatite pastes established on the market: Ostim® (aap Implantate AG, Berlin, Germany), SINTlife (Finceramica Faenza S.p.A, Italy) and ReproBone *novo*™ (Ceramisys Ltd., Sheffield, UK). Although there are several reports in the literature on the behaviour of Ostim® *in vivo*, fewer reports exist on investigations involving SINTlife and ReproBone *novo*™. The majority of the reports published on nHA pastes have been published within the last 7 years, thereby highlighting the current interest in this novel class of materials.

Ostim® is prepared through a wet precipitation reaction involving the addition of orthophosphoric acid into a calcium hydroxide suspension [51] and has been reported to contain a range of nanoscale hydroxyapatite mineral content from 35 wt. % [51] to 59.6 wt.% [52] in combination with water. Transmission electron micrographs of dried Ostim® paste display needle-like HA particles with a high aspect ratio (length of particle / width of particle). The particles have been reported to be 100 x 20 x 3 nm in size [53]. Several papers have reported the particle size as 18 nm [54] but this is an incorrect interpretation of Rietveld refinement results obtained from X-ray diffraction data that can only provide crystallite sizes which may be present in much larger particles.

SINTlife is a nanoscale hydroxyapatite paste substituted with magnesium ions with particle sizes of 30-40 nm [55]. The preparation of the material involves the addition of calcium nitrate, magnesium nitrate and ammonium dihydrogen phosphate solutions into a dilute solution of ammonium hydroxide to maintain the pH above 9 for the duration of the reaction [56]. The solution is stirred in a carbon dioxide-free environment to reduce carbonate substitution into the HA. This is followed by a hydrothermal treatment at 120 °C followed by filtering, washing and drying stages. For more information regarding magnesium-substituted hydroxyapatite see section 2.5.1.1 *Substitutions Intended to Enhance the Bioactivity of Hydroxyapatite*.

In the past decade, Ostim® and SINTlife have been investigated for a wide range of bone regeneration applications to enhance healing throughout the body. These nanoscale hydroxyapatite pastes have been tested against conventional bone graft materials in a variety of procedures. Firstly, the biocompatibility of Ostim® has been investigated *in vitro*. However, one set of *in vitro* tests provided poor viability results for primary human osteoblast and mesenchymal stem cells cultured on Ostim®. It was suggested that the high water content of the material was likely to have reduced the osmotic potential of the culture conditions, thereby resulting in cell death [54]. Ostim®

has been extensively tested in a range of animals including rabbits, goats, pigs, minipigs and hamsters. In these animal trials Ostim® was generally found to possess potent osteoconductivity. It was reported in several papers that the rapid and thorough osteointegration of Ostim® may have hindered the complete resorption of the material [57]. Although Ostim® was found to resorb at an early stage after implantation [58], there are reports that showed the cessation of Ostim® degradation 4 weeks [59] and 6 weeks [60] after implantation. Indeed, many animal investigations have described the incomplete resorption of Ostim® after 12 weeks [59, 61] and 1 year [57]. In contrast, Thorwarth *et al.* [62] reported the complete resorption of Ostim® 6 months after implantation into critical size porcine calvarial defects. In the same study, when Ostim® was combined with autogenous bone, complete resorption occurred in 12 weeks.

Many studies observed favourable results for Ostim® compared with other materials. Ostim® was found to reduce cement penetration in acetabular bone impaction grafting [58] and Busenlechner *et al.* [2] found that the use of Ostim® led to a higher degree of bone formation compared to particulate deproteinised bovine bone mineral (Bio-Oss®). The presence of Ostim® was also found to be beneficial for treating critical size rabbit defects compared with the use of a bovine derived porous HA scaffold (Cerabone®) [3]. Laschke *et al.* [51] reported evidence to suggest that Ostim® guided vascularisation during degradation after 14 days *in vivo* in dorsal skinfold chambers of Syrian golden hamsters.

Similar promising results have been found with the use of Ostim® in clinical trials. Ostim® has been investigated as a material for use in a variety of bone fracture situations such as void filling of tibial compression fracture zones [63], complicated metaphyseal radial fractures [64], comminuted distal radial fractures [65] and calcaneal fractures [53]. Ostim® has also been tested in various maxillofacial surgeries including sinus floor augmentation [66, 67], intrabony peri-implantitis

defects [68], periodontal intrabony defects [69, 70], alveolar bone healing following tooth extraction [71] and lateral alveolar ridge augmentation [72]. In these applications Ostim® was generally found to be a suitable material due to its easy handling characteristics and its good biocompatibility and osteoconductivity thereby encouraging beneficial bone formation. Strietzel *et al.* [72] and Zaffe *et al*. [67] reported only a small amount of Ostim® presence 6 months after implantation for alveolar ridge augmentation and 12 months after implantation for sinus floor augmentation respectively.

Clinical trials performed using SINTlife paste have included treatments for tibial osteotomy [55] and sinus grafts [73]. In these applications, SINTlife showed a limited resorption capacity. An improved resorption capacity was observed when SINTlife was mixed with allogeneic lyophilised human bone chips to form DBSint [55]. The nanocomposite DBSint showed significantly higher osteointegration than the lyophilised bone chips. It was also noted that the radio density of SINTlife was different from that of mineralised bone [55] thereby providing a useful means of monitoring the presence of the bone substitute.

ReproBone *novo*™ is a nanoscale hydroxyapatite paste with a particle size of 30 – 50 nm and a mineral content of 38 wt. % [74]. Although ReproBone *novo*™ has not been investigated as widely as Ostim® or SINTlife, early reports suggest that it has the ability to encourage bone tissue healing in the same way as other nanoscale hydroxyapatite pastes. When ReproBone *novo*™ paste was combined with hydroxyapatite and β-tricalcium phosphate biphasic granules to fill tooth extraction sockets in dogs, the nanoscale hydroxyapatite paste was completely resorbed within 8 weeks. At this time point, remnants of the granules still remained. In this study, the granulated ReproBone *novo*™ construct presented superior biological results when compared to the self-hardening bone cementum group which displayed fibrous tissue encapsulation and a lower degree of bone tissue regeneration [75, 76].

Despite very encouraging experimental and clinical data, more general concerns exist regarding the safety of materials at the nanoscale. A review on the use of nanoscale materials in orthopaedic surgery conceded that the health effects of nanoscale materials are essentially unknown [77]. Safety considerations include the potential release of nanoparticles during *in vivo* degradation, and the subsequent transport and metabolism via the blood. Investigations involving the injection of nHA into mice concluded that the target organs of the blood-borne particles were the lungs, liver and spleen [78]. These investigations into the long term safety involved the repeated injection of nHA particles every 2 weeks over a 2 year period, with no chronic damage or long term side effects reported. The study concluded that nHA particles may be an effective drug carrier in appropriate concentrations as the lethal dose of the nHA suspension was caused by the blockage of capillaries [79]. The general consensus is that more studies need to be carried out in order to fully understand the potential risks associated with the use of nanoscale materials *in vivo*. However, the studies to date on nanoscale hydroxyapatite pastes have showed promising results with no specific concerns raised regarding the harmful migration of nHA throughout the body.

Therefore based on the current evidence in the literature, it can be concluded that nanoscale hydroxyapatite paste-like materials present a promising new class of bone augmentation materials which may be superior to current clinical treatments. In particular the combination of these pastes with granules or bone chips generally provides superior handling characteristics and a better biological response, than the use of granules or bone chips alone. For information regarding the manufacture and characterisation of nHA see section 2.5.2 *Nanoscale Hydroxyapatite Production Methods*.

2.5 Hydroxyapatite Chemistry

Before considering the methods to produce nanoscale hydroxyapatite, it is important to understand the chemistry and structure of hydroxyapatite (HA) and elemental substitutions which may impart favourable properties. Hydroxyapatite is a calcium phosphate mineral with the formula $Ca_{10}(PO_4)_6(OH)_2$. Therefore the stoichiometric calcium: phosphorus ratio for HA is 1.67. HA has been widely used in medical and dental applications during the last few decades due to its similarity to the mineral phase of bone and tooth enamel. Moreover, HA has excellent bioactivity and biocompatibility. It is considered as an osteoconductive material due to its ability to provide a beneficial environment for new bone apposition [28].

HA possesses the highest stability, density and insolubility of the calcium phosphates. In bone and tooth enamel, hydroxyapatite is present in its hexagonal crystal structure form. An alternative crystal structure for HA also exists, namely the monoclinic form in which the hydroxyl groups are stacked in a column and point in the same direction; in hexagonal HA the adjacent hydroxyl groups point in opposite direction [80]. Since the stability of the monoclinic form is sensitive even to a small amount of foreign ions [9], it is the hexagonal structure HA that is commonly prepared using precipitation and sol-gel techniques. Hexagonal HA has a $P6_3/m$ space group with the unit cell dimensions of a = b = 0.9432 nm, c = 0.6881 nm [81]. Two different calcium cation sites exist in the crystal structure: Ca(I) and Ca(II), see Figure 2.2. In a unit cell of HA, 4 Ca(I) atoms are tightly bound to 6 oxygen atoms, whilst sharing 3 weaker oxygen bonds. The Ca(I) atoms are arranged parallel to OH- channels and are aligned in precise columns. Deviation in the metal-oxygen interactions for the Ca(I) affect the entire lattice. Meanwhile 6 Ca(II) are enclosed by 7 oxygen atoms. The Ca(II) atoms are staggered, belonging to consecutive layers, which allows for random local displacements without affecting the entire unit cell structure [9].

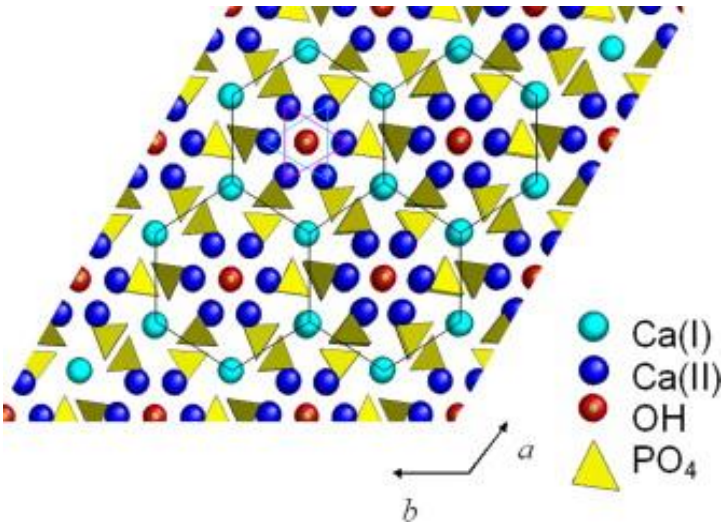

Figure 2.2. Hydroxyapatite crystal structure viewed along the c-axis. Note the different positions of Ca(I) and Ca(II). Reproduced with permission from reference [9].

The stages in the precipitation of hydroxyapatite have been investigated from 1965 [82]. This report demonstrated the importance of an ageing step in the production of crystalline HA. Firstly an amorphous product was formed which slowly crystalizes until an apatite structure is observed. The final stage is characterised by a gradual increase of crystallinity caused by an enlargement of particle size and a reduction of the concentration of dissolved calcium in the solution. The growth of the crystals is said to occur through Ostwald ripening, where smaller soluble crystals are re-deposited of the surface of the larger crystal. It is believed Posner clusters ($Ca_9(PO_4)_6$), described as the growth unit of hydroxyapatite, may be involved in the process of Ostwald ripening. Specifically, it has been reported that Posner clusters of 0.8 nm in height may partake in selective hexagonal packing during the formation of HA [83]. Posner clusters exist in the known precursors of hydroxyapatite, namely octacalcium phosphate and amorphous calcium phosphate [83, 84]. The Ostwald ripening process is considered as thermodynamically favourable due to the reduction of Gibbs free energy in the system; smaller particles are considered to have a high surface energy as a result of their large surface area to volume ratio. Therefore the reduction of surface area forms more stable, larger particles.

Hydroxyapatite undergoes thermal decomposition into β-tricalcium phosphate (β-TCP). There are reports of the thermal decomposition of HA ranging from 1050 °C to over 1450 °C [85]. It was reported by Cihlar *et al.* that the most generally accepted mechanism of HA thermal decomposition [85] is:

$$Ca_{10}(PO_4)_6(OH)_2 \leftrightarrow 2\beta\text{-}Ca_3(PO_4)_2 + Ca_4(PO_4)_2O + \uparrow H_2O$$

However there are also reports providing an alternative decomposition reaction [86-88]:

$$Ca_{10}(PO_4)_6(OH)_2 \leftrightarrow 3\beta\text{-}Ca_3(PO_4)_2 + CaO + \uparrow H_2O$$

In particular, calcium-deficient HA [89] and nanoscale HA [90] have been found to decompose to β-TCP at lower temperatures than stoichiometric HA. For example, Bianco *et al.* [90] reported the appearance of a β-TCP phase when nanoscale HA powders were sintered above 800 °C.

2.5.1 Substituted Hydroxyapatites

Apatite is considered to be a very flexible mineral in its ability to allow for a vast range of elemental substitutions. Indeed, apatite is able to around accommodate half of the elements in the periodic table [12]. Some possible substitutions of biological interest are listed in Table 2.4. The substitution of different elements into the HA crystal lattice affect the unit cell structure. These changes affect many material properties including crystallinity, crystal strain, hardness, thermal stability and solubility [12]. Furthermore, if the substitution does not balance the charge of the original ion, vacancies are created within the crystal structure. Cationic substitutions can occur over the whole range of occupation (e.g. substitution of Sr^{2+}, Cd^{2+}, Pb^{2+} for Ca^{2+}) [9], or to a limited extent for smaller ions which inhibit crystal nucleation and growth e.g. Mg^{2+} and Zn^{2+} [56, 91, 92]. Similarly, the anionic substitution of Cl^- or F^- can replace all the OH^- ions in the HA crystal structure. Carbonate substitution has also been reported to inhibit the growth of crystals resulting in poorly crystalline products with an increased

solubility. On the other hand, the substitution of F^- resulted in a product with increased crystallinity and a lower solubility. Advantageously, these substitutional effects allow for the tailoring of material properties, which can allow for the material to be optimised for a range of different biological functions. For example, the use of fluoride in toothpaste and drinking water creates a degree of fluorine substituted apatite on the tooth surface which is more resistant to corrosion in an acidic environment [93, 94].

Complications can arise when trying to distinguish if the ions have successfully substituted into the crystal structure or if the ions are present in an amorphous phase or adsorbed onto the crystal surface. Unfortunately there is discrepancy in the literature regarding the terms ‘substitution’ and ‘doping’ when describing chemical modifications to hydroxyapatite. Some researchers use the term interchangeably, whereas others regard substitution as the replacement of an atom in the crystal cell structure, whereas doping is the adherence of ions or particles on the surface of the crystal cell. Certainly in some cases it is not known which eventuality has occurred. Many researchers investigate the change in unit cell parameters to determine whether the introduction of a smaller or larger ion has caused a change in the unit cell dimensions. With the view to improve the bioactivity of hydroxyapatite, several elemental substitutions have been reported in the literature.

Table 2.4. Hydroxyapatite substitutions of biological interest; general formula $M_{10}(XO_4)_6Y_2$ [9, 12].

M	**XO_4**	**Y**
Ca^{2+}	PO_4^{3-}	OH^-
Sr^{2+}	CO_3^{2-}	F^-
Ba^{2+}	VO_4^{3-}	Cl^-
Cd^{2+}	AsO_4^{3-}	Br^-
Pb^{2+}	SiO_4^{4-}	
Zn^{2+}	SO_4^{2-}	
Mg^{2+}		
Mn^{2+}		
Ni^{2+}		
Cu^{2+}		
Co^{2+}		
Ag^+		
Na^+		
K^+		
Al^{3+}		
Y^{3+}		

2.5.1.1 Substitutions Intended to Enhance the Bioactivity of Hydroxyapatite

Silicon-substituted Hydroxyapatite

Silicon is the most prevalent HA substitution published in the literature. Historically, silicon-containing Bioglass was the first synthetic material to bond with living tissue and was discovered by Larry Hench in 1969 [95]. Silicon is a biologically relevant substitution as it was found to have a significant effect on the early stages of bone matrix production when cockerel chicks were fed silicon-deficient diets. In this study, bones from chicks fed silicon-deficient diets were found to have considerably less collagen present than chicks fed a silicon-enriched diet. Furthermore the silicon-deficient chicks developed shorter and narrower skulls with abnormal areas displaying fewer trabeculae and less calcification [96]. Silicon has also been located in the unmineralised osteoid regions in young bones of mice and rats suggesting that it has an important role in the mineralisation of bone [97].

It has been reported that the maximum amount of silicon that can be successfully substituted into the HA crystal is 5 wt. % [97]. It should be noted that the maximum amount of silicon which could theoretically be incorporated into the HA crystal by replacing all of the phosphorus is approximately 20 wt. %. Due to the non-isoelectronic substitution of SiO_4^{4-} for PO_4^{3-} the hydroxyapatite crystal can accommodate the extra negative charge by creating new anionic vacancies [97]. Therefore, the substitution of silicate ions into HA is not energetically favourable during crystal growth and it has been proposed that silicate ions only substitute with subsequent thermal treatment at 900 °C to displace residual carbonate ions [98]. The substitution of the silicate ion is also responsible for a decrease in the surface charge which in turn will allow a higher dissolution rate [97]. This has been proposed as an explanation for the difference in *in vivo* activity.

The most popular method to synthesise silicon-substituted HA has been via precipitation methods [97] which use silicon sources such as silicon acetate [99].

Balas *et al.* [100] demonstrated the importance of a basic pH during the precipitation of silicon-substituted HA. Silicon-substituted hydroxyapatite synthesised at a pH lower than 11 was found to decompose into β-TCP at a temperature of 950 °C. A review article by Boanini *et al.* [9] states that XRD is not a sensitive enough technique to distinguish between silicon and phosphorus due to their very similar isoelectronic states. Instead neutron diffraction is suggested to provide a clearer understanding on the presence and position of these atoms.

Although there is evidence to suggest that silicon substitution enhances the bioactivity of HA [99], little is understood on the precise mechanisms by which the presence of silicon affects bone cells. A critical view by Bohner [101] suggests that silicon ions may be released by the materials and then have an active and direct effect on cellular behaviour. Another proposed theory is that the chemical and physical difference induced by the presence of silicon has an indirect effect on the cells when they interact with the surface of the modified biomaterial. Bohner concluded that it is still not clear whether the presence of silicon has a positive effect on the biological response of silicon-substituted calcium phosphates. However, Bohner also concedes that there is converging evidence that the addition of silicon to calcium phosphates such as HA and α-TCP modifies the *in vivo* behaviour of the material. For example, an *in vivo* study by Patel *et al*. [102] found a significantly greater bone ingrowth for 0.8 wt. % silicon-substituted HA granules compared to phase pure HA granules which had been implanted in the femoral condyle of rabbits.

Interestingly, silicon-substituted hydroxyapatite was found to be osteoinductive in an ectopic ovine model. It should be noted that the stoichiometric HA was also found to be osteoinductive in this model which is unusual, since HA is not commonly accepted to have osteoinductive properties. However, significantly more bone formation and bone attached to the implant surface was observed in the silicon-substituted HA group [103].

Magnesium-substituted Hydroxyapatite

Magnesium is another substitution which has been investigated in the literature due to its biological relevance; biological apatite is known to contain a higher amount of magnesium at the start of the calcification process which then decreases as calcification progresses [104]. Although magnesium is a known inhibitor of HA nucleation and growth, a limited amount of substitution is possible.

Interestingly, Bigi *et al.* [56] recognised that an apatite phase could not be formed when magnesium was present between 35 – 50 at. %. In this range the product was found to be completely amorphous due to the ability of magnesium to inhibit the crystallisation of HA. Below this range, increasing the amount of magnesium causes a decrease in crystal size. Above this range, different crystalline phases are formed displaying the inability of the HA crystal lattice to accommodate the magnesium atoms at a level higher than 7 at. %. The amount of magnesium able to substitute into the lattice is limited by the inability of the magnesium atom to substitute into the Ca(I) position. Instead magnesium atoms are only able to substitute into the Ca(II) sites which form the channels surrounding hydroxyl ions (see Figure 2.2). This has been attributed to the shorter metal oxygen distance provided by these sites. Magnesium was found to preferentially adsorb onto the crystal surface when it was fully accommodated by the HA lattice. This has promoted research regarding magnesium-doped hydroxyapatite which has been found to have a higher solubility than hydroxyapatite potentially through a reduction in crystallisation in conjunction with increased surface hydration [105].

It can be difficult to confirm the effective substitution of magnesium using conventional XRD analysis due to the decrease in HA crystallinity. Furthermore, low temperature precipitation methods can be prone to multi-substitutions such as carbonate-substitution in conjunction with magnesium-substitution which can further complicate XRD patterns. The presence of magnesium in HA has been found to cause thermal

instability; it was reported by Bigi *et al.* [56] that the presence of magnesium causes the thermal decomposition of the magnesium-substituted HA to a magnesium-substituted β-TCP above 500 °C.

Magnesium-substituted hydroxyapatite has been found to have promising results regarding its *in vivo* activity. For example a study by Crespi *et al.* [106] compared the use of magnesium-enriched HA and autologous bone in maxillary sinus grafting. Although the autologous bone group displayed higher vital bone levels, *ex vivo* osteoblast expansion revealed that the magnesium-enriched HA had caused higher expression of osteoblast differentiation markers and bone formation markers which are also associated with a lower osteoclastic activity. Unfortunately, no details are given regarding the amount of magnesium present or the source of the material which makes it difficult to understand whether this material is magnesium-substituted or magnesium-doped HA. For more information regarding the *in vivo* behaviour of nanoscale magnesium-substituted HA paste (SINTlife) see section 2.4 *Nanoscale Hydroxyapatite Bone Augmentation Pastes*.

Carbonate-substituted Hydroxyapatite

As described earlier, the substitution of carbonate ions into hydroxyapatite is of particular interest due to the carbonate content of bone mineral. Indeed, bone apatite is said to contain between 2.3 and 8 wt. % carbonate [11]. For this reason, carbonate-substituted HA is a biomimetic substitution which has attracted attention due to its potential to encourage bone tissue regeneration. Carbonate ions (CO_3^{2-}) are able to substitute into two sites within the HA crystal structure. A-type carbonate substitution is when carbonate ions substitute into the hydroxyl ion site, whereas the carbonate ion occupancy of the phosphate group site is known as B-type substitution. The most biologically relevant substitution is a mixed A- and B-type which corresponds to the distribution of carbonate in biological apatite [11]. The presence of carbonate reduces the crystal growth and crystallinity of HA. These factors may account for the increased

solubility of carbonated hydroxyapatite, which has been proposed to contribute to its increased bioactivity [9].

A recent *in vitro* study concluded that the effects of carbonated HA on the behaviour of human osteoblast-like cell line MG63 were not dose dependent on the amount of carbonate. Differentiation, osteoprotegerin and vascular endothelial growth factor A (VEGF-A) levels were all decreased with carbonated HA (3.88, 4.85 and 5.82 wt. %) when compared to conventional HA [107]. In contrast the activity of osteoclasts was stimulated on carbonated HA [108], and in fact osteoblast activity increased after the osteoclastic presence on carbonated HA [109].

In vivo studies have concluded that carbonated HA has enhanced bioactivity due to its higher solubility and ability to stimulate osteoclastic resorption; indeed these two factors are intrinsically linked. For instance, Porter *et al*. investigated the behaviour of carbonated HA granules in an ovine model. The carbonate-containing HA (1.2 and 2.05 wt. %) was more soluble than the HA with no carbonate content. Furthermore, the bone surrounding the carbonated HA displayed a higher degree of organisation, including the presence of collagen fibrils. It was concluded that the increased solubility of the carbonated HA may have activated osteoclasts, which in turn further accelerated the material breakdown [110]. In order to better understand the mechanisms regarding the increased bioactivity on carbonated HA, Spence *et al.* investigated the dual effect of carbonated HA and the osteoclast suppressing drug zoledronate. It was concluded that osteoclast activity was responsible for the increased osteoconductivity observed for carbonated HA implants [111].

Strontium-substituted Hydroxyapatite

Strontium substitution into hydroxyapatite is of particular interest due to the use of strontium compounds in the treatment of osteoporosis [112]. Osteoporosis is a common metabolic bone disease among post-menopausal women that causes the

weakening of bone tissue through over resorption of existing bone tissue and a decrease in bone deposition. This often results in fractures which can require patients to undergo traumatic joint replacement procedures. Oral dosage of strontium compounds, such as strontium ranelate, have been used successfully in the treatment of osteoporosis. It has been found that these strontium compounds have the ability to increase bone deposition whilst reducing bone resorption [112, 113] which has the positive effect of increasing the strength of bone, thus reducing the occurrence of fractures. More specifically, strontium ranelate has been found to increase pre-osteoblast replication, osteoblast differentiation, collagen type I synthesis and bone mineralisation whilst reducing osteoclast differentiation [114]. This has led to interest in the field of strontium-substituted hydroxyapatite. Even in this form, strontium has been found to have a beneficial effect on bone formation, namely by stimulating osteoblast-like cells whilst inhibiting osteoclastic activity [115]. However, only a limited amount of papers have been published regarding the production and characterisation of Sr-HA which are discussed in detail below.

Although the exact mechanisms of strontium action on bone cells are not fully understood, several theories have been proposed. Due to the use of the drug for reducing fractures in osteoporotic patients, research regarding the effect of strontium on bone cells usually investigates the effect of strontium ranelate on bone cell cultures. In this form, strontium is said to have a pharmacological effect on bone cell activity i.e. strontium directly exerts a biochemical or physiological effect. Furthermore the molecular mechanisms of strontium on bone cells have also been investigated [116]. The action of strontium on bone cells, particularly osteoblasts and osteoclasts, directly affects the rate of bone formation. Firstly, strontium reduces osteoclast activity and differentiation, thereby reducing bone resorption levels; this effect manifests through various actions including increased osteoclastic apoptosis and disruption to osteoclast adhesion [117]. Secondly, strontium stimulates osteoblast differentiation

and activity which increases bone deposition [117]. Finally, strontium has also been found to reduce the adipogenic differentiation of mesenchymal stromal cells, thereby effectively encouraging osteoblastic differentiation [118].

The cellular effects listed above are caused by various molecular mechanisms which activate multiple signalling pathways. Namely, strontium can act through the calcium-sensing receptor to increase the proliferation of osteoblastic cells. Osteoclast apoptosis and reduced osteoclastic differentiation is also stimulated by the effect of strontium on the calcium-sensing receptor. However, studies on knock-out animals with no calcium-sensing receptor, have shown that other pathways are also stimulated by strontium. For instance, the stimulation of the nuclear factors of activated T-cells (NFATc) pathway upregulates the expression of osteoblastic differentiation genes [119], although the precise mechanism by which NFATc is activated by strontium is unknown. Furthermore, strontium has been found to have an effect on the receptor activator of nuclear factor kappa-B (RANK) / receptor activator of nuclear factor kappa-B ligand (RANKL) / osteoprotegerin (OPG) system [116]. RANK is a cell membrane receptor present on the surface of osteoclast cells and their precursors. When RANKL binds to RANK osteoclast formation is stimulated as well as the activity and longevity of mature osteoclast cells. OPG inactivates RANKL by binding to it, thereby reducing its effect on osteoclast cells. Specifically, strontium increases OPG and decreases RANKL production which reduces osteoclast production and activity; this in turn reduces the resorption of bone tissue [120]. Furthermore, a study investigating strontium-substituted bioactive glasses reported the genetic upregulation of alkaline phosphatase, collagen type 1 α-chain and osteocalcin for strontium-containing samples [121].

The higher atomic number of strontium when compared to calcium results in the higher radiopacity of strontium-containing materials. For instance, studies regarding strontium HA bone cement [122] and strontium calcium phosphate bone cements

[123] reported higher radiopacity for the materials containing greater amounts of strontium. This could beneficially aid *in vivo* placement and monitoring of implants.

Strontium can be substituted into hydroxyapatite over the whole range of composition which causes a linear expansion of the lattice parameters [124, 125] due to the larger ionic radius of strontium (0.12 nm) when compared to calcium (0.099 nm). At low concentrations strontium has been found to display a preference for the Ca(I) site, whereas at higher strontium concentrations a slight preference for the Ca(II) site has been observed [125]. Low levels of strontium substitution cause a decrease in crystallinity. At higher strontium concentrations, increases in the size of crystals and the crystallinity of the material have been observed [125]. A computational study by Matsunaga *et al.* [126] indicated that for biological apatite mineralisation, strontium ions can be more favourably substituted into octacalcium phosphate (OCP) by ion exchange rather than straight into hydroxyapatite. Since OCP is a known precursor to hydroxyapatite, this provides an insight as to how strontium-substituted hydroxyapatite may be synthesised in wet chemical reactions.

Strontium-substituted hydroxyapatite has been prepared by various methods including wet precipitation and sol-gel methods. Typical strontium precursors used include strontium nitrate and strontium hydroxide. Low temperature wet precipitation methods have used to produce strontium-substituted hydroxyapatite powders [115, 125, 127], with one study preparing strontium-substituted-HA powders over the whole range of possible composition (0-100 at. %) [124]. It should be noted that these studies did not involve high temperature sintering stages, potentially due to the thermal instability of substituted apatites.

Several papers regarding the sol-gel synthesis of strontium-substituted hydroxyapatite reported the thermal instability of strontium-substituted HA samples. Hanifi *et al.* [128] reported the emergence of a β-TCP phase after sintering at 600 °C. It was proposed by Renaudin *et al.* [129] that strontium-substituted β-TCP was being

synthesised in the thermal decomposition of strontium-substituted HA. This was confirmed by Rietveld refinement studies investigating the changes in unit cell parameters of HA and β-TCP with strontium substitution into the two materials. Strontium HA has also been investigated in the form of coatings applied using sputtering techniques. Recent analysis of Sr-HA coatings by Boyd *et al.* demonstrated the changes in XRD patterns and FTIR spectra for coatings with increased amount of strontium [130, 131].

Strontium-substituted hydroxyapatite has been found to have a marked biological effect on osteoblasts at a relatively low level of substitution (3-7 at. %) [115]. Increased levels of alkaline phosphatase activity, collagen type I production and osteocalcin production were observed for osteoblasts cultured on Sr-HA samples. Furthermore osteoclast numbers were found to be reduced on the strontium-containing samples, even at 1 at. % strontium incorporation. As an explanation as to how strontium-substituted HA promoted bioactivity, it was proposed that the presence of strontium causes a destabilising effect which in turn increases the solubility of strontium-substituted hydroxyapatite. Increases in solubility will result in a higher concentration of ions to interact with the bone cells. A study by Zhang *et al*. concluded that 10 at. % strontium-substituted HA promoted the highest levels of alkaline phosphatase activity and MG63 viability compared to 0, 40 and 100 at. % strontium-substituted HA [132]. Interestingly it was also reported that the effect of Sr alone was not enough to stimulate the higher levels of proliferation and ALP activity observed for MG63 cells on strontium-substituted HA pellets; instead it was proposed that a joint effect between the strontium, calcium and phosphorus could be responsible for the biological effects observed [133]. Recently, it was reported that strontium-substituted hydroxyapatite gels promoted proliferation and the differentiation of mesenchymal stem cells in an osteogenic manner. Specifically, alkaline phosphatase, osteopontin and osteocalcin markers were upregulated demonstrating

the enhanced osteogenic differentiation. However, due to the change in particle morphology when different amounts of strontium were present, it could not be concluded whether the changes in *in vitro* response were due to the direct effect of strontium or due to an indirect effect of particle morphology, or a combination of the two effects. Furthermore, only strontium-substituted nHA gels of up to 20 at. % Sr content were investigated; by considering strontium content only up to one fifth, an optimal Sr concentration may have been overlooked [134].

Few *in vivo* studies are available concerning the response of SrHA. However, in one study, 10 at. % SrHA cement was found to interact differently than HA with cancellous and cortical bone in a rabbit hip replacement model. The SrHA cement induced the formation of a 70 µm apatitic layer when in contact with cancellous bone, whereas a layer of only 1 µm thickness was formed on the cement in contact with cortical bone. Furthermore, the different compositions of the apatite layers suggested different rates of cement dissolution had occurred at the different sites. It was proposed that these differences may be due to the presence of active osteoclasts at the cancellous bone site whereas no osteoclasts were observed at the cortical bone site [135].

2.5.1.2 Antibacterial Hydroxyapatite Substitutions

As well as substitutions to increase the bioactivity of HA, some researchers have performed substitutions to impart antibacterial properties. Ions such as zinc, copper and silver have been investigated for this purpose. Although not fully understood, the broad mode of action of antibacterial ions reduces the likelihood of bacterial resistance developing. For example, as well as disrupting ATP production and DNA replication, it has also been suggested that antibacterial ions induce changes in cell membrane permeability and affect the transportation of protons. Furthermore, the production of reactive oxidative species affects several components of the cell wall, membrane and other intracellular components, ultimately causing cell death [136].

Zinc-substituted Hydroxyapatite

Zinc is regarded as an essential biological element and has a particularly vital role in bone metabolism, since it is known to be present at the active sites of hundreds of enzymes [136]. For example, an increase in alkaline phosphatase activity and bone DNA content was observed when rats were given a low dose of zinc [137]. Therefore the development of zinc-substituted HA has been considered for bioactive and antibacterial purposes. Zinc has been shown to inhibit osteoclastic differentiation and stimulate osteoblast activity, thereby promoting bone formation [138]. Murine pre-osteoblast cells cultured on zinc-substituted HA surfaces were found to display significantly increased cell proliferation, alkaline phosphatase activity and osteocalcin production [139]. Few published articles are available detailing the in *vivo* response of zinc-substituted hydroxyapatite. However, an *in vivo* experiment by de Lima *et al.* concluded that zinc-substituted HA granules were found to increase the rate of angiogenesis and were resorbed at a faster rate than stoichiometric HA [140].

Although zinc is a fairly potent inhibitor of HA crystal growth [92] it is still possible to perform zinc substitution using wet precipitation reactions [91, 92, 141]. So far it has been suggested that the successful substitution of zinc ions for calcium ions in the HA crystal occurs up to approximately 20 at. %. In a similar fashion to other ions such as magnesium, zinc preferentially substitutes into the Ca(II) site. The incorporation of zinc is associated with a decrease in HA crystallinity and thermal stability with partial decomposition to zinc-substituted β-TCP reported after sintering at 500 °C [92].

The antibacterial activity of zinc-substituted HA has been reported [142] and a zinc content of 1.6 wt. % was found to exhibit antibacterial properties whilst enhancing bioactivity [143]. Investigations regarding a zinc-doped β-TCP and HA composite ceramic reported the increased bioactivity of osteoblast cells when the zinc level was 0.6 – 1.2 wt. %. However, a zinc content higher than 1.2 wt. % was found to have

cytotoxic effects due to zinc release, which highlighted the sensitivity of cells to small changes in metallic composition [144].

Copper-substituted Hydroxyapatite

Copper is involved in a variety of metabolic processes and has been known for its antibacterial properties since the Egyptian times. It was discussed that as well as the disruption to the bacterial structures and functions previously discussed for antibacterial ions, copper ions also increase macrophage ability to inactivate bacteria [145].

Reported synthesis methods of copper-substituted hydroxyapatite include hydrothermal [146], ion exchange [147] and wet precipitation methods [142, 148]. In these methods copper nitrate [146, 148] , acetate [147] and oxide [142] have all been used as copper sources. The ion exchange method described by Li *et al*. involved the precipitation of HA followed by subsequent drop wise addition of the metal salt solution into the HA slurry. This study suggested that the substitution process involved initial rapid formation of surface complexes followed by the partial dissolution of HA whereupon the copper ions would exchange with the calcium HA ions [147]. The attempted substitution of copper by Stanic *et al.* resulted in a reduction in the stoichiometric ratio ((Ca+Cu)/P) for HA demonstrating the probable formation of a copper-substituted calcium-deficient apatite [142].

Conflicting reports exist on the antibacterial efficacy of copper-substituted HA. Kim *et al.* reported that the antibacterial effect of copper and zinc were difficult to observe whereas clear antibacterial effects were observed for silver-substituted samples [148]. Conversely, it was reported by Stanic *et al.* that copper- and zinc-substituted HA samples showed clear antimicrobial activity against *Escherichia coli, Staphylococcus aureus* and *Candida albicans* [142]. High antibacterial activity was also observed against *E. coli* for copper-substituted HA. However, the same paper

concluded that copper-substituted HA coatings were unsuitable for implants due to the cytotoxicity of copper ions to osteoblasts [147].

Silver-substituted Hydroxyapatite

Few detailed reports have been published on the synthesis and antibacterial activity of silver-doped nHA research to date. The majority of reports which have been published mainly focussed on a substitution approach, whereby the amount of calcium is reduced in an attempt to substitute silver into the HA crystal lattice [149-154]. However the drawback with this approach is that if the silver does not readily incorporate into the HA phase, calcium-deficient HA is likely to precipitate which possesses different properties than stoichiometric HA; particularly its' thermal stability. Many studies do not report the level of silver successfully incorporated into the product and therefore it is not possible not know what changes are caused by the incorporation of silver and what changes are caused by the production of calcium-deficient HA. Furthermore the substitution of silver into the HA crystal lattice may limit the diffusion and therefore the antimicrobial activity of the silver hydroxyapatite.

Several researchers use the terms 'doped' and 'substituted' interchangeably when reporting on silver incorporation into HA. It would be beneficial for clarity if investigators used 'substitution' when silver was attempted to be substituted into the lattice and doped when silver was incorporated on the surface. Two reports where silver nanoparticles were introduced on the surface of the HA particles used the term 'nano composite' which provided a clear distinction as to what the aim of the methods were [155, 156].

A variety of methods have been used to synthesise silver hydroxyapatite materials including the sol-gel method [157, 158] and ionic exchange by immersion of HA in a silver salt solution [159]. However the most popular method is the wet precipitation method. Several researchers used the chemical precursors of calcium nitrate, silver

nitrate and ammonium phosphate [150, 151]. However, this approach may allow the formation of highly stable silver ammonium product, thereby limiting the amount of silver available for incorporation into the HA phase [160]. Alternatively, chemicals including calcium hydroxide and phosphoric acid were used in combination with silver nitrate [161]. An interesting approach by Ipekoglu *et al.* investigated the formation of a silver-substituted calcium-deficient HA using rapid microwave assisted processing [162]. Other approaches include the synthesis of HA followed by subsequent doping with silver nanoparticles [155, 156]. For these investigations TEM images clearly display the presence of silver nanoparticles closely associated with the HA particles.

In the literature, the antimicrobial activity of silver HA powders and coatings have been tested against a range of bacteria including *E. coli* [151, 152, 156], *S. aureus* [149, 161, 163], methicillin-resistant *S. aureus* [157] and *C. albicans* [154]. It has been widely reported that even very low levels of silver incorporation contribute to an effective antimicrobial response. This suggests that low levels of silver may be suitable for achieving a suitable antimicrobial response whilst maintaining good levels of biocompatibility for host cells.

However, it should be noted that bacterial genes for silver resistance have been identified and concerns have been raised regarding silver-resistant bacteria [164-166]. In detail, silver resistance is often encoded with plasmid genes. The resistance genes can code for proteins which act to transport silver out of the bacterial cell [166]. With this in mind, silver is widely used to reduce infections suggesting that the benefits of using silver as an antimicrobial agent, particularly the low risk to human health, generally outweigh the risks of the evolution of silver-resistant bacteria.

2.5.1.3 Hydroxyapatite Standards in Relation to Substituted Nanoscale Hydroxyapatite Materials

No standards were found specifically regarding nHA materials or HA paste materials. However, several standards are available regarding the quality of HA required for the production of surgical implants, specifically in the form of blocks and coatings [167-170].

In terms of allowable limits of elements apart from calcium, phosphorus, oxygen and hydrogen, two references were found in the current standards. Firstly, in BS ISO 13175-3:2012 'Implants for surgery – calcium phosphates' it is specified that any impurity with a ratio of more than 1000 mg/kg must be identified and its influence on bone healing shall be assessed [169]. The influence on biocompatibility will specifically be assessed using ISO 10993-1. Secondly, ISO 13779-6:2015 for HA powders used as raw materials for manufacturing of surgical implants or coatings stated that any chemical element except for calcium, phosphorus, hydrogen and oxygen likely to be present with a mass fraction more than 500 mg/kg shall be identified, quantified and indicated on the certificate of compliance on the batch [170]. Therefore, for the commercialisation of substituted nHA materials it would be necessary to prepare an alternative quality standard system which may be based on parts of the currently available standards. Based on the current standards it would be necessary to assess the biocompatibility of any substituted nHA material using ISO 10993-1 to ensure the material was suitable to develop for clinical use.

2.5.2 Nanoscale Hydroxyapatite Production Methods

Conventionally, materials may be described as 'nano' if one or more of their dimensions are less than 100 nm [171]. Nanoscale hydroxyapatite is expected to have increased biocompatibility when compared to microcrystalline HA due to its very large surface area to volume ratio. Nanoscale hydroxyapatite materials can be

considered to be biomimetic since biological apatite is present in the body at the nanoscale (see Figure 2.1).

Research into nanoscale hydroxyapatite materials is a relatively new field with the first report of the synthesis of nanocrystalline hydroxyapatite in 1995 using a spray dry method [172]. Since then, numerous methods have been employed to synthesise nanoscale hydroxyapatite including biomimetic synthesis, mechanochemical and combustion processes [173]. Two prevalent methods are the wet precipitation and sol-gel methods.

Firstly the wet precipitation method usually involves the drop-wise addition of a phosphorus solution into a calcium solution or vice versa. An alkaline pH (commonly 9 or above) is maintained to ensure the formation of hydroxyapatite instead of brushite which is thermodynamically favourable at a lower pH. Typical combinations of reagent are listed in Table 2.5. Titration by means of a peristaltic pump offers more reproducible conditions and better controllability as when compared to the use of a burette. The titration step is followed by rigorous stirring and often an ageing step, to allow time for the growth of hydroxyapatite crystals. The poor colloidal stability of hydroxyapatite results in its precipitation out of the main solution. Typically the hydroxyapatite suspension is then washed by centrifugation or filtration, dried and sintered. The smallest particle sizes reported in the literature were achieved with use of dispersal agents such as Darvan 7 [174] and hexadecyl(cetyl) trimethyl ammonium bromide [25]. For instance, spherical nanoscale HA particles of size 80, 40 and 20 nm were synthesised using 0.6, 0.9 and 1.2 mM of hexadecyl(cetyl) trimethyl ammonium bromide respectively.

Table 2.5. Typical reagents used in the wet precipitation method to produce nanoscale hydroxyapatite.

Calcium precursor	Phosphorus precursor	Reagent to control pH	References
Calcium hydroxide	Orthophosphoric acid	None	[89, 90, 174-176]
		Ammonium hydroxide	[177]
		Sodium hydroxide	[178]
Calcium chloride	Disodium hydrogen phosphate	None	[25]
	Ammonium hydrogen phosphate	Ammonium hydroxide	[179]
	Sodium phosphate	Sodium hydroxide	[86, 176]
Calcium nitrate	Diammonium hydrogen phosphate	Ammonium hydroxide	[90, 180, 181]
	Phosphoric acid		[182]

The sol-gel method contains similar stages as the wet precipitation method, starting with titration and mixing steps. Reagents typically used in the sol-gel method are listed in Table 2.6. Calcium nitrate is commonly used as the calcium precursor and the sol-gel method can involve the use of organic precursors such as triethyl phosphite. Inconveniently, the use of triethyl phosphite requires a lengthy hydrolysis stage which can be up to 24 h [183]. Unlike the wet precipitation method, the sol-gel method involves an intermediate gel phase which is said to promote molecular level mixing of the calcium and phosphorus precursors [184]. The gel can develop after a heating stage, usually at 60 or 80 °C. As a result the hydroxyapatite powder is said to require a lower sintering temperature as when compared to the wet precipitation method [183]. The prepared gel is effectively a hydrated network of metal hydroxide bonds.

Table 2.6. Typical reagents used in the sol-gel method to produce nanoscale hydroxyapatite.

Calcium precursor	Phosphorus precursor	Reagent to control pH	References
Calcium nitrate	Ammonium phosphate	Ammonium hydroxide	[185]
		None	[186]
	Triethyl phosphite	None	[184, 187-189]
	Phosphorus pentoxide	None	[88, 190, 191]
	Phosphoric acid	Ammonium	[192]
Calcium acetate	Triethyl phosphite	None	[188]

As discussed above, there are a wide variety of papers published in the literature regarding the wet precipitation and sol-gel synthesis of nanoscale hydroxyapatite. The main advantages of wet precipitation and sol-gel methods are the relative ease of production, especially that expensive equipment is not necessarily required. Furthermore these methods lend themselves well to the introduction of other ions and therefore may be most suitable for the production of substituted nHA materials.

Unfortunately, the quality of the papers regarding the wet precipitation and sol-gel production of nHA is variable. For instance, some papers do not use transmission electron microscopy (TEM) which is required to ensure that the synthesised product is indeed nanoscale [86, 186]. Similarly, some studies only use a limited amount of characterisation techniques which leave the reader unable to understand the precise physico-chemistry of the nHA produced [88, 89, 191]. Furthermore, it is often very difficult to draw conclusions on how the alteration of particular process parameter affects the properties of the nHA produced due to the various synthesis conditions used in different papers. Indeed, research recently published by our group has demonstrated the physico-chemical differences in nHA produced by different

synthesis methods which highlights the need to perform detailed characterisation techniques to fully understand the nature of the synthesised product [193]. Therefore, for this PhD program it was necessary to review several methods in order to select those that may be most suited to the production of (a) nHA, (b) substituted nHA, and (c) substituted nHA on an industrial scale.

2.5.2.1 Material Characterisation of nHA

A variety of materials characterisation methods have been used to investigate the properties of nanoscale hydroxyapatite. Firstly, X-ray diffraction is commonly used to detect the crystal phases present in a sample. The technique involves monitoring the diffraction of X-rays as they pass through the crystal lattice. Each characteristic lattice structure gives rise to a specific XRD pattern. However, difficulties can arise when using conventional materials characterisation techniques to analyse nanoscale materials. For example, it can be difficult to distinguish between X-ray diffraction patterns from very small crystals and amorphous materials, due to both materials not possessing long-range order [194]. Specifically, short range order is generally used to describe the ordering between an atom and its nearest neighbours. All liquids and solids are considered to possess short range order. Long range order however, can only be observed in solids or crystalline solids where adjacent crystal lattices provide order over a much longer length scale which may be tens or hundreds of atomic distances [195]. As a result, alternative characterisation techniques including Raman spectroscopy and Fourier-Transform Infrared (FTIR) spectroscopy are increasing in popularity as useful tools to investigate such materials [196]. These particular techniques provide information on the chemical bonds present in the studied material, which can highlight the presence of different chemical structures. The incident radiation may interact with the sample in several ways including absorption and emission of infrared radiation. However, samples must be kept as dry as possible to reduce the intensity of the water band which can obscure spectral features. An

alternative mode of FTIR does not require the production of potassium bromide discs; instead the powder material may be placed in contact with a crystal with a high reflective index (e.g. diamond) when the material is examined using FTIR in attenuated total reflectance (FTIR-ATR).

Other characterisation tests performed on nanoscale HA materials in the literature include transmission electron microscopy (TEM), thermogravimetric and differential thermal analyses (TG/DTA) and the Brunauer-Emmett-Teller (BET) method [174, 179]. In TEM an electron beam is used to image nanoscale features of the sample. However when performing this technique the nanoscale HA can be damaged with the high energy of the electron beam at high intensity. Thermogravimetric analysis records the weight of a sample as it is heated to high temperature, typically 1200 or 1300 °C. On the other hand, differential thermal analysis records the heat flow from the sample material which provides information regarding the chemical events that occur at elevated temperatures. These techniques can allow for the high temperature stability of the nHA to be investigated. The BET method allows measurement of the specific surface area of materials by studying the level of gas adsorption.

Inductively coupled plasma (ICP) techniques including mass spectrometry (MS) and atomic absorption spectrometry (AAS) have been used to give quantitative chemical compositions of nHA materials [86, 177]. This can also allow for parameters such as the calcium: phosphorus ratio to be calculated. This technique requires for the sample to be acid digested prior to analysis. Alternatively X-ray fluorescence (XRF) can be used for quantitative chemical analysis. XRF involves suspending a powder sample in molten glass which is then cooled and analysed for specific elements by monitoring the specific fluorescent response of the material to X-ray illumination.

2.5.2.2 Biological Characterisation of nHA

The papers regarding the *in vitro* biocompatibility of nHA usually test a powder or coating form, with very few papers reporting the biological behaviour of injectable nHA. However, early evidence suggests that nHA in powder and coating forms possesses potent osteoconductive properties. It is believed that the superior biological activity of nanoscale HA when compared to micron scale HA is due to several factors. Firstly, the higher specific surface area of nHA allows greater levels of protein absorption [197]. Specifically, it was reported that nHA absorbed a greater amount of vitronectin than micron scale HA [198]. The absorption of protein onto a biomaterial allows for cells to subsequently adhere to the surface. Therefore the ability of a biomaterial to adhere protein can be a strong indicator of its' biological response especially in terms of integration [197]. It has also been confirmed that nHA surfaces can promote cellular attachment. For instance, a study by Guo *et al.* reported greater levels of human osteoblast attachment on nHA when compared to micron scale HA [199]. The cellular morphology of attached osteoblasts was more physiologically relevant with less cell spreading observed on nHA in combination with a greater degree of mineralisation. Therefore it was concluded that nHA has greater bioactivity than micron HA. These affects are again potentially due to the greater surface area and corresponding protein absorption provided by nHA [199].

Furthermore, nHA has been reported to upregulate osteogenic gene expression in rat mesenchymal stromal cells (MSCs). In detail, alkaline phosphatase (ALP), core binding factor alpha 1 (Cbfa1), and the alpha 1 chain of type 1 collagen (COL1A1) were upregulated thereby stimulating the osteogenic differentiation of the MSCs. Furthermore the osteogenic protein expression of ALP and COL1A1 was higher for the cells cultured on nHA compared with a micron HA control [200]. It has also been suggested that the biomimetic nature of nHA inherently allows for a better biological response and higher levels of osteointegration in turn [14].

As well as stimulating cellular attachment and differentiation, nHA has also been reported to enhance cellular viability [199]. For example, when mesenchymal stromal cells were cultured on microscale and nanoscale particles of hydroxyapatite, greater cell viability and proliferation were observed for the cells cultured on the smallest nanoscale particles tested (20 nm). Furthermore the growth of osteosarcoma cells was found to be inhibited when cultured on the smallest nHA particles [25].

The majority of recent papers investigating the *in vivo* response of nHA materials involve the production of a polymer nHA composite scaffold or the application of a nHA coating. The application of nHA as an implant coating generally improves the level of osteointegration to a noticeable degree. For instance, when nHA has been applied as a coating to titanium bone screws, it has been found that nHA enhances the osteointegration which provides better stabilisation compared with micron HA coatings [201]. Similarly, Cheng *et al.* reported that the application of an nHA coating stimulated better osteointegration resulting in higher removal torque values for titanium screw implanted in rat tibia compared with no nHA coating [202]. When applied to the surface of a PLGA porous scaffold, the nHA coating was found to stimulate a higher degree of bone formation than observed with uncoated scaffolds [203]. A nanostructured surface design was also found to improve new bone formation and mineralisation on macroporous HA scaffolds in rat calvarial defects [204].

Regarding nHA polymer composite materials, an nHA chitosan composite powder had a lower osteogenic potential than nHA powder alone when investigated *in vitro* and in a rat calvarial defect [205]. PLA composites were also improved in terms of biocompatibility when nHA was incorporated. Specifically, a lower inflammatory response was observed with the increased presence of nHA. This was suggested to be due to the slower release of degradation products. The mechanical strength of the implants was also improved with nHA addition [206].

For information regarding the *in vivo* response of nanoscale HA paste materials see section 2.4 *Nanoscale Hydroxyapatite Bone Augmentation Pastes*.

2.6 Summary of Literature Review

This review has highlighted the importance of healthy bone for a good quality of life. There is clearly a significant socio-economic need for improved bone substitution materials since the current gold standard of autologous bone has severe limitations. Early evidence suggests that nanoscale hydroxyapatite materials may possess superior properties for bone repair in terms of bioactivity and resorbability. Furthermore, the advantageous injectability of nanoscale HA paste materials aids the minimally invasive placement of the bone graft. These materials have also shown promising results in initial *in vivo* tests in animals and in preliminary clinical trials, possibly promoting bone formation to a higher degree than control materials. Furthermore, the potential of performing elemental substitutions on nanoscale HA materials presents an opportunity to develop novel materials for bone regeneration with superior characteristics. Although many nHA production methods have been published in the literature, it is unclear which methods may be most suited for the production of substituted nHA pastes in an industrial batch process. Relatively few papers have been published in the areas of strontium and silver addition to nHA systems which have a great potential to impart advantageous properties. This review has identified the benefits of developing ‘off the shelf’ novel bone augmentation materials with enhanced bioactive and/or antimicrobial properties thereby providing direct benefits for the patient and the surgeon.

3. Aims and Objectives

Chapter 2 concluded that nanoscale calcium phosphates have great potential as injectable synthetic bone graft substitutes that may promote healing and tissue regeneration. While much has been published on the preparation of simple nHA, relatively little has been reported on the fabrication of these materials for use as injectable bone substitutes, in particular as chemically modified systems to provide advanced functionality. The aim of this PhD program was therefore to develop and evaluate processes suitable for the production of injectable basic and inorganically modified nHA materials, and to assess their biocompatibility and advanced functionality for application in regenerative medicine. The specific objectives were:

1. To compare and contrast published methods for nHA synthesis in order to select those that appeared best-suited for chemical modification and commercial scale-up. This will involve the production of nHA using a variety of wet chemical precipitation and sol-gel methods. The nHA produced will then be characterised using a range of techniques including X-ray diffraction (XRD), X-ray fluorescence (XRF) and transmission electron microscopy (TEM). From these results, the most promising method(s) will be selected for the subsequent development of chemically modified compositions.

2. To further develop the most promising methods identified above in order to investigate the effect of process parameters on the nHA produced. Specifically, the method parameters will be altered and materials characterisation techniques (XRD and TEM) will be carried out in order to ascertain the effects of experimental conditions on the chemical nature and morphology of the nHA produced.

3. To investigate the preparation of strontium-substituted nHA paste and gel. The optimised methods developed from objective 2 will be used as the basis to prepare a series of strontium-substituted nHA pastes and gels. Comprehensive materials

characterisation will be performed including XRD, XRF, TEM and Fourier transform infrared spectroscopy in attenuated total reflectance mode (FTIR-ATR). The direct and indirect *in vitro* biocompatibility of the materials will be investigated in order to assess their suitability as bone augmentation materials.

4. To investigate the preparation of silver-substituted and/or doped nHA paste. The method developed in objective 2 will also be used to produce a range of silver-doped nHA pastes with a range of silver contents. After the silver-doped nHA pastes have been characterised using the techniques listed for objective 3, the antibacterial activity of the pastes will be investigated using agar diffusion and broth dilution methods.

Specifically, the ideal strontium content of the paste or gel would be the content at which bioactivity is increased to an optimal degree. This may be difficult to conclude without *in vivo* assessment, and it could be that a range of strontium contents promote good osteoconductive properties. Similarly, the optimal silver content of the paste would be where the paste displays an effective antibacterial response whilst possessing a low toxicity to human cells, thereby promoting good bone tissue regeneration.

On completion of this project, methods will have been developed and described in detail for the production of chemically modified nanoscale hydroxyapatite pastes. The intention was to add beneficial biological and antibacterial properties, and these will have been assessed as part of the experimental programme. This research will significantly add to current knowledge in the field, indicating how chemically modified nHA paste and gels may have enhanced biological properties and clinical potential. This will in turn assist the development of new medical devices with enhanced properties for bone tissue regeneration, bringing them closer to commercial manufacture and clinical use.

4. Materials and Methods

4.1 Materials

Table 4.1. Reagents used in synthesis and characterisation of nHA.

Reagent	Molecular formula	Molecular weight ($g.mol^{-1}$)	Supplier
Ammonium hydroxide 28 %	NH_4OH	35.05	Alfa Aesar (UK)
Ammonium phosphate dibasic	$(NH_4)_2HPO_4$	132.06	Sigma Aldrich (UK)
Calcium chloride dihydrate	$CaCl_2{\cdot}2H_2O$	147.01	
Calcium hydroxide	$Ca(OH)_2$	74.09	
Calcium nitrate tetrahydrate	$Ca(NO_3)_2{\cdot}4H_2O$	236.15	
Distilled water	H_2O	18.02	-
Ethanol	C_2H_6O	46.07	Fisher Scientific (UK)
Methanol	CH_3OH	32.04	Alfa Aesar (UK)
Phosphoric acid (85 %)	H_3PO_4	98.00	Sigma Aldrich (UK)
Potassium hydroxide	KOH	56.11	
Potassium phosphate dibasic trihydrate	$K_2HPO_4{\cdot}3H_2O$	228.22	
Silver nitrate	$AgNO_3$	169.87	
Strontium hydroxide octahydrate	$Sr(OH)_2{\cdot}8H_2O$	265.76	
Strontium nitrate	$Sr(NO_3)_2$	211.63	
Triethyl phosphite	$(C_2H_5)_3PO_4$	166.16	
Zinc chloride	$ZnCl_2$	189.36	

Table 4.2. Consumables used in biological characterisation experiments.

Item	Supplier / Manufacturer
For antibacterial evaluation	
Brain heart infusion (BHI) agar	Oxoid (UK)
Brain heart infusion (BHI) broth	
For *in vitro* biocompatibility	
L-glutamine	Sigma Aldrich (UK)
Live/Dead staining kit	
Minimum Essentials Media Eagles (α-modification) (α-MEM)	
Non-essential amino acid	
Penicillin / streptomycin	
Phosphate buffered saline	
Trypsin EDTA	
Foetal calf serum (FCS)	Labtech International Ltd. (UK)
PrestoBlue® cell viability reagent	Fisher Scientific (UK)

4.2 Methods

4.2.1 Evaluation of Wet Precipitation and Sol-gel Methods for Nanoscale Hydroxyapatite Synthesis (Methods 1 - 4)

4.2.1.1 Wet Precipitation Synthesis of Nanoscale Hydroxyapatite

Method 1: Acid-base Reaction of Calcium Hydroxide and Phosphoric Acid Based on Prakash et al. [176]

Calcium hydroxide (1.85 g (25 mmol)) was suspended in 250 mL distilled water using a hotplate magnetic stirrer set to 400 rpm. Prior to the titration, the calcium hydroxide suspension was heated to 60 °C and stirred for 1 h. The hotplate magnetic stirrer was

then left on throughout the titration. A phosphoric acid solution was prepared by dissolving 1.73 g (15 mmol) of 85 wt. % phosphoric acid in 250 mL distilled water. The phosphoric acid solution was then added to the calcium solution at a rate of 3.5 $mL.min^{-1}$ with a peristaltic pump. The solution was stirred for a further 2 h after the phosphoric acid addition was completed and then left to cool to room temperature overnight. The precipitate which had settled overnight was washed three times by pouring off the clear liquid on top of the sediment and adding 500 mL distilled water. This procedure was followed by stirring at 400 rpm for 1 min and then the precipitate was left to settle over a 2 h period in between washes. Finally the suspension was dried at 60 °C in an oven, ground in an agate mortar and pestle and half of the sample was sintered. The furnace was programmed to heat at 10 $°C.min^{-1}$ to a temperature of 1000 °C which was maintained for 2 h before the sample cooled to room temperature overnight. The resulting nHA powders were then stored in a vacuum desiccator. See schematic diagram for overview of method (Figure 4.1).

Method 2: Reaction of Calcium Chloride and Potassium Phosphate Based on Fluidinova Patent Example 3 [207]

Calcium chloride dihydrate (3.68 g (25 mmol)) was dissolved in 250 mL distilled water and stirred at approximately 400 rpm. Meanwhile, 3.42 g (15 mmol) of potassium phosphate dibasic trihydrate was dissolved in 250 mL distilled water. A 1 M potassium hydroxide solution was made by dissolving 5.57 g potassium hydroxide in distilled water to make a volume of 100 mL. The pH of the calcium and the phosphorus solutions were adjusted to 11 and 12 respectively by adding the appropriate amount of 1 M potassium hydroxide solution. The phosphorus solution was then titrated into the stirred calcium solution at approximately 3 $mL.min^{-1}$ using a peristaltic pump. The solution was stirred for 1 h after the titration was completed and then left to settle overnight. The solution was washed, ground and sintered using the same process as described for method 1.

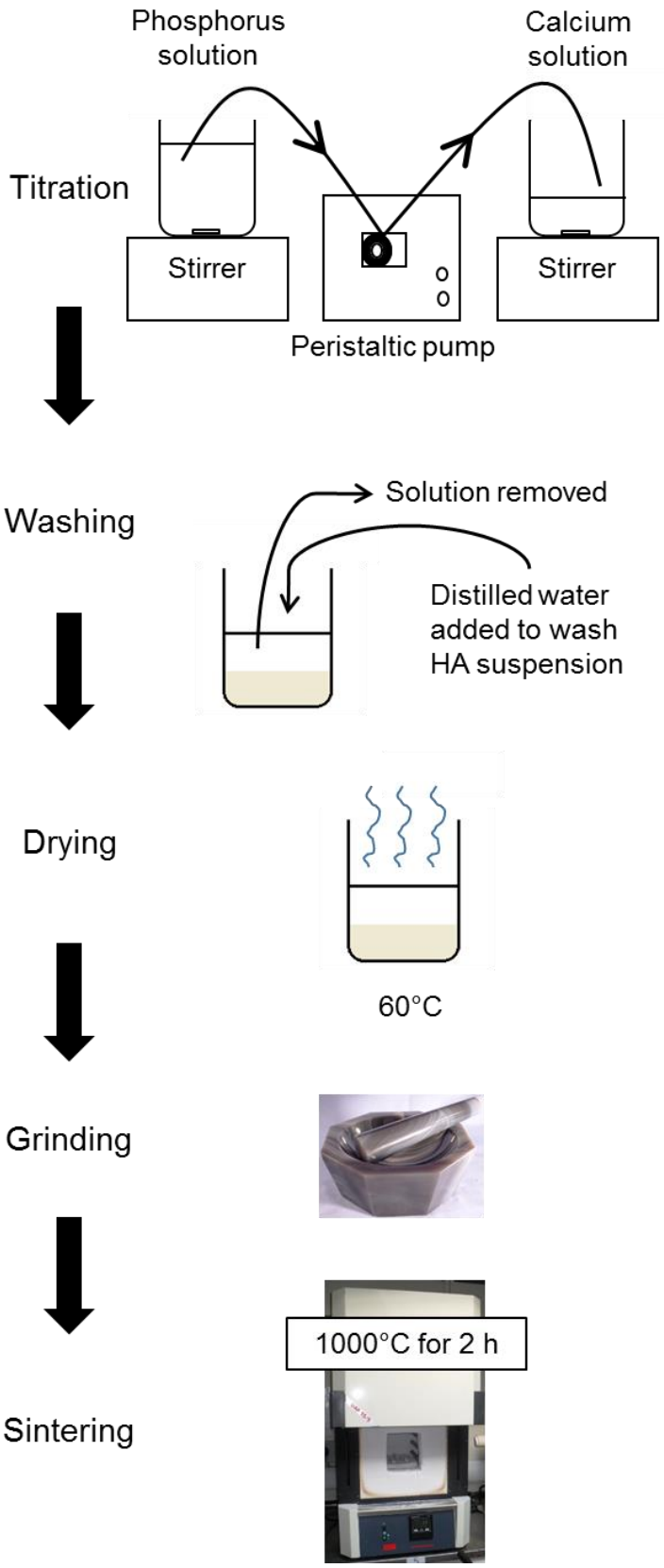

Figure 4.1. Schematic diagram showing production stages for method 1-3.

4.2.1.2 Sol-gel Synthesis of Nanoscale Hydroxyapatite

Method 3: Reaction of Calcium Nitrate and Ammonium Phosphate Based on Fluidinova Patent Example 2 [207]

Calcium nitrate tetrahydrate (5.91 g (25 mmol)) was dissolved in 250 mL distilled water and stirred at approximately 400 rpm. Similarly, 1.98 g (15 mmol) of ammonium phosphate dibasic was dissolved in 250 mL distilled water. The pH of the calcium and the phosphorus solutions were then adjusted to 11 and 12 respectively by adding 1 M potassium hydroxide solution. The phosphorus solution was titrated into the stirred calcium solution at approximately 3 $mL.min^{-1}$ using a peristaltic pump, followed by 1 h of stirring at 400 rpm after the titration was completed. The suspension was then left to settle overnight. The solution was washed, ground and sintered using the same process as described for method 1.

Method 4: Reaction of Calcium Nitrate and Triethyl Phosphite Based on Liu et al. [184]

Firstly, 22.48 g (95 mmol) of calcium nitrate tetrahydrate was dissolved in 40 mL ethanol using a magnetic stirrer. Triethyl phosphite (10 mL (58 mmol)) was dissolved in 5.6 mL distilled water and 10 mL ethanol. The solutions were covered and stirred for 30 min to allow the phosphite to hydrolyse. The pH of the calcium and phosphorus solutions were adjusted to pH 10 using 28 % ammonium hydroxide solution. The calcium nitrate solution was then titrated using a peristaltic pump at 3 $mL.min^{-1}$ into the hydrolysed phosphorus solution under vigorous stirring which was continued until 5 min after the titration. The solution was then aged at room temperature for at least 24 h. The suspension was dried overnight on a hotplate at 60 °C until a gel was obtained. The gel was further dried in an oven at 80 °C. The dried powder was crushed with a mortar and pestle before being sintered at 500, 550 or 600 °C for 2 h. The powders were then washed to remove any soluble impurities such as ammonium

hydroxide or ammonium nitrate. Firstly, each sample was divided between 4 tubes and 40 mL distilled water was added to each tube. The powder was shaken until it was in suspension and then sonicated for 5 min. The tubes were centrifuged at 3500 rpm for 10 min. The supernatant was poured off and 40 mL distilled water was added again. This sonication-centrifugation cycle was repeated 4 times in total. After the fifth rinse approximately 20 mL methanol was added to each tube and the powder suspension was poured into Petri dishes and left in a fume hood for the methanol to evaporate. After approximately 3 h, powders were placed in oven at 37 °C. Powders were then stored in a vacuum desiccator.

4.2.2 Development of Selected Synthesis Methods (Methods 1 and 3)

Methods 1 and 3 were selected for further development due to their advantages over methods 2 and 4, as discussed in section 6.1 *Evaluation of Wet Precipitation and Sol-gel Methods of Nanoscale Hydroxyapatite Synthesis (Methods 1 - 4*). Several parameters were altered in an attempt to obtain an optimal nHA product using the most simple and cost-effective method.

4.2.2.1 Method 1: Acid-base Reaction of Calcium Hydroxide and Phosphoric Acid

The synthesis parameters of method 1 (specified in section 4.2.1.1) were then altered in order to optimise the nHA obtained. The parameters investigated were:

1. Phosphoric acid solution addition rate (method 1-B)

   The rate of the phosphorus solution addition was increased by pouring the phosphoric acid solution into the calcium hydroxide suspension (addition rate of approximately 100 $mL.s^{-1}$). The results were compared to the previous results obtained when the phosphorus solution was titrated into the calcium suspension at 3.5 $mL.min^{-1}$ (method 1-A). This rapid addition rate was then used in all subsequent method alterations detailed below.

2. Temperature of reaction (method 1-C)

   The temperature of the synthesis was decreased to room temperature and compared with the previous results obtained when the reaction was carried out at 60 °C. Similarly, all subsequent method alterations listed below were also carried out at room temperature.

3. Concentration of reactants (method 1-D)

   The concentration of the reactants was then increased by suspending 3.70 g (50 mmol) of calcium hydroxide in 500 mL distilled water and dissolving 3.46 g (30 mmol) of phosphoric acid in 250 mL distilled water. For this experiment the stirring time of the HA suspension after phosphoric acid addition was decreased from 2 h to 1 h.

4.2.2.2 Method 3: Reaction of Calcium Nitrate and Ammonium Phosphate

The synthesis parameters of method 3 were then investigated and compared to the results obtained using the original method (as specified in section 4.2.1.2). The following parameters were investigated:

1. pH of the calcium and phosphorus solutions (methods 3-B, 3-C and 3-D)

   The pH of the calcium and phosphorus solutions was altered using potassium hydroxide solutions to investigate their effect on the nHA produced (Table 4.3). For all subsequent experiments, the pH of the calcium and phosphorus solutions were adjusted to 11 and 12 respectively.

2. Phosphorus solution addition rate (method 3-E)

   The rate of the phosphorus solution addition was increased by pouring the phosphorus solution into the calcium solution (addition rate of approximately 100 $mL.s^{-1}$). The results were compared to the previous results obtained when the phosphorus solution was titrated into the calcium solution at 3 $mL.min^{-1}$. This rapid addition rate was then used in all subsequent preparations.

3. Concentration of reactants (method 3-F)

   The concentration of the reactants was increased by suspending 11.81 g (50 mmol) of calcium nitrate tetrahydrate in 500 mL distilled water and dissolving 3.96 g (30 mmol) of ammonium phosphate dibasic in 250 mL distilled water.

Table 4.3. Calcium and phosphorus solution pH investigated for nHA synthesis using method 3.

Method reference	**pH of calcium solution**	**pH of phosphorus solution**	**Potassium hydroxide solution used for pH adjustment (M)**
3-A	11	12	1
3-B	11	11	1
3-C	10	10	0.5
3-D	9	9	0.1

4.2.3 Synthesis of Strontium-substituted Nanoscale Hydroxyapatite (Optimised Methods 1 and 3)

When the range of strontium substituted nHA were prepared it was considered which substitution levels would be most likely to promote optimal bone regeneration. Relatively low levels of strontium substitution (i.e. below 10 at. %) were likely to promote a beneficial biological response as suggested in the literature review. Furthermore substituted nHA with lower levels of strontium may be easier to progress through regulatory barriers due to their relative similarity to hydroxyapatite. However, the investigation of more unstable compositions (i.e. 50 at. % Sr) may have more clearly demonstrated how differences in solubility affect the properties of the biomaterial system. Furthermore, the 100 at. % strontium-substituted nHA was likely to have a similarly low level of solubility to the calcium nHA so provided a good comparison as to the effects that calcium or strontium alone may have not only on the material properties, but also on the precipitation of these materials.

4.2.3.1 Optimised Method 1

The substitution of strontium into the calcium hydroxyapatite crystal lattice (0, 2.5, 5, 10, 50 and 100 at. %) was then performed by adding the appropriate amount of strontium hydroxide octahydrate alongside the appropriate amount of calcium hydroxide to 500 mL distilled water (Table 4.4). The calcium / strontium hydroxide suspension was then stirred for 1 h at 400 rpm prior to the rapid addition of the 30 mmol (dissolved in 250 mL distilled water) phosphoric acid solution and then stirred for 1 h. The strontium-substituted nHA suspensions were washed at least three times with 500 mL distilled water. Additional washes were carried out until the conductivity was below 15 $\mu S.cm^{-1}$. However washing was discontinued if the conductivity did not decrease by 10 $\mu S.cm^{-1}$ with 4 subsequent washes. The nHA suspensions were then dried and sintered in the same method as described in method 1.

Table 4.4. Amount of reagents required for the optimised method 1 synthesis of the range of strontium-substituted nHA.

Amount of Sr (at. %)	Calcium hydroxide amount		Strontium hydroxide octahydrate amount	
	g	mmol	g	mmol
0	3.70	50	0	0
2.5	3.61	48.75	0.33	1.25
5	3.52	47.5	0.66	2.5
10	3.33	45	1.33	5
50	1.85	25	6.64	25
100	0	0	13.29	50

4.2.3.2. Optimised Method 3

The substitution of strontium into the calcium hydroxyapatite crystal lattice was then performed by dissolving the appropriate amount of strontium nitrate alongside the appropriate amount of calcium nitrate tetrahydrate in 500 mL distilled water (Table 4.5). Ammonium phosphate (3.96 g (30 mmol)) was dissolved in 250 mL distilled water. The pH of the calcium / strontium nitrate solution and the ammonium phosphate solution were then adjusted to 11 and 12 respectively using 1 M potassium hydroxide solution. The phosphorus solution was poured into the calcium / strontium solution which was then stirred for 1 h at 400 rpm and the nHA suspension was left to settle overnight. The strontium-substituted nHA suspensions were then washed at least three times with 500 mL distilled water. Additional washes were carried out until the conductivity was below 15 $\mu S.cm^{-1}$. However washing was discontinued if the conductivity did not decrease by 10 $\mu S.cm^{-1}$ with 4 subsequent washes. The nHA suspensions were then dried at 60 °C and ground in a mortar and pestle. Due to excessive thermal decomposition at 1000 °C, 100 at. % strontium nHA was sintered

at 500, 700 and 850 °C for 2 h in order to investigate its thermal stability. Powders were then stored in a vacuum desiccator.

Table 4.5. Amount of reagents required for the optimised method 3 synthesis of the range of strontium-substituted nHA.

Amount of Sr (at. %)	**Calcium nitrate amount**		**Strontium nitrate amount**	
	g	**mmol**	**g**	**mmol**
0	11.81	50	0	0
2.5	11.51	48.75	0.26	1.25
5	11.22	47.5	0.53	2.5
10	10.63	45	1.06	5
50	5.90	25	5.29	25
100	0	0	10.58	50

4.2.4 Synthesis of Silver-doped Nanoscale Hydroxyapatite (Altered Method 1)

To maintain a high level of biocompatibility the silver doping level was kept relatively low (i.e. below 10 at. %). However, it was also useful to investigate how the presence of silver may have affected the precipitation reaction when the level of silver doping was increased. Therefore higher levels, i.e. 10 at. % silver-doping, were also investigated in order to understand the sensitivity of the silver-doped nHA precipitation.

4.2.4.1 Altered Method 1

A range of silver-doped nHA powders (0, 2, 5 and 10 at. %) were prepared by adding the appropriate amount of silver nitrate to the 50 mmol calcium hydroxide suspension (Table 4.6). The silver / calcium suspension was stirred at 400 rpm and heated to 60 °C on a hotplate stirrer for 1 h followed by the rapid addition of the 30 mmol phosphoric acid solution. The suspension was stirred and heated for a further hour before being left to cool and settle overnight. The suspension was washed 3 times with 500 mL distilled water. The suspensions were dried and sintered using the same procedure as described in method 1.

Table 4.6. Amount of silver nitrate required for the method 1 synthesis of the range of silver-doped nHA.

Silver dopant level (at. %)	**Silver nitrate amount**	
	g	**mmol**
0	0	0
2	0.17	1
5	0.42	2.5
10	0.85	5

4.2.5 Characterisation Techniques used for the Evaluation and Development of Nanoscale Hydroxyapatite Synthesis Methods

4.2.5.1 X-ray Diffraction (XRD)

Nanoscale hydroxyapatite powder samples were prepared for XRD by depositing a small amount of PVA glue onto an acetate film. nHA powder was then mixed with the PVA glue, and was treated with a hot air gun until dried. Qualitative phase analysis was performed on powdered samples using X-ray diffraction (STOE IP, Phillips) with Cu $K_{\alpha 1}$ radiation, λ = 0.15406 nm. The diffractometer was operated at 40 kV and 35 mA, with a 2θ range of 10-60°. The resulting patterns were analysed using ICDD PDF 4+ software. See Table 4.7 for XRD database cards used to identify phases present in the samples. For the final optimised range of materials the full width at half maximum for the (002) diffraction peak before and after high temperature sintering was measured by hand in order to demonstrate the change in the crystallite size of the samples, in accordance with the Scherrer equation [208]:

$$\text{Crystallite size (nm)} = \frac{0.9\,\lambda}{\text{FWHM}\cos\theta}$$

Where: λ = 0.15406 nm (incident Cu $K_{\alpha 1}$ x-ray radiation), FWHM = full width half maximum of the (002) XRD diffraction peak, θ = Bragg angle.

Table 4.7. X-ray diffraction cards used to identify phases observed in nHA XRD patterns. Quality rating in descending order: * (high-quality), I (indexed), C (calculated).

Compound	Card	Quality rating
Hydroxyapatite ($Ca_{10}(PO_4)_6(OH)_2$)	9-432	I
β-tricalcium phosphate (β-$Ca_3(PO_4)_2$)	04-014-2292	*
Calcium oxide (CaO)	48-1467	C
Ammonium nitrate (NH_4NO_3)	8-452	I
Brushite ($CaHPO_4.2H_2O$)	72-1240	C
2.4 at. % strontium-substituted hydroxyapatite ($Ca_{9.76}Sr_{0.24}(PO_4)_6(OH)_2$)	04-016-2959	I
5 at. % strontium-substituted hydroxyapatite ($Ca_{9.5}Sr_{0.5}(PO_4)_6(OH)_2$)	04-016-3585	I
10 at. % strontium-substituted hydroxyapatite ($Ca_9Sr_1(PO_4)_6(OH)_2$)	60-0648	I
50 at. % strontium-substituted hydroxyapatite ($Ca_5Sr_5(PO_4)_6(OH)_2$)	34-479	I
100 at. % strontium-substituted hydroxyapatite ($Sr_{10}(PO_4)_6(OH)_2$)	33-1348	*
β-tristrontium phosphate (β-$Sr_3(PO_4)_2$)	24-1008	*
Silver phosphate (Ag_3PO_4)	6-505	*
Silver (Ag)	4-783	I

4.2.5.2 Transmission Electron Microscopy (TEM)

Powder samples were placed in ethanol and were prepared for transmission electron microscopy by ultrasonic dispersion for 15 min. The ethanol solution was then pipetted onto a 400 mesh copper grid coated with a holey thin carbon film (Agar

Scientific). Morphological evaluation of the HA particles was carried out using the FEI Tecnai G2 Spirit TEM at an accelerating voltage of 80 kV. TEM was mainly carried out on the unsintered samples due to the increase in particle size observed during sintering. Increased particle sizes were not desired due to the aim of nanoscale material production. However, for method 4, the sintered particles were imaged since a HA phase was not detected prior to sintering.

4.2.5.3 X-ray Fluorescence (XRF)

0.2 g of sample powder was used for XRF analysis for the initial evaluation of the nHA production methods 1 - 4 due to limited sample size. For subsequent XRF analyses 0.8 g of sample powder was used. The sample powder was combined with 8 g of lithium tetraborate (ICPH, Malzéville, France). This mixture was melted into a glass disc in a furnace at 1200 °C. The glass discs were analysed in an XRF spectrometer (PW2440 Philips) to determine the elemental composition of the samples.

4.2.5.4 Fourier Transform Infrared Spectroscopy in Attenuated Total Reflectance Mode (FTIR-ATR)

A small amount of powder was placed on top of the diamond in the attenuated total reflectance mode adapter and was compressed onto the surface of the diamond. 32 scans were performed from 4000 – 500 cm^{-1} with a resolution of 4 cm^{-1} (Thermo Scientific Nikolet Spectrometer, Unicam Ltd. England). 64 background scans were initially taken with an empty set up and this scan was then subtracted from all subsequent scans.

4.2.5.5 Radiopacity of Strontium-substituted Nanoscale Hydroxyapatite Powders

0.1 g of powder (0, 2.5, 5, 10, 50, 100 at. % Sr) was placed in a 96 well plate (n = 3). An X-ray image was taken with 0.25 s exposure time and developed in a dark room. Firstly the films were placed in developer solution for 4 min followed by a 2 min rinse

in running water. The films were then placed in a fixative solution for 4 min followed by a 30 min rinse in running water. The films were then left to dry overnight before being scanned and analysed using Quantity One software to obtain quantitative values for the radiopacity of the materials. The radiodensity of the materials was expressed in mm of aluminium.

4.2.6 Production of Nanoscale Hydroxyapatite Paste and Gel Materials

The different between a gel and a paste is not formally defined in the literature. For this project, a gel was defined as a translucent stable suspension which had a higher water content that the correspondingly opaque paste.

4.2.6.1 Strontium-substituted Nanoscale Hydroxyapatite Paste Production using Optimised Method 1

The final production protocol described in section 4.2.2.1 *Optimised Method 1: Synthesis of Strontium-substituted nHA* was used to synthesise the final range of strontium-substituted nHA paste materials (0, 2.5, 5, 10, 50 and 100 at. % Sr). Instead of the suspensions being dried completely in the oven, the drying was stopped when the paste had an approximate water content of 80 wt. %. This water content was selected due to the formation of a stable paste suspension which had good injectable properties when loaded into a syringe. The water content was confirmed by completely drying a small amount of the paste at 80 °C and calculating the mass loss % using the equation shown below. The pastes were then stored in sealed universal tubes, sterilised by gamma irradiation and were loaded into 1 mL syringes prior to use.

$$\text{Water content of paste (wt. \%)} = \frac{\text{Initial mass of paste} - \text{mass of dried paste}}{\text{Initial mass of paste}} \times 100$$

4.2.6.2 Strontium-substituted Nanoscale Hydroxyapatite Gel Production using Optimised Method 3

Similarly the final production protocol described in section 4.2.2.2 *Optimised Method 3: Synthesis of Strontium-substituted nHA* was used to synthesise the final range of strontium-substituted nHA gel materials (0, 2.5, 5, 10, 50 and 100 at. % Sr). The gels were dried until a water content of approximately 90 wt. % was obtained. The sol-gel optimised method 3 allowed for the formation of a stable gel-like suspension with a higher water content (90 wt. %) than any stable suspension which could be produced using optimised method 1. This allowed the comparison of injectable nHA materials with different water contents. The water content was confirmed and the gels were stored in the same manner as described above for the paste materials.

4.2.6.3 Silver-doped Nanoscale Hydroxyapatite Paste Production using Method 1

Silver-doped nHA pastes (0, 2, 5 and 10 at. %) were prepared using the protocol described in section 4.2.2.1 *Method 1: Synthesis of Silver-doped nHA.* These materials were dried at 60 °C until a paste of 85 wt. % water content was obtained. The water content was confirmed and the pastes were stored in the same manner as described in section 4.2.6.1 Strontium-substituted Nanoscale Hydroxyapatite Paste Production using Optimised Method 1.

4.2.7 Characterisation of Nanoscale Hydroxyapatite Paste and Gel Materials

4.2.7.1 In Vitro Evaluation of Strontium-substituted Nanoscale Hydroxyapatite Paste and Gel Produced using Optimised Methods 1 and 3

The *in vitro* biocompatibility of the strontium-substituted nHA paste and gels (0, 2.5, 5, 10, 50 and 100 at. % Sr) produced using optimised method 1 and method 3 respectively were investigated; the indirect and direct biocompatibility were assessed using light microscopy (Eclipse TS100, Nikon), PrestoBlue® assays and Live/Dead fluorescence imaging. Prior to use, all paste and gel materials were sterilised using 25kGy γ-irradiation from a cobalt 60 source (Swann-Morton Ltd., Sheffield, UK). The biocompatibility protocols were provided by the IMCOSS project [209] and were based on the ISO 10993-5 biocompatibility testing standard [210].

The following media was prepared and used for cell culture (v/v %): 87 % α-MEM, 10 % FCS, 1 % penicillin-streptomycin, 1 % L-glutamine and 1 % non-essential amino acids. MG63 human osteosarcoma cell line was grown in T75 flasks. When 70-80 % confluent, the flasks were washed twice with 10 mL phosphate buffered saline (PBS) used each time. 2 mL trypsin-EDTA was added and the flasks were incubated for 5 min at 37 °C, 5 % CO_2. The detachment of the cells from the flasks was monitored using light microscopy. When the cells were detached, 4 mL FCS was added to neutralise the trypsin. The cell suspension was placed in a tube and centrifuged for 5 min at 1000 rpm. The supernatant was carefully removed and the cell pellet was resuspended in an appropriate amount of media for cell counting using a haemocytometer. The cells were then seeded for experiments or seeded for further growth in T75 flasks.

Firstly, indirect cellular toxicity was investigated by incubating 0.5 mL of Sr nHA paste / gel material (0, 2.5, 5, 10, 50 and 100 at. % Sr) with 5 mL media for 24 h at 37 °C to produce pre-conditioned media. Preconditioned media for a commercially available

nHA paste (ReproBone *novo*™, Ceramisys Ltd.) was prepared following the same procedure, and 5 mL of media was also incubated without any material present for a non-material control. At the same time, 50,000 MG-63 human osteoblast-like cells in 1 mL media were seeded in each well of a 24 well plate and incubated for 24 h (n = 3). After 24 h incubation, the pre-conditioned media was centrifuged at 1000 rpm for 5 min. The media on the cells was replaced by 1 mL preconditioned media and the cells were incubated again for 24 h. Light microscopy images were then obtained to assess the growth of the cells in the pre-conditioned medium. A PrestoBlue® assay was carried out using a 10 v/v % dilution of the PrestoBlue® in complete media; 1 mL of the PrestoBlue® media solution was added to each well. After 1 h, 200 µL was taken out of each well and placed in a 96 well plate. The fluorescence of the samples was read on a fluorescent plate reader (Infinite M200, Tecan) with 535 nm excitation and 590 nm emission wavelengths used. After the PrestoBlue® assay the wells were washed twice with 1 mL PBS and 400 µL of Live/Dead stain, prepared according to the manufacturer's instructions, was added to each well and incubated for 15 min at 37 °C, 5 % CO_2. The wells were then washed with PBS before being imaged using a fluorescence microscope (Axiovert 200M, Zeiss). The experiment was repeated three times to obtain n = 9.

For direct toxicity assays 100 µL of paste or gel (0, 2.5, 5, 10, 50, and 100 at. % Sr) was placed into a 24 well plate (n = 3). Direct cellular viability was also tested for ReproBone *novo*™ (Ceramisys, Ltd.) using the same protocol alongside the paste or gel samples. A 1 mL cell suspension containing 50,000 MG63 cells was then added to each well alongside control wells containing no material. Paste / gel wells with no cells present were also prepared to act as a material control. The 24 well plates were then incubated for 48 h at 37 °C, 5 % CO_2. After 48 h, light microscopy was used to image cells growing alongside the paste / gel materials. Cellular viability was then tested using a PrestoBlue® assay. To prevent the disruption and loss of paste or gel

from the wells, 100 µL PrestoBlue® reagent was directly added to the wells, after 100 µL media had been removed. After 1 h, 200 µL of the solution was transferred to a 96 well plate for fluorescent analysis as detailed above. After the PrestoBlue® assay the wells were washed twice with 1 mL PBS and 400 µL of Live/Dead stain was added to each well and incubated for 15 min at 37 °C, 5 % CO_2. The wells were then washed with PBS before being imaged using fluorescent microscopy as described above. Unfortunately the dead cells could not be imaged due to red background fluorescence from residual PrestoBlue® media solution which had absorbed into the pastes and gels. The experiment was repeated three times to obtain n = 9.

All PrestoBlue® assays results were expressed as the mean of the three triplicate repeats (n = 9). Statistical analyses were tested for significance using a one way ANOVA test with Tukey's multiple comparisons test applied using GraphPad Prism 6 software.

4.2.7.2. Antibacterial Evaluation of Silver-doped nHA Paste Produced Using Method 1

Preparation of Brain-heart Infusion (BHI) Agar and Broth

BHI agar plates were prepared by dissolving 4.7 g BHI agar powder in 100 mL of distilled water. The solution was autoclaved and then placed in a water bath at 55 °C to cool. The liquid agar was then poured into plastic Petri dishes and left to set, before being stored at 4 °C. BHI broth was prepared by dissolving 3.7 g BHI broth powder in 100 mL distilled water and sterilised in an autoclave. *S. aureus* (Oxford strain) and *P. aeruginosa* (clinical isolate SOM-1) were cultured on BHI agar plates at 37 °C, 5 % CO_2.

Agar Diffusion Assay for Silver-doped nHA Pastes

10 mL of BHI broth was inoculated with a single colony of *S. aureus* or *P. aeruginosa* and agitated in a rotary incubator at 37 °C, 5 % CO_2 overnight. 400 µL of bacterial

suspension with an optical density (O.D) of 1.5 at 600 nm were prepared. The bacterial suspensions were then spread over the surface of the agar plate using a spreader. 0.15 mL of each of the silver-doped nHA paste materials (0, 2, 5 and 10 at. % Ag) were then placed on top of the agar plates before incubation overnight. The plates were imaged and 3 agar plugs were removed using a plastic Pasteur pipette from the agar directly surrounding each paste material. The plugs were placed in a 10 mL universal tube with 4 mL distilled water and 40 µL of ultra-pure nitric acid before being heated at 70 °C for 2 h to dissolve the agar plugs. The samples were then analysed for silver content using inductively coupled plasma-mass spectrometry (ICP-MS, Elan DRCII, Perkin Elmer).

Suspension Culture for Silver-doped nHA Pastes

10 mL of BHI broth was inoculated with a single colony of *S. aureus* or *P. aeruginosa* and agitated in a rotary incubator at 37 °C, 5 % CO_2 overnight. Bacterial suspensions with an optical density (O.D.) of 0.05 at 600 nm were prepared. Paste suspensions for each of the silver-doped nHA paste materials (0, 2, 5 and 10 at. % Ag) were then prepared by placing 0.2 g paste in an Eppendorf tube with 1 mL BHI broth and agitating it using a vortex mixer. 50 µL of BHI broth was placed in all wells of a 96 well plate. A serial dilution was then performed by adding 50 µL of paste suspension to the first well, mixing and transferring 50 µL of suspension to the next well and so on. This process was repeated 11 times, with four repeats for each material. Three of the rows were then inoculated with 50 µL bacterial suspension whilst 50 µL BHI broth was added to one row to act as a material control. BHI broth acted as a negative control and BHI broth inoculated with 50 µL bacterial suspension acted as a positive control. The plates were incubated overnight after which the optical density of the wells at 600 nm was recorded using a plate reader (POLARstar Galaxy, BMG Labtech). The optical density of the material controls were subtracted from the suspension cultures. The minimum inhibition concentration (MIC) for the pastes was

calculated as the concentration of paste at which the optical density of the culture had reduced by 50 %.

5. Results

5.1 Evaluation of Wet Precipitation and Sol-gel Methods for Nanoscale Hydroxyapatite Synthesis (Methods 1 - 4)

5.1.1 Wet Precipitation Synthesis of Nanoscale Hydroxyapatite

5.1.1.1 Method 1: Acid-base Reaction of Calcium Hydroxide and Phosphoric Acid

XRD patterns showed that HA was the only detectable phase precipitated from method 1 (Figure 5.1). However, after sintering treatment at 1000 °C for 2 h a low intensity calcium oxide peak was detected alongside a main phase of HA. TEM micrographs of the HA produced by method 1 (Figure 5.2) displayed that needle-like nHA particles with a high aspect ratio (length of particle / width of particle) of approximately 6.5 were produced during the reaction. The nHA particles produced were typically 130 nm long and 20 nm wide.

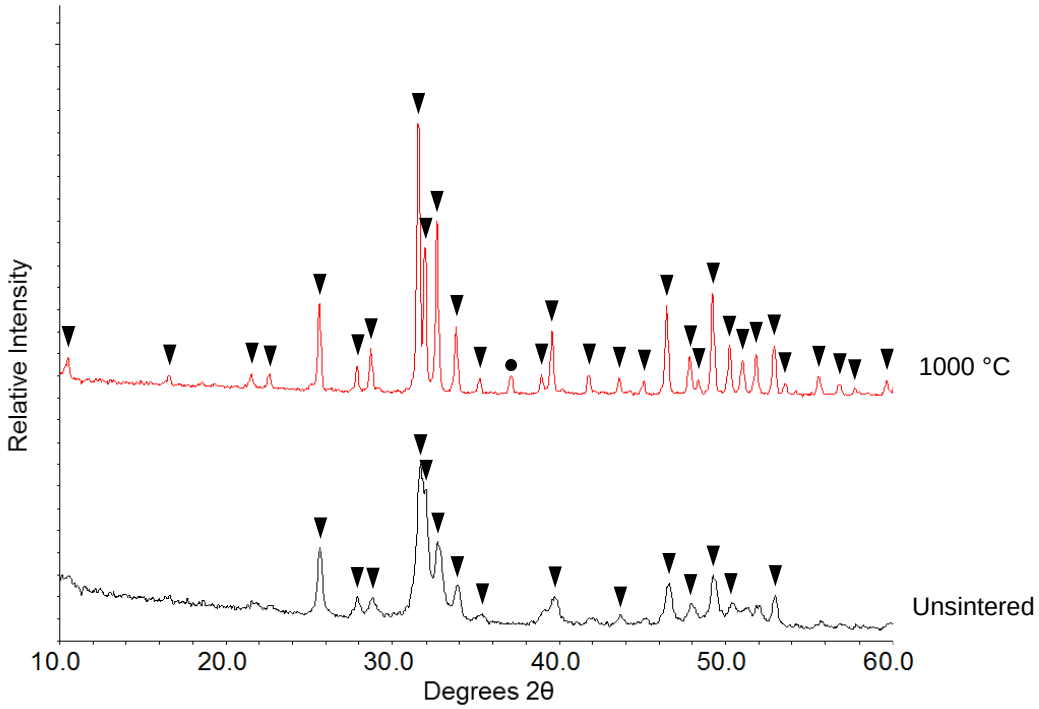

Figure 5.1. XRD patterns of nHA powder prepared by method 1. The unsintered sample (black) and sample sintered at 1000 °C for 2 h (red) are displayed. Peak labels: ▼ hydroxyapatite; ● calcium oxide.

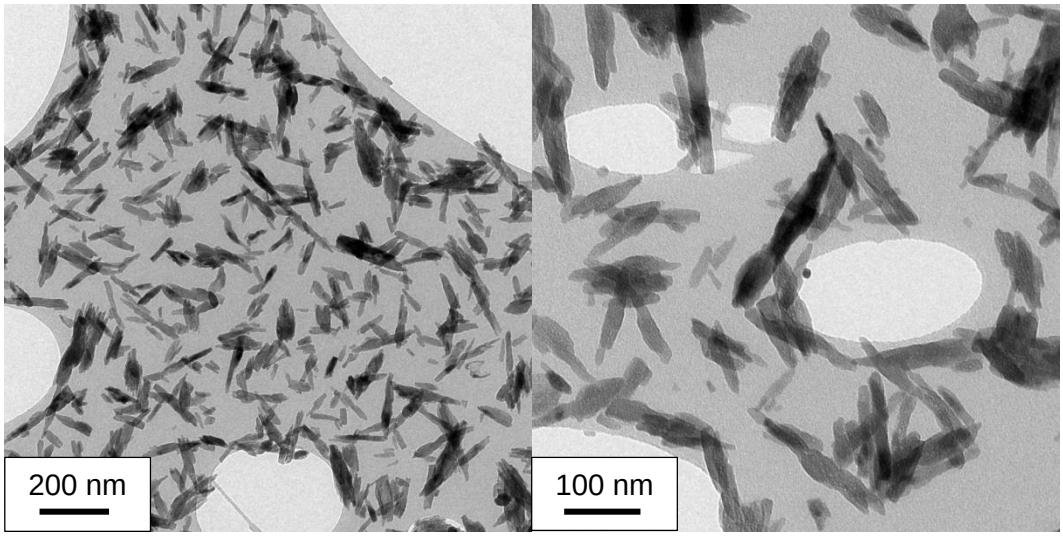

Figure 5.2. TEM micrographs of unsintered nHA powder prepared by method 1.

5.1.1.2. Method 2: Reaction of Calcium Chloride and Potassium Phosphate

XRD patterns displayed that the main phase precipitated using method 2 was HA (Figure 5.3). After heat treatment the product was found to completely decompose into β-tricalcium phosphate (β-TCP). Needle shaped nHA particles were also produced during this reaction (Figure 5.4). However, these particles have a noticeably smaller aspect ratio than the particles produced using the method 1. Average particle sizes were 110 nm by 30 nm providing an aspect ratio of 3.7.

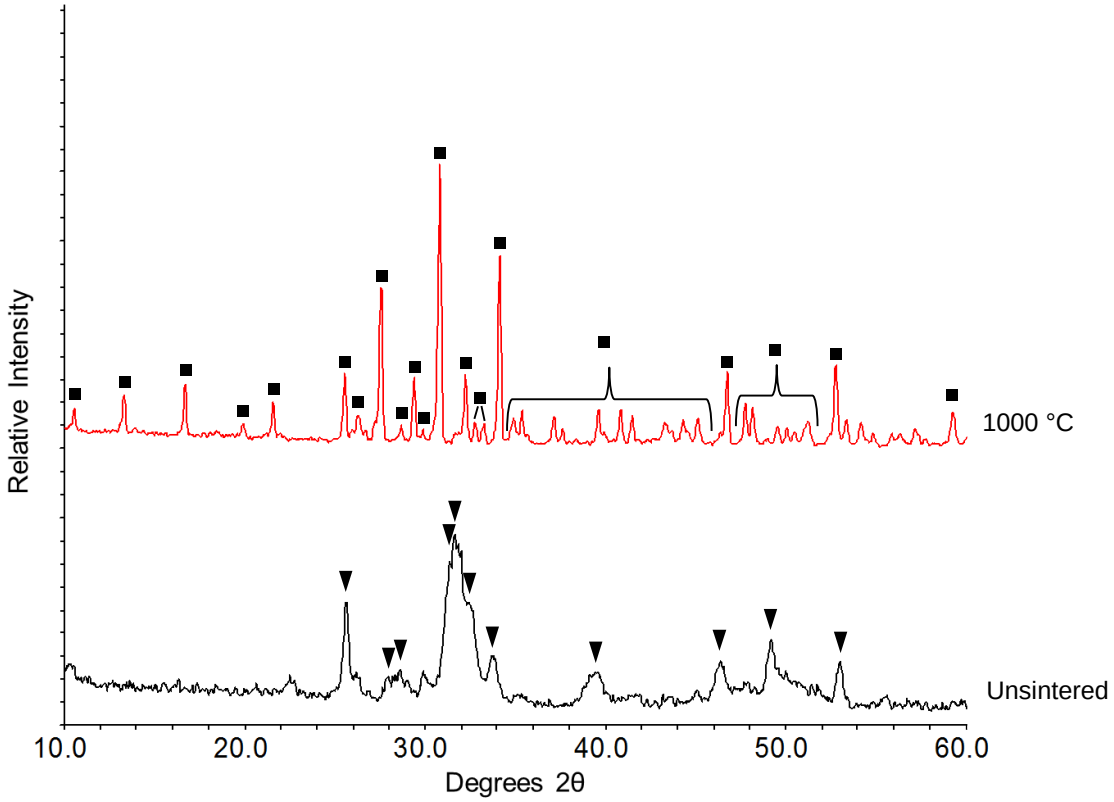

Figure 5.3. XRD patterns of nHA powder prepared using method 2. The unsintered sample (black) and sample sintered at 1000 °C for 2 h (red) are displayed. Peak labels: ▼ hydroxyapatite; ■ β-tricalcium phosphate.

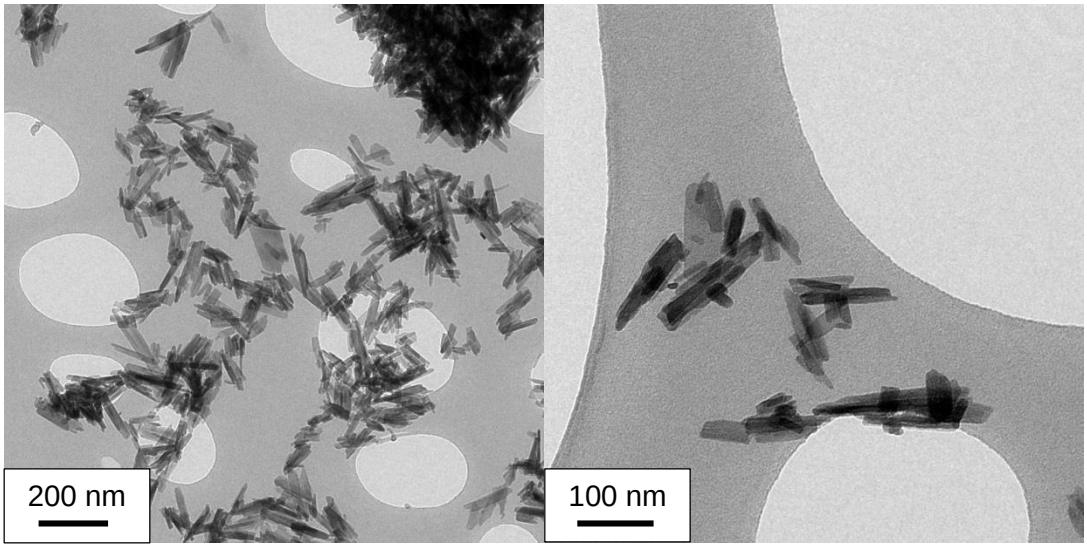

Figure 5.4. TEM micrographs of unsintered nHA powder prepared using method 2.

5.1.2 Sol-gel Synthesis of Nanoscale Hydroxyapatite

5.1.2.1 Method 3: Reaction of Calcium Nitrate and Ammonium Phosphate

HA was successfully produced using method 3 as shown by XRD patterns (Figure 5.5). However, after sintering a minor phase of β-TCP was detected alongside the main HA phase. nHA particles produced using method 3 were approximately 30 nm by 20 nm and were therefore much smaller and had a lower aspect ratio (1.5) than the particles produced using the wet precipitation methods 1 and 2 (Figure 5.6).

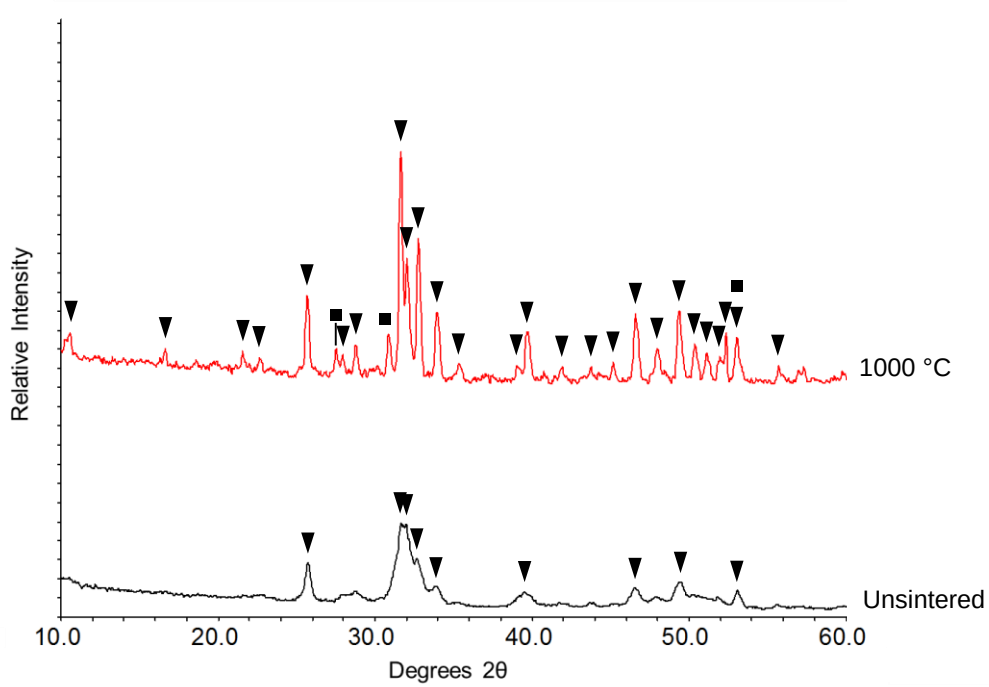

Figure 5.5. XRD patterns of nHA powder prepared using method 3. The unsintered sample (black) and sample sintered at 1000 °C for 2 h (red) are displayed. Peak labels: ▼ hydroxyapatite; ■ β-tricalcium phosphate.

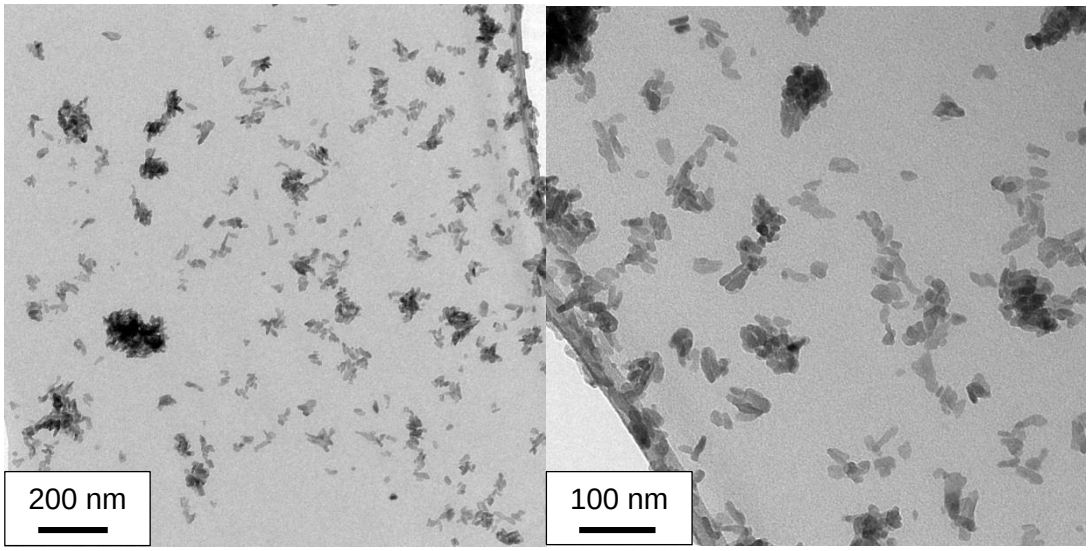

Figure 5.6. TEM micrographs of unsintered nHA powder prepared using method 3.

5.1.2.2 Method 4: Reaction of Calcium Nitrate and Triethyl Phosphite

Prior to sintering, no phases were detected by XRD for the method 4 product displaying its amorphous nature (Figure 5.7). After sintering the product at 500, 550 and 600 °C a main HA phase was detected (Figure 5.8). Ammonium nitrate was detected in the sintered samples particularly when sintered at 500 and 550 °C. When the product was sintered at 600 °C, β-TCP was detected alongside a decreased amount of ammonium nitrate. The nHA particles produced using this method were noticeably larger and more rounded than the particles produced using methods 1-3. Little variation was observed between the particle sintered at different temperatures; typical particle morphology shown in Figure 5.9. The particles were approximately 100 nm by 80 nm and had an average aspect ratio of 1.25.

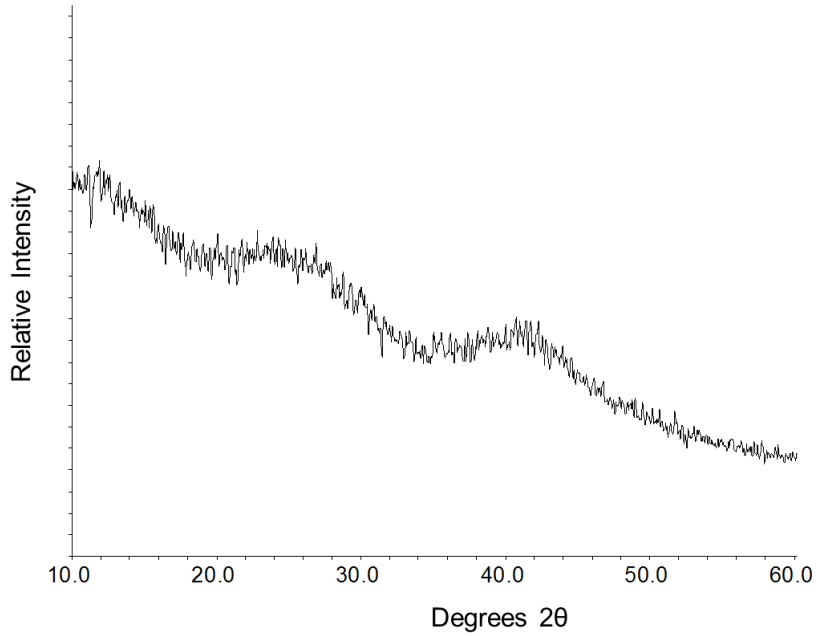

Figure 5.7. XRD pattern of unsintered powder prepared using method 4 at pH 10. No identifiable crystalline phases were detected.

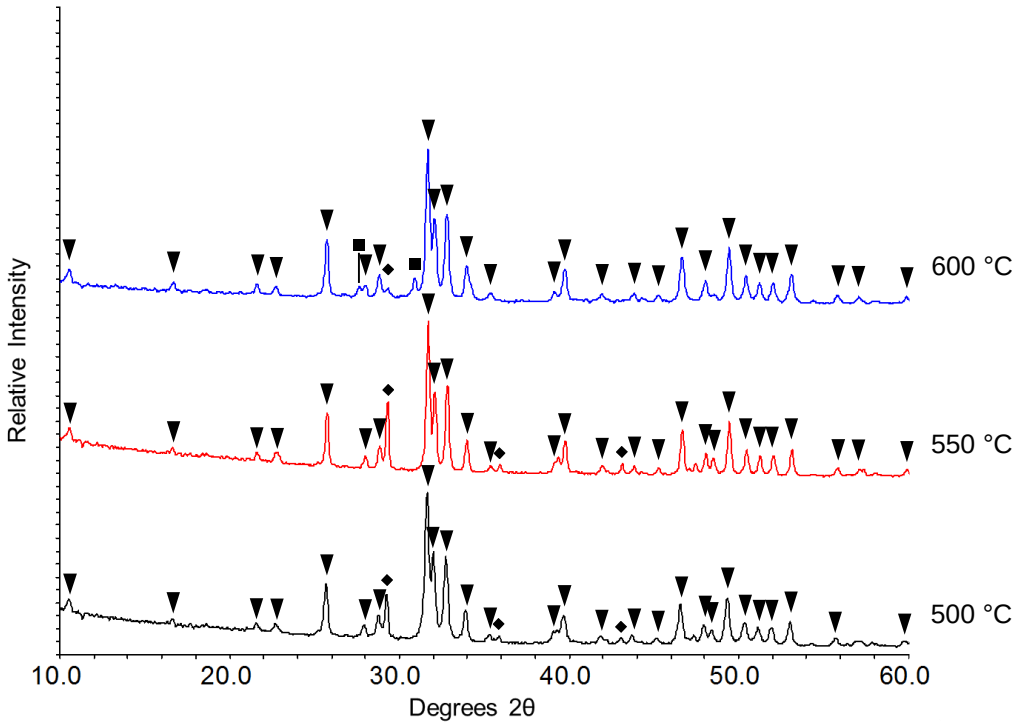

Figure 5.8. XRD patterns of nHA powder prepared using method 4 at pH 10. The samples sintered at 500 (black), 550 (red) and 600°C for 2 h (blue) are displayed. Peak labels: ▼ hydroxyapatite; ■ β-tricalcium phosphate; ◆ ammonium nitrate.

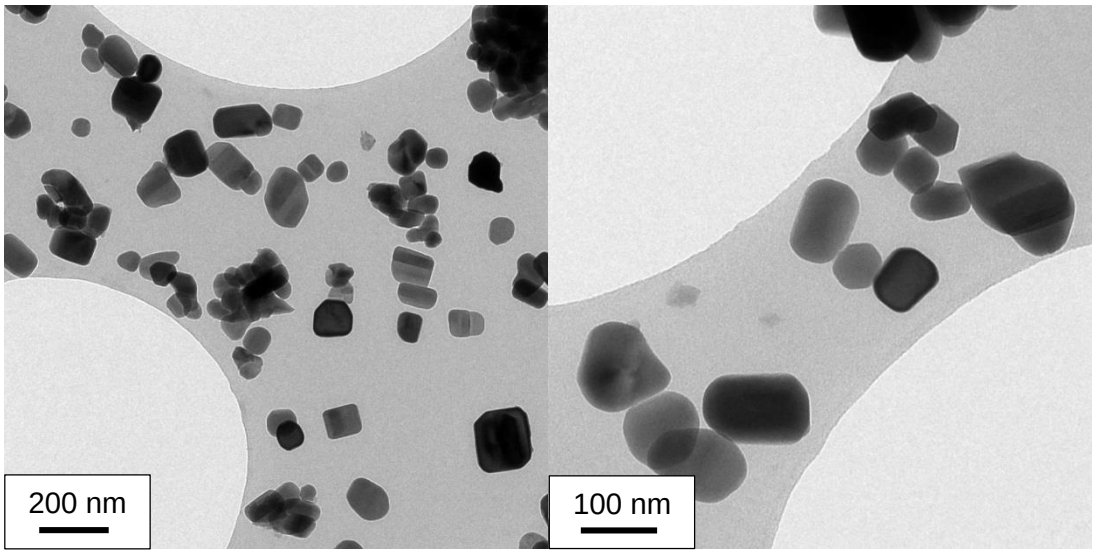

Figure 5.9. TEM micrographs of nHA powder sintered at 550 °C prepared using method 4 at pH 10.

5.1.3 X-ray Fluorescence Results for the Evaluation of Production Methods (Methods 1 - 4)

XRF results showed that the HA produced using the different methods tended to vary from the stoichiometric calcium to phosphorus ratio of 1.67 (Table 5.1). The method 1 product had excess calcium present (Ca:P 1.70) whereas the other wet precipitation method (method 2) produced HA which was noticeably calcium-deficient (Ca:P 1.38). The large variations in the calcium to phosphorus ratios of the materials produced using method 4 raised concerns regarding the chemical homogeneity of these samples. The samples produced using the method 4 tended towards excess calcium rather than calcium deficiency. For example, the samples synthesised at pH 10 had Ca:P ratios of 1.75, 1.93 and 1.60 when sintered at 500, 550 and 600 °C respectively.

Table 5.1. XRF results for nHA production methods 1 – 4.

Production method		**pH**		**Sintering temperature (°C)**	**Calcium: phosphorus molar ratio**
		Ca sol^{n}	**P sol^{n}**		
Wet precipitation	Method 1	11.4	1.8	1000	1.70
	Method 2	11	12	1000	1.38
Sol-gel	Method 3	11	12	1000	1.51
	Method 4	10	10	500	1.75
				550	1.93
				600	1.60

5.2 Development of Selected Synthesis Methods (Methods 1 and 3)

5.2.1 Method 1: Acid-base Reaction of Calcium Hydroxide and Phosphoric Acid

The development of method 1 involved changing the parameters in order to determine their effect on the nHA produced. Firstly, it was observed that by increasing the phosphoric acid solution addition rate into the calcium hydroxide suspension, no calcium oxide was observed in the sintered HA product as seen in method 1-A; instead a minor phase of β-TCP was detected (method 1-B) (Table 5.2). There was also a change in the particle morphology when the phosphoric acid addition rate was increased, i.e. rapid mixing (method 1-B), with the particle aspect ratio decreasing from approximately 6.5 to 1.3. When the temperature was decreased with rapid mixing (method 1-C) there was a noticeable reduction in the conductivity of the nHA suspension prior to washing (Table 5.3), which suggested that less residual calcium hydroxide was present. No other phase or particle morphology changes were observed for the other incremental method alterations including the increase in reactant concentration (method 1-D) (Figure 5.10).

Table 5.2. Summary of XRD analysis on method 1 development.

Method reference	Method details				Phases detected in XRD pattern of unsintered sample	Phases detected in XRD pattern of sample sintered at 1000 °C for 2 h
	Addition rate of phosphoric acid solution	Reaction temperature (°C)	Reactant concentrations			
			Calcium hydroxide (mmol) / suspended in volume of distilled water (mL)	Phosphoric acid (mmol) / dissolved in volume of distilled water (mL)		
1-A	3.5 $mL.min^{-1}$	60	25 / 250	15 / 250	HA	HA + CaO
1-B	100 $mL.s^{-1}$	60	25 / 250	15 / 250	HA	HA + βTCP
1-C	100 $mL.s^{-1}$	25	25 / 250	15 / 250	HA	HA + βTCP
1-D	100 $mL.s^{-1}$	25	50 / 500	30 / 250	HA	HA + βTCP

Table 5.3. Effect of temperature on conductivity of suspensions prepared using phosphoric acid addition rate of 100 mL.s^{-1} with reactant concentrations of 25 / 250 and 15 / 250 (mmol.mL^{-1}) for the calcium hydroxide suspension and phosphoric acid solution respectively.

Sample reference	**Reaction temperature (°C)**	**Conductivity of nHA suspension prior to washing (µS.cm^{-1})**
1-B	60	161
1-C	25	21

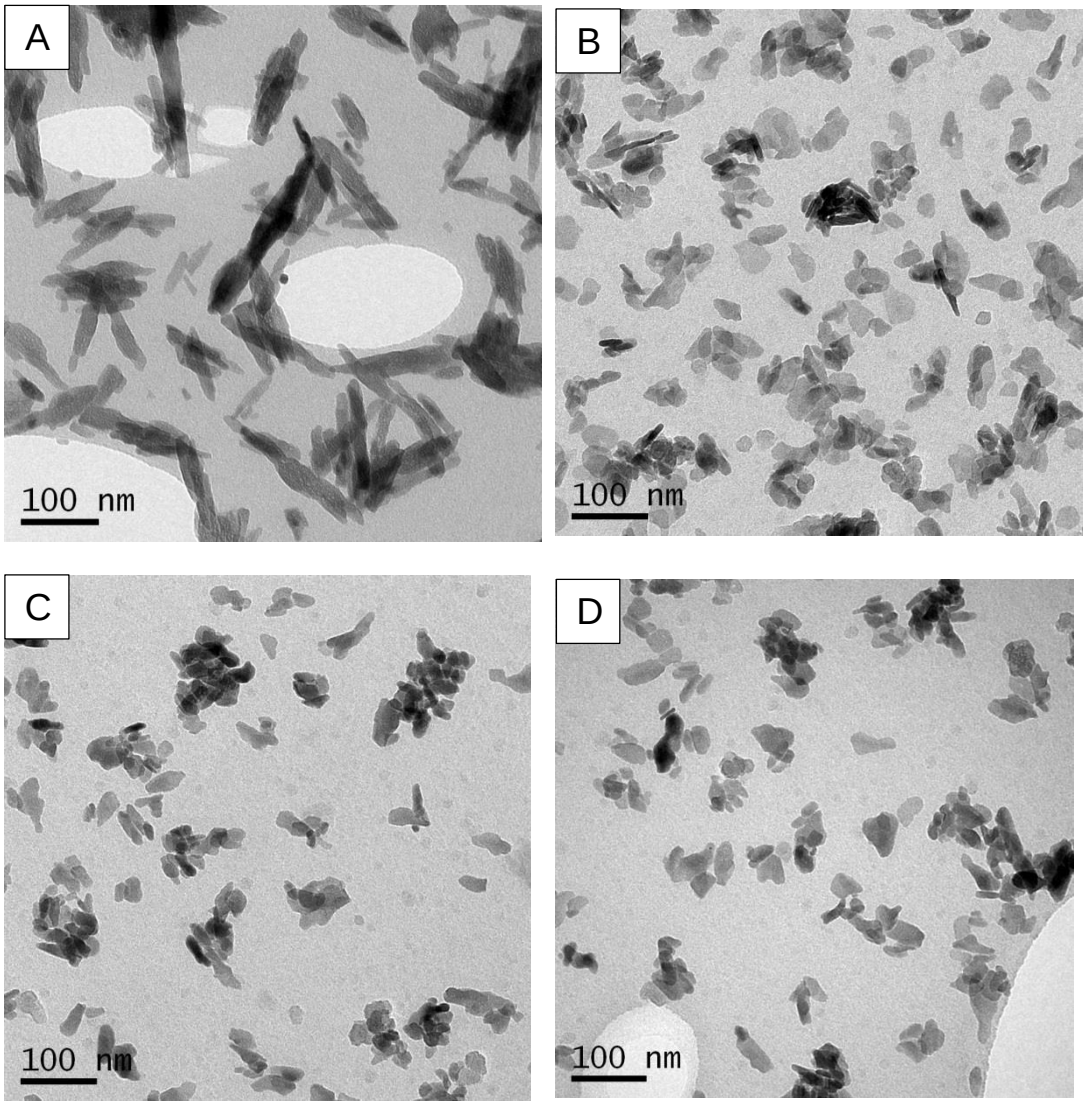

Figure 5.10. TEM micrographs showing particle morphology when incremental changes were made using method 1: (A) original method (1-A); (B) Phosphoric acid solution addition rate increased (1-B); (C) Reaction performed at room temperature (1-C); (D) Increased concentration of reaction (1-D).

5.2.2 Method 3: Reaction of Calcium Nitrate and Ammonium Phosphate

The development of method 3 showed that a high pH was critical to produce a pure HA precipitated product with high thermal stability. The level of thermal stability was assessed by the relative intensity of the β-TCP peaks when compared to the HA peaks, which indicated the proportion of the HA which had decomposed into β-TCP. Indeed, the amount of β-TCP detected in the sintered product increased as the pH

was decreased. When the calcium and phosphorus solution pH was adjusted to 9 (method 3-D), the main phase of the sintered product was β-TCP (Table 5.4). The increase in phosphorus solution addition rate and concentration of reactants did not have an effect on the phases produced (method 3-E compared to method 3-A). The particle size increased slightly for the increased phosphorous solution addition rate (Figure 5.11). Specifically the average particle size was 30 x 20 nm for the original method 3-A and 40 x 20 nm for method 3-E. The particle size further increased to 50 x 30 nm with an increase in the reactant concentration (method 3-F).

Table 5.4. Summary of XRD analysis on method 3 development.

Method reference	Method details					Phases detected in XRD pattern of unsintered sample	Phases detected in XRD pattern of sample sintered at 1000 °C for 2 h
	pH		Phosphorus solution addition rate	Reactant concentrations			
	Calcium solution	Phosphorus solution		Calcium nitrate (mmol) / dissolved in volume of distilled water (mL)	Ammonium phosphate (mmol) / dissolved in volume of distilled water (mL)		
3-A	11	12	3 mL.min^{-1}	25 / 250	15 / 250	HA	HA + β-TCP
3-B	11	11	3 mL.min^{-1}	25 / 250	15 / 250	HA	HA + β-TCP
3-C	10	10	3 mL.min^{-1}	25 / 250	15 / 250	HA	HA + β-TCP
3-D	9	9	3 mL.min^{-1}	25 / 250	15 / 250	HA + brushite	β-TCP + HA
3-E	11	12	100 mL.s^{-1}	25 / 250	15 / 250	HA	HA + β-TCP
3-F	11	12	100 mL.s^{-1}	50 / 500	30 / 250	HA	HA + β-TCP

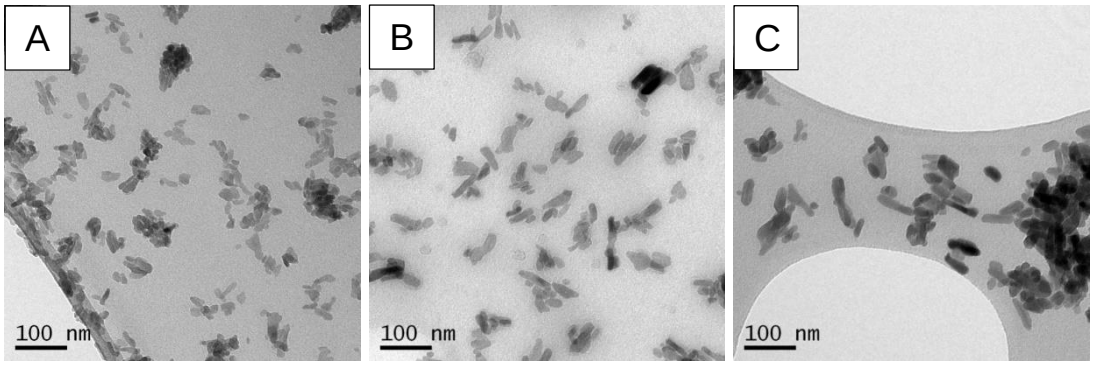

Figure 5.11. TEM micrographs displaying particle morphology when incremental changes were made using method 3: (A) Original method (3-A); (B) Phosphorus solution addition rate increased (3-E); (C) Increased concentration of reactants (3-F).

5.3 Synthesis of Strontium-substituted Nanoscale Hydroxyapatite (Optimised Methods 1 and 3)

5.3.1 Optimised Method 1: Synthesis of Strontium-substituted Nanoscale Hydroxyapatite

The addition of strontium into optimised method 1 caused a peak shift to lower degrees 2θ in the XRD patterns for the apatite phase produced when greater amounts of strontium were used in the method (Figure 5.12 and Figure 5.13). This peak shift to lower degrees 2θ was also observed for the minor phase of strontium-substituted β-tricalcium phosphate which was present only after high temperature treatment.

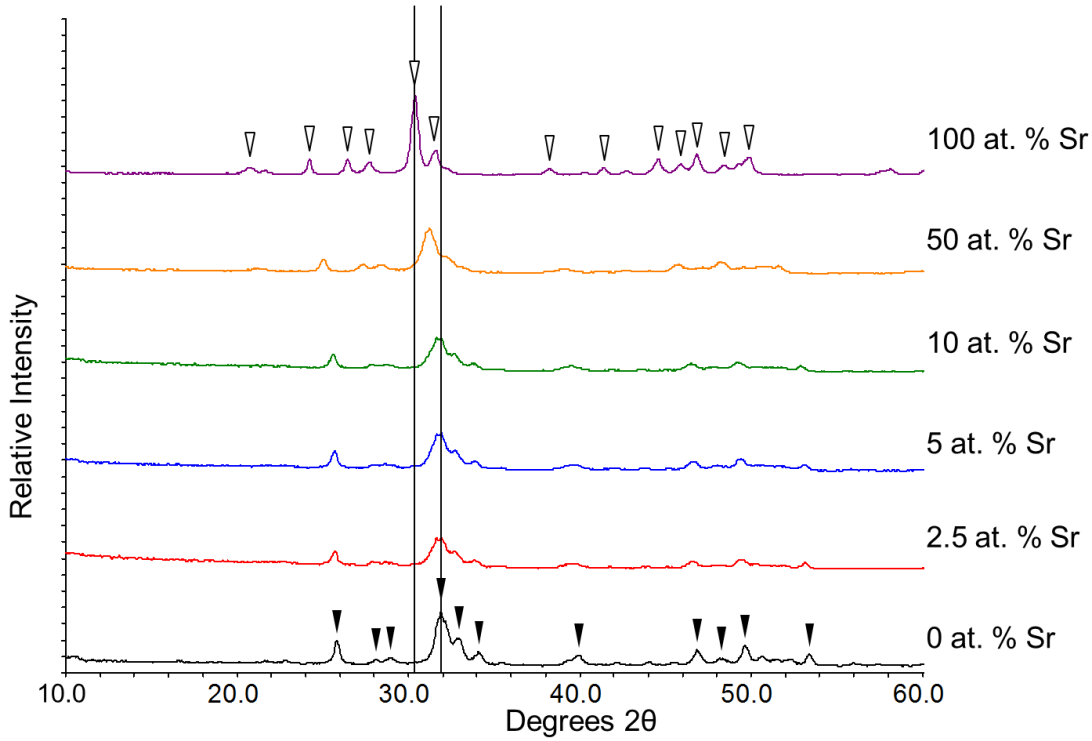

Figure 5.12. XRD patterns of unsintered strontium-substituted HA powders (0, 2.5, 5, 10, 50 and 100 at. % Sr) produced using optimised method 1. Peak labels: ▼ hydroxyapatite; ▽ strontium hydroxyapatite.

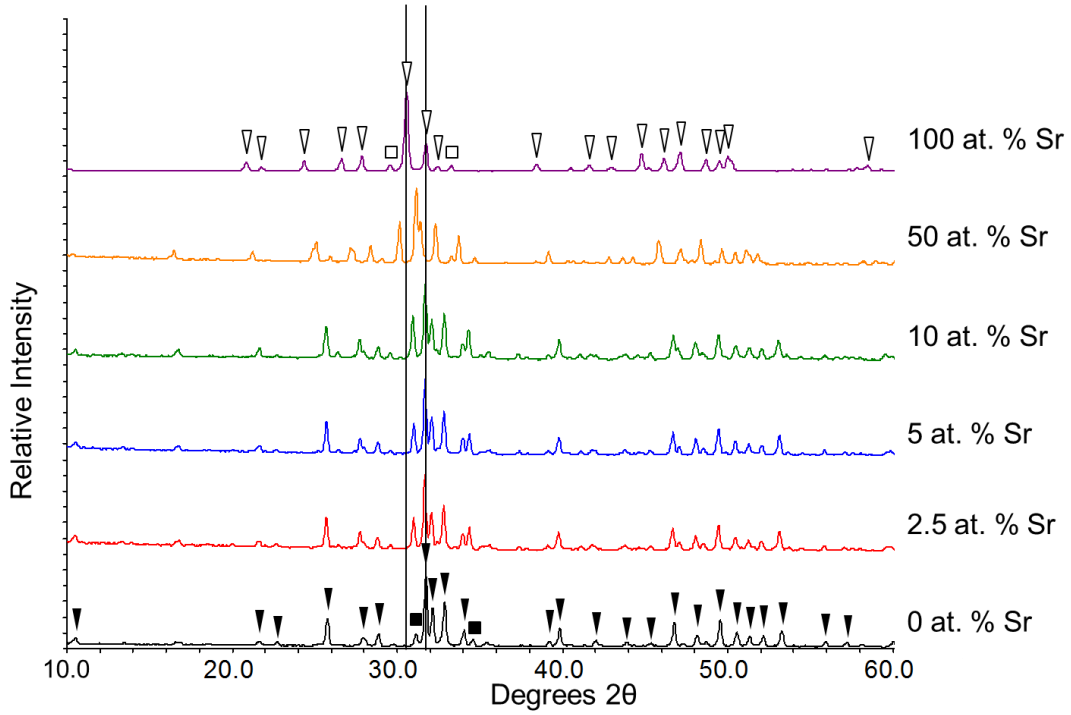

Figure 5.13. XRD patterns of strontium-substituted HA powders (0, 2.5, 5, 10, 50 and 100 at. % Sr) produced using optimised method 1 sintered at 1000 °C for 2 h. Peak labels: ▼ hydroxyapatite; ■ β-tricalcium phosphate; ▽ strontium hydroxyapatite; □ β-tristrontium phosphate.

The full width half maximum of the (002) XRD peak for the sintered strontium-substituted nHA samples was consistently lower than for the corresponding unsintered samples, except for the sample with 100 % strontium (Table 5.5). This demonstrated the sharpening of the diffraction peaks for the majority of the sintered samples. The reduction of the FWHM corresponds with an increase in crystallite size, in accordance with the Scherrer equation [208].

Table 5.5. Full width half maximum (FWHM) values for (002) XRD peak located between 24 and 26 degrees 2θ of strontium-substituted nHA produced using optimised method 1.

Sr (at. %)	**FWHM of (002) XRD peak (Degrees 2θ)**	
	Unsintered	**Sintered**
0	0.37	0.20
2.5	0.35	0.20
5	0.38	0.19
10	0.36	0.23
50	0.40	0.25
100	0.24	0.24

Particles of 100 at. % strontium-substituted hydroxyapatite had a larger aspect ratio (4.5) than any other level of strontium substitution (e.g. 0 at. % Sr nHA particles had an aspect ratio of 1.7). The particles produced using 2.5, 5, 10 and 50 at. % Sr appeared to be composed of smaller crystallites which were agglomerated together. This was in contrast the particles produced at 0 and 100 at. % Sr which had well defined edges (Figure 5.14).

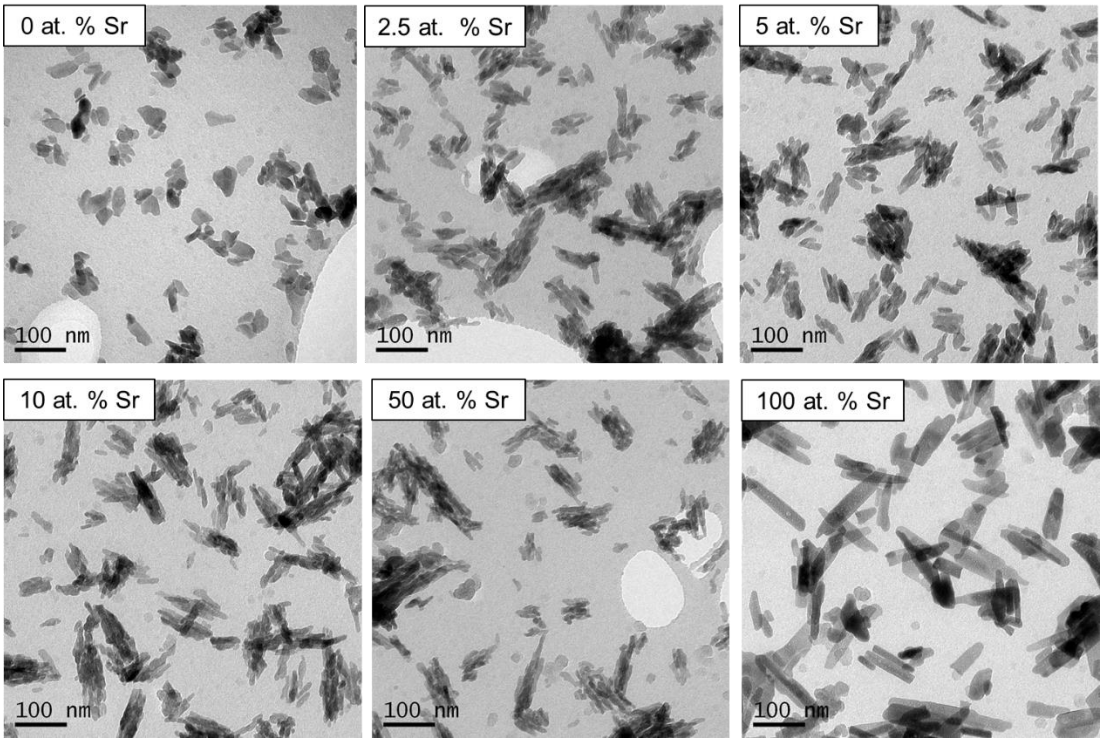

Figure 5.14. TEM micrographs of unsintered strontium-substituted HA powders (0, 2.5, 5, 10, 50 and 100 at. % Sr) produced using optimised method 1.

XRF data showed the accurate incorporation of strontium into the product, with the product Sr / (Sr+Ca) close to the attempted substitution level (Table 5.6). However the calcium and strontium to phosphorus ratios were lower than expected particularly for the 100 % strontium sample, which had a Sr:P ratio of 1.50. The sample with 0 at. % Sr had the calcium to phosphorus ratio (1.63) that was closest to the stoichiometric value (1.67).

Table 5.6. XRF results for strontium-substituted nHA powders produced using optimised method 1.

Experimental Sr / (Sr + Ca) molar %	**Sr / (Sr + Ca) molar % calculated from XRF data**	**(Ca + Sr) / P molar ratio**
0	0.02	1.63
2.5	2.45	1.57
5	4.83	1.57
10	9.55	1.56
50	49.67	1.58
100	99.79	1.50

The FTIR-ATR spectra of the range of unsintered strontium-substituted nHA powders displayed the presence of the characteristic bands for hydroxyapatite [11, 211]: 3750 cm^{-1} (OH^- stretch v_{OH}); 1086 and 1022 cm^{-1} (PO_4^{3-} v_3); 962 cm^{-1} (PO_4^{3-} v_1); 630 cm^{-1} (OH^- libration δ_{OH}); 600 and 570 cm^{-1} (PO_4^{3-} v_4). Additional band allocation for the unsintered samples: broad peak centred around 3400 cm^{-1} (absorbed water molecules); 1455 and 1410 cm^{-1} (CO_3^{2-} v_3); 880 cm^{-1} (CO_3^{2-} v_2). The band at around 880 cm^{-1} may also be associated with hydrogen phosphate (P-OH v_2), but it is generally accepted that the strong CO_3^{2-} v_2 band obscures this activity [212]. The absorbed water and carbonate groups (Figure 5.15 and Figure 5.16) were removed during high temperature sintering (Figure 5.17 and Figure 5.18). There was a clear shift in the position of the phosphate group bands (1086, 1022 and 962 cm^{-1}) to a lower wavenumber when increased amount of strontium were incorporated. Specifically, the highest degree of band wavenumber shift was observed for the 100 at. % strontium sample, followed by the lower amount of strontium incorporation levels respectively (Figure 5.16 A and Figure 5.18 A). Shoulders on the phosphate group bands were observed for the sintered samples which corresponded to the presence

of β-TCP or β-tristrontium phosphate (β-TSP) [211]; approximate positions of 990 cm^{-1} (for 0 at. % Sr), 974 cm^{-1} (for 2.5 and 5 at. % Sr) and 1023 cm^{-1} (for 100 at. % Sr). The bands for the phosphate group activity for the 50 at. % Sr nHA were not as clearly defined (i.e. not as sharp) as the other Sr contents. This was observed for both the unsintered and sintered samples. The carbonate bands for the 50 and 100 at. % Sr nHA samples were also less defined when compared to the other Sr contents (Figure 5.16 B).

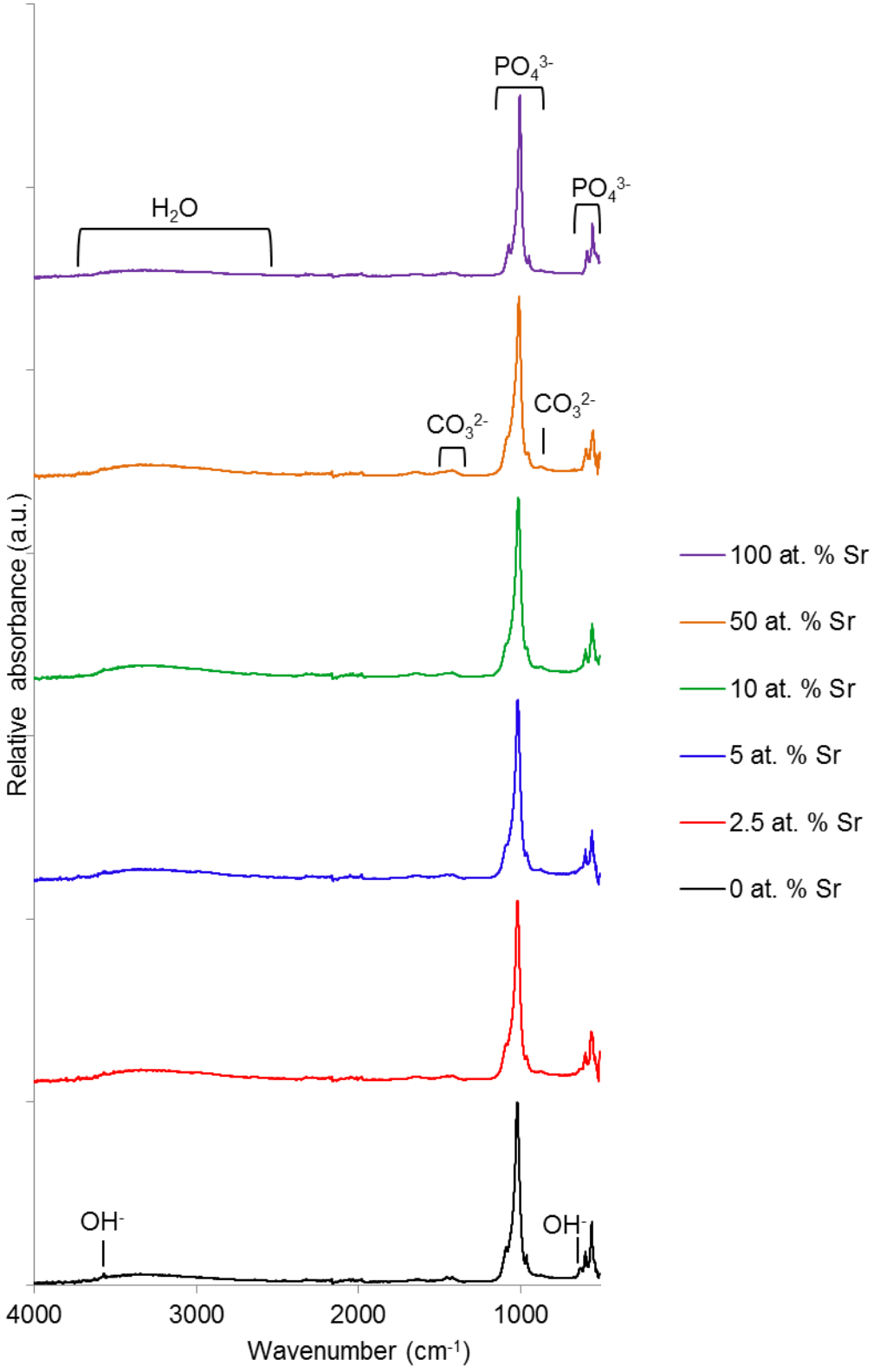

Figure 5.15. FTIR-ATR spectra of unsintered strontium-substituted nHA powders (0, 2.5, 5, 10, 50 and 100 at. % Sr) produced using optimised method 1.

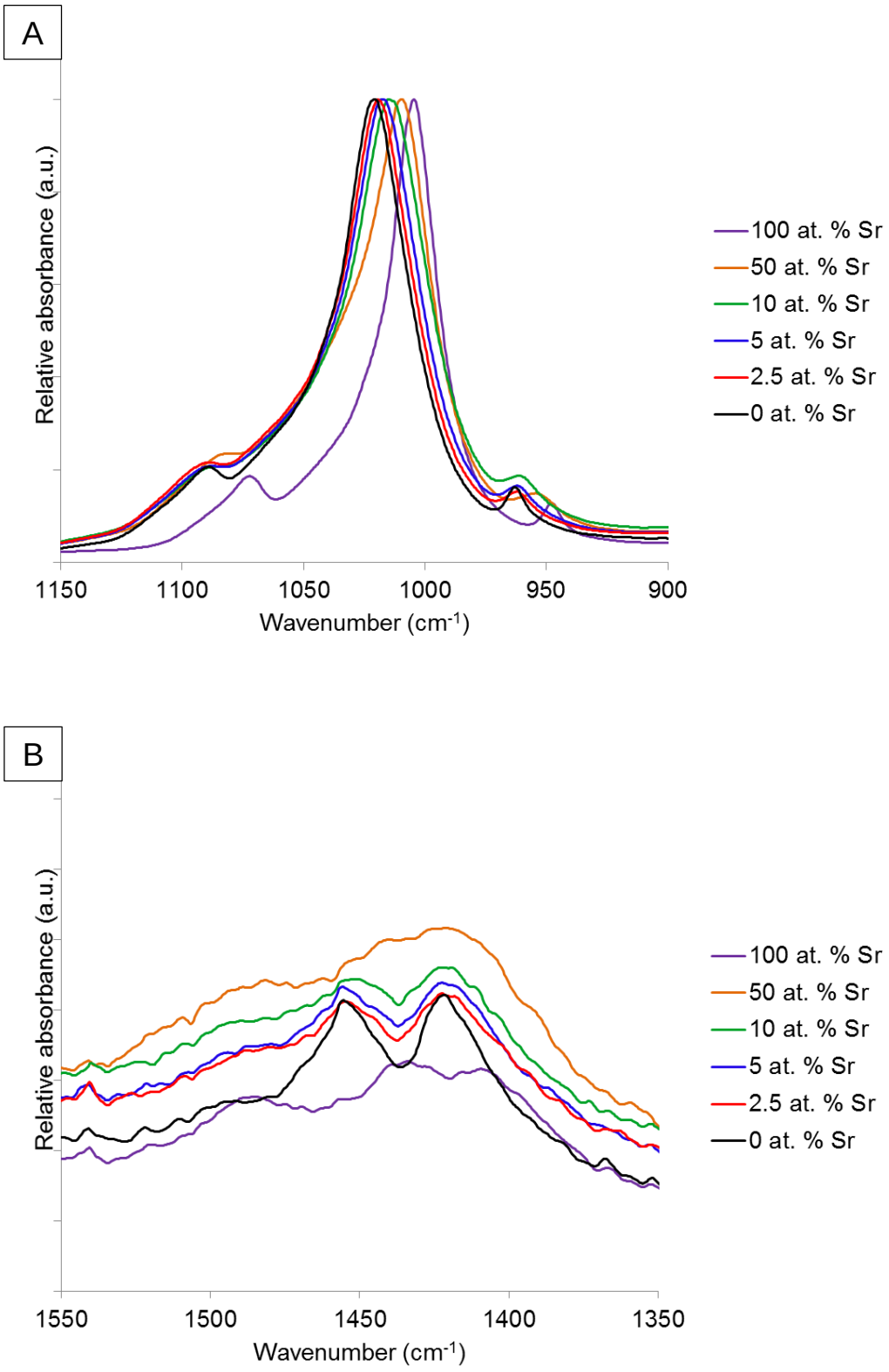

Figure 5.16. FTIR-ATR spectra of unsintered strontium-substituted nHA powders (0, 2.5, 5, 10, 50 and 100 at. % Sr) produced using optimised method 1. (A) 1150 – 900 cm^{-1}: phosphate group bands. (B) 1550 - 1350 cm^{-1}: carbonate group bands.

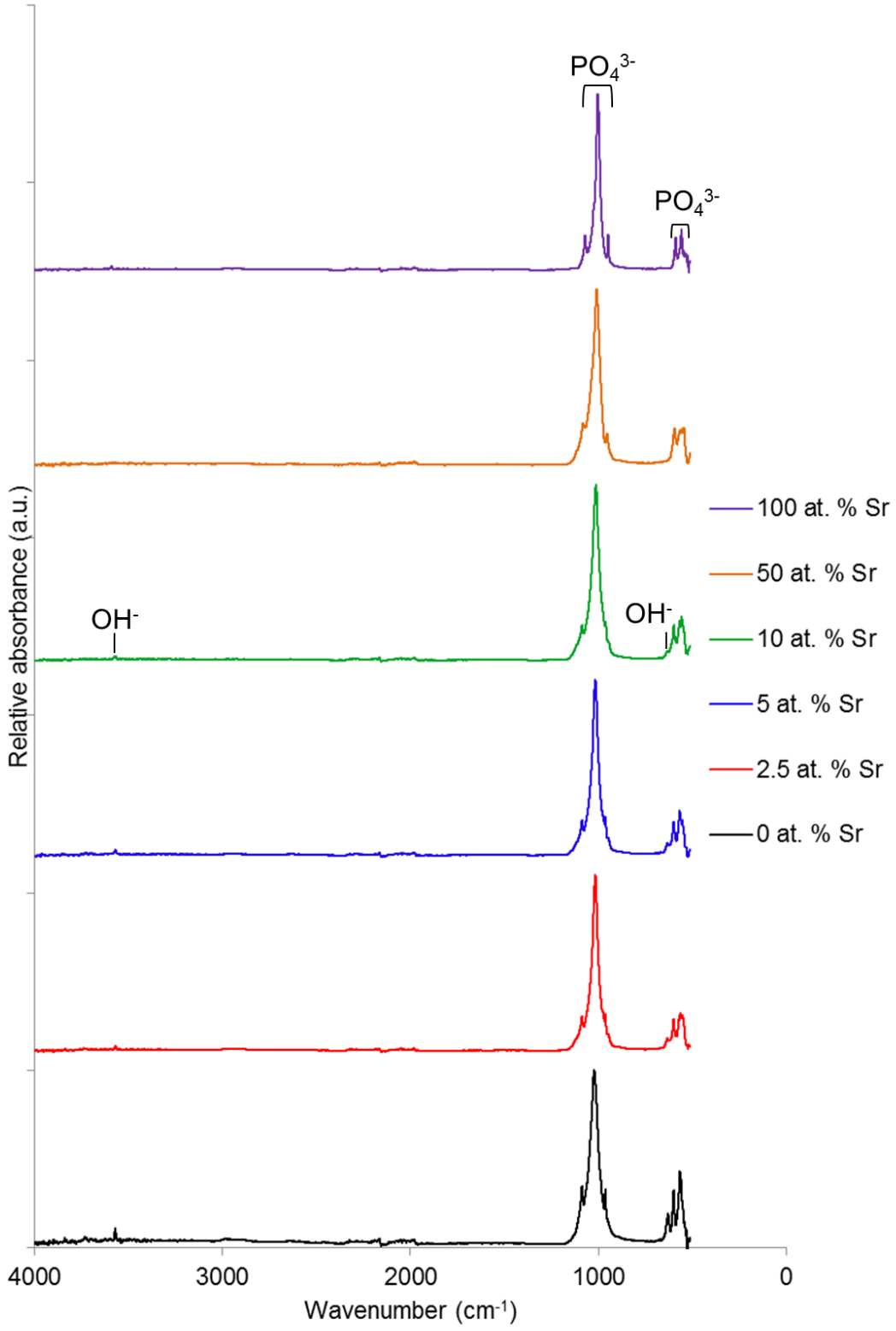

Figure 5.17. FTIR-ATR spectra of strontium-substituted nHA powders (0, 2.5, 5, 10, 50 and 100 at. % Sr) sintered at 1000 °C for 2 h produced using optimised method 1.

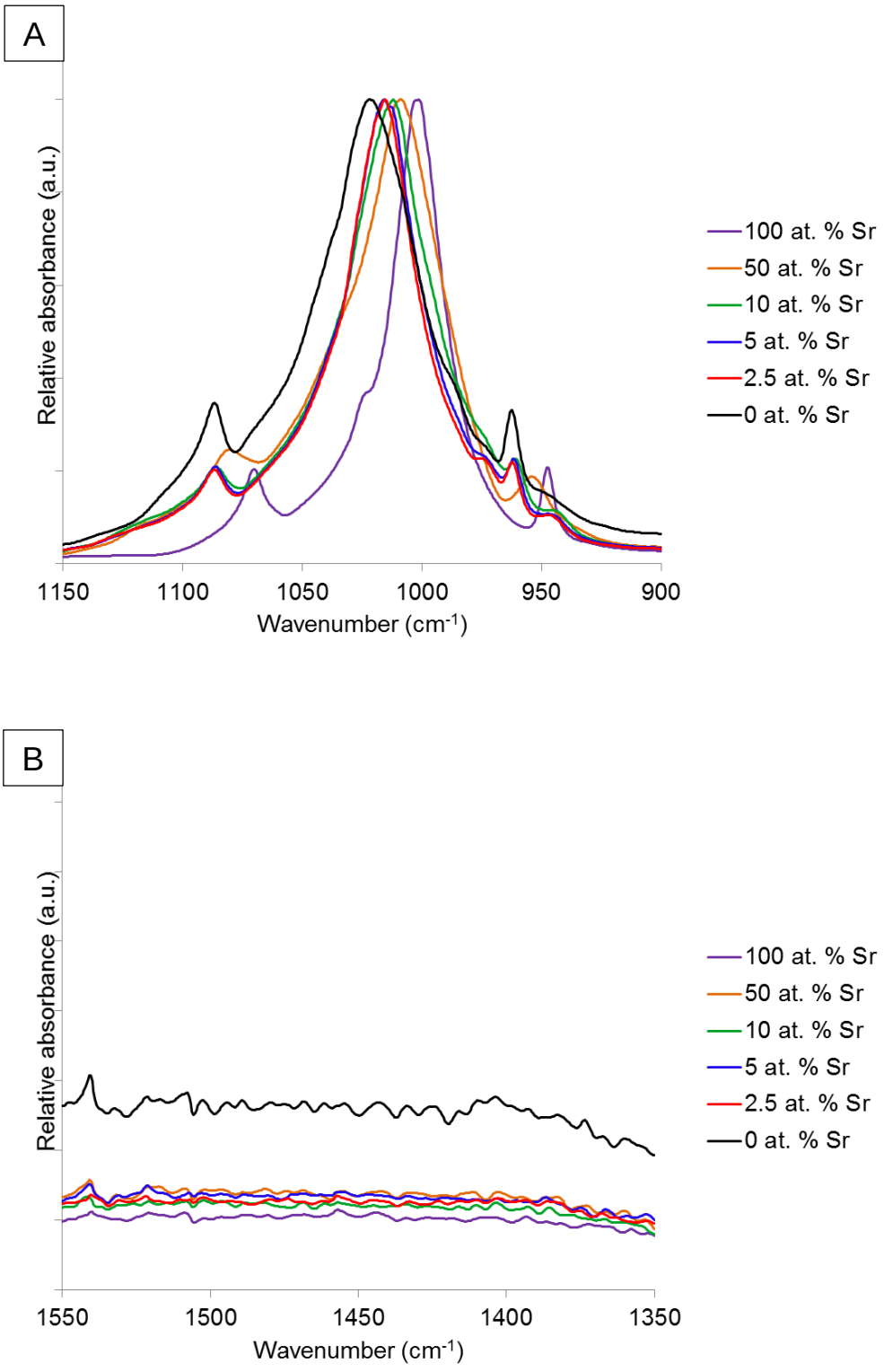

Figure 5.18. FTIR-ATR spectra of strontium-substituted nHA powders (0, 2.5, 5, 10, 50 and 100 at. % Sr) sintered at 1000 °C for 2 h produced using optimised method 1. (A) 1150 – 900 cm^{-1}: phosphate group bands. (B) 1550 - 1350 cm^{-1}: carbonate group bands.

The radiopacity of the strontium-substituted nHA powders increased with increasing strontium content in a non-linear manner (Figure 5.20).

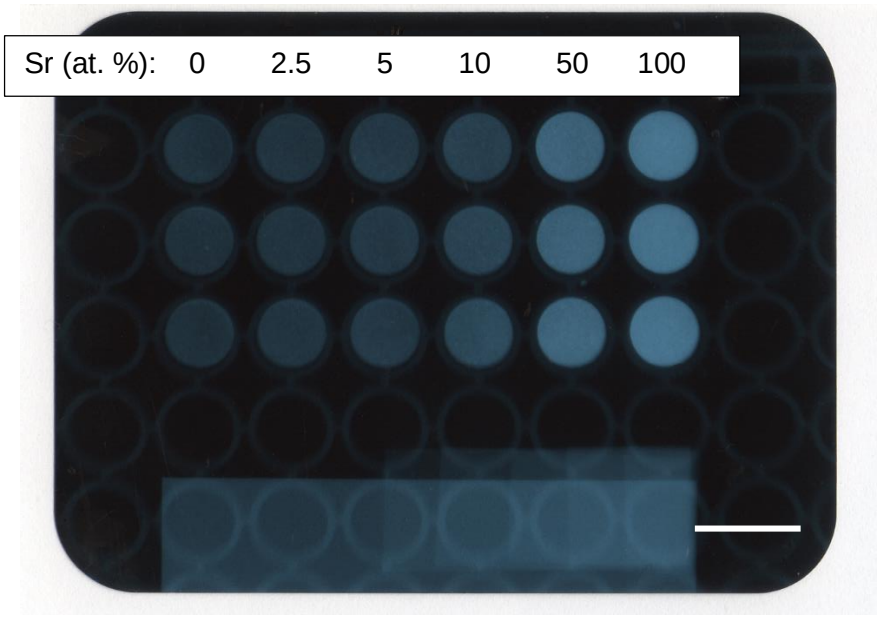

Figure 5.19. Radiograph of strontium-substituted nHA powders (0, 2.5, 5, 10, 50 and 100 at. % Sr) produced using optimised method 1, n=3, with aluminium step wedge used for quantification. Scale bar = 1 cm.

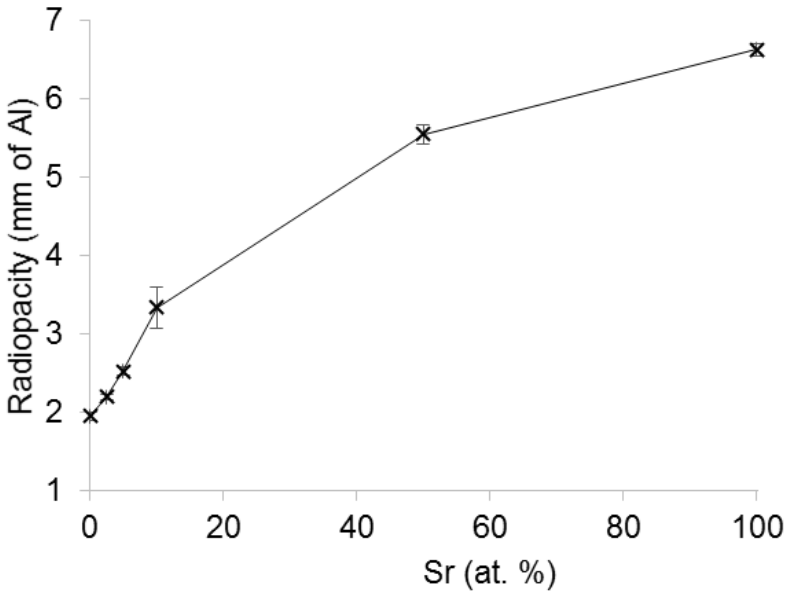

Figure 5.20. Quantification of radiopacity of strontium-substituted nHA powders (0, 2.5, 5, 10, 50 and 100 at. % Sr) produced using optimised method 1, n=3. Error bars: ± S.D.

5.3.2 Optimised Method 3: Synthesis of Strontium-substituted Nanoscale Hydroxyapatite

XRD patterns for the range of strontium-substituted nHA powders (0, 2.5, 5, 10, 50 and 100 at. % Sr) produced using optimised method 3 displayed the same peak shift relationship (Figure 5.21) as the Sr nHA produced using optimised method 1; i.e. the XRD peaks shifted to lower degrees 2θ for increased amounts of Sr. The thermal stability of the calcium nHA produced using optimised method 3 was relatively high, with only minor traces of β-TCP observed when sintered at 1000 °C (Table 5.4, method 3-F). This was in contrast to the 100 at. % Sr nHA produced which underwent significant thermal decomposition at 700 °C and almost complete thermal decomposition at 850 °C (Figure 5.22). Therefore there was no suitable single sintering temperature which could be used to increase the sharpness of the diffraction peaks of the entire range of strontium-substituted nHA without causing excessive thermal decomposition.

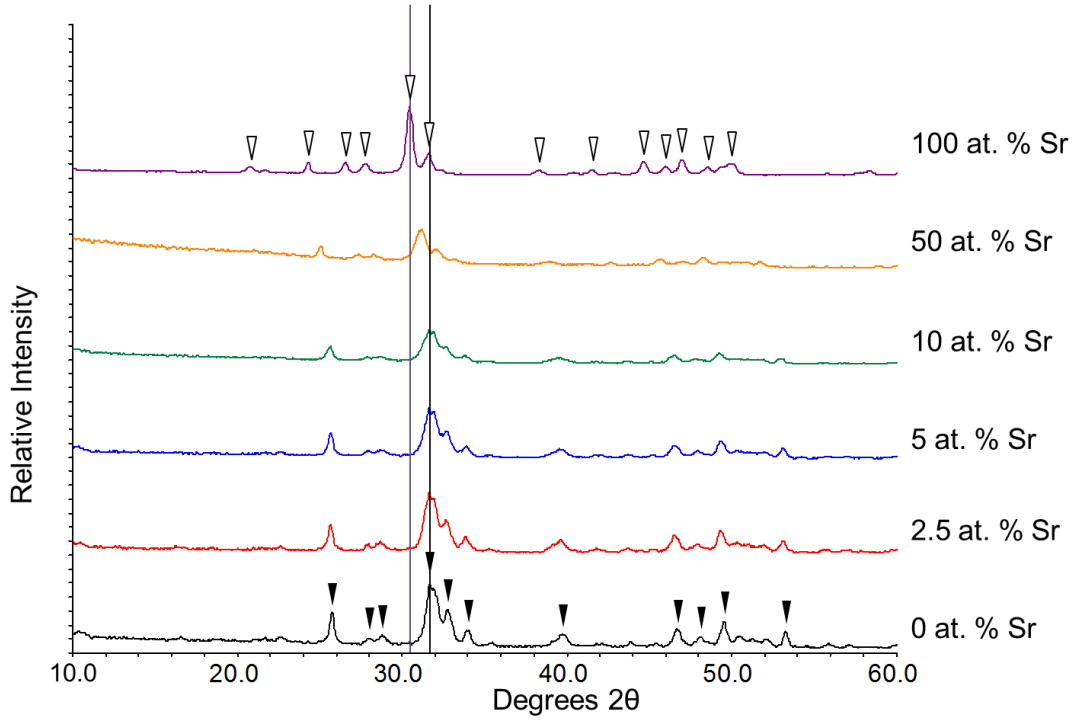

Figure 5.21. XRD patterns of unsintered strontium-substituted nHA powders (0, 2.5, 5, 10, 50 and 100 at. % Sr) produced using optimised method 3. Peak labels: ▼ hydroxyapatite; ▽ strontium hydroxyapatite.

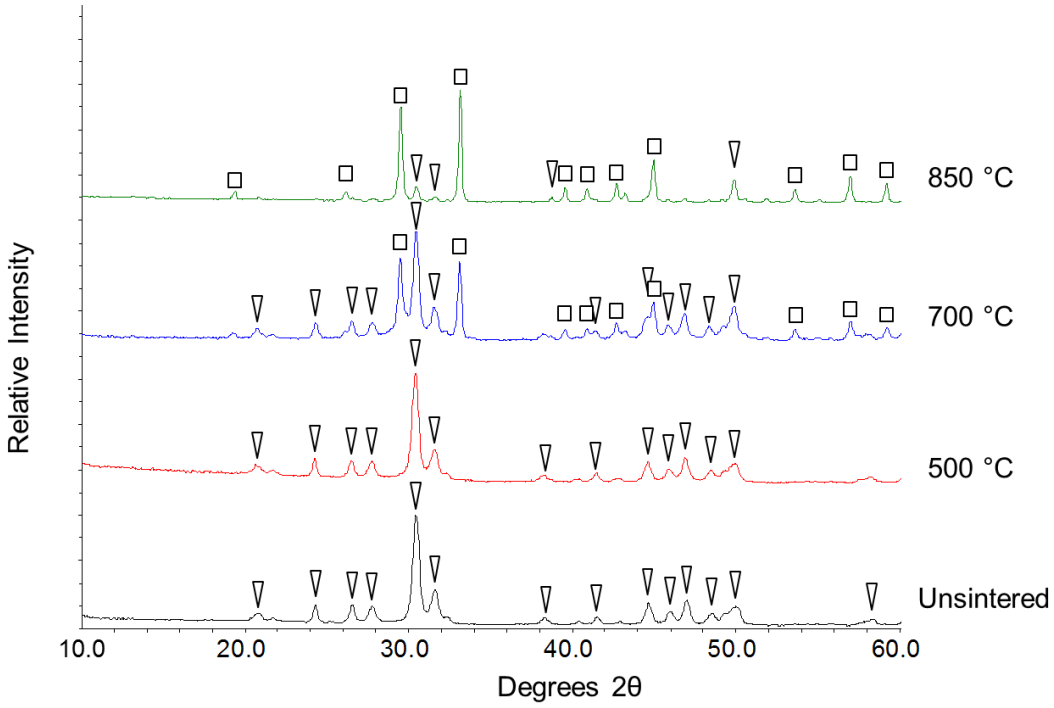

Figure 5.22. XRD patterns of 100 at. % strontium-substituted nHA powder produced using optimised method 3: unsintered and sintered at 500, 700 and 850 °C. Peak labels: ▽ strontium hydroxyapatite; □ β-tristrontium phosphate.

The increase in the aspect ratio for the 100 at. % strontium-substituted HA produced using optimised method 3 (Figure 5.23) was more pronounced than observed for optimised method 1 (Figure 5.14). Specifically, the aspect ratio for the nHA produced using optimised method 3 increased from 2.5 for the sample with 0 at. % Sr to 6 for the 100 at. % Sr sample.

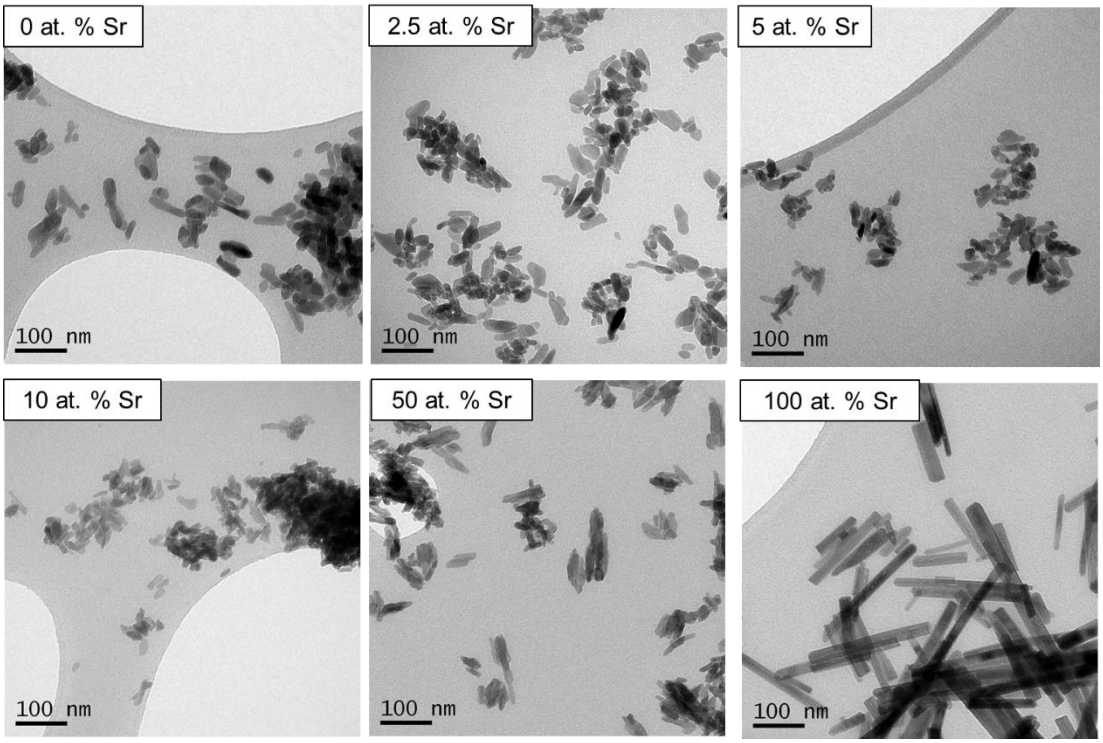

Figure 5.23. TEM micrographs of unsintered strontium-substituted HA powders (0, 2.5, 5, 10, 50 and 100 at. % Sr) produced using optimised method 3.

XRF data displayed the successful incorporation of strontium into the HA in a similar ratio to that which was used in the method (Table 4.1). The (Ca+Sr)/P molar ratios were again lower than the stoichiometric value of 1.67, with the 0 at. % strontium sample (1.59) closest to the stoichiometric value.

Table 5.7. XRF results for strontium-substituted nHA produced using optimised method 3.

Experimental Sr / (Sr + Ca) molar %	**Sr / (Sr + Ca) molar % calculated from XRF data**	**(Ca + Sr) / P molar ratio**
0	0.01	1.59
2.5	2.32	1.56
5	4.81	1.50
10	9.01	1.54
50	45.11	1.48
100	99.91	1.52

FTIR-ATR spectra (Figure 5.24 and Figure 5.25) confirmed the presence of an apatite-like phase with characteristic bands for hydroxyapatite as listed in section 5.3.1 *Optimised Method 1: Synthesis of Strontium-substituted Nanoscale Hydroxyapatite*. Absorbed water and carbonate group activity were also observed in these samples alongside the characteristic hydroxyapatite phosphate and hydroxyl group activity. As observed for the Sr nHA produced using optimised method 1, there was a clear shift to a lower wavenumber of the phosphate group bands (1086, 1022 and 962 cm^{-1}) when increasing amounts of strontium were present (Figure 5.25 A). Similarly for the results obtained for the optimised method 1, the peaks for the phosphate group band for the 50 at. % Sr nHA were not as defined as the other Sr contents. Also the carbonate group bands for the 50 and 100 % at. Sr nHA samples were less defined when compared to the other Sr contents (Figure 5.25 B).

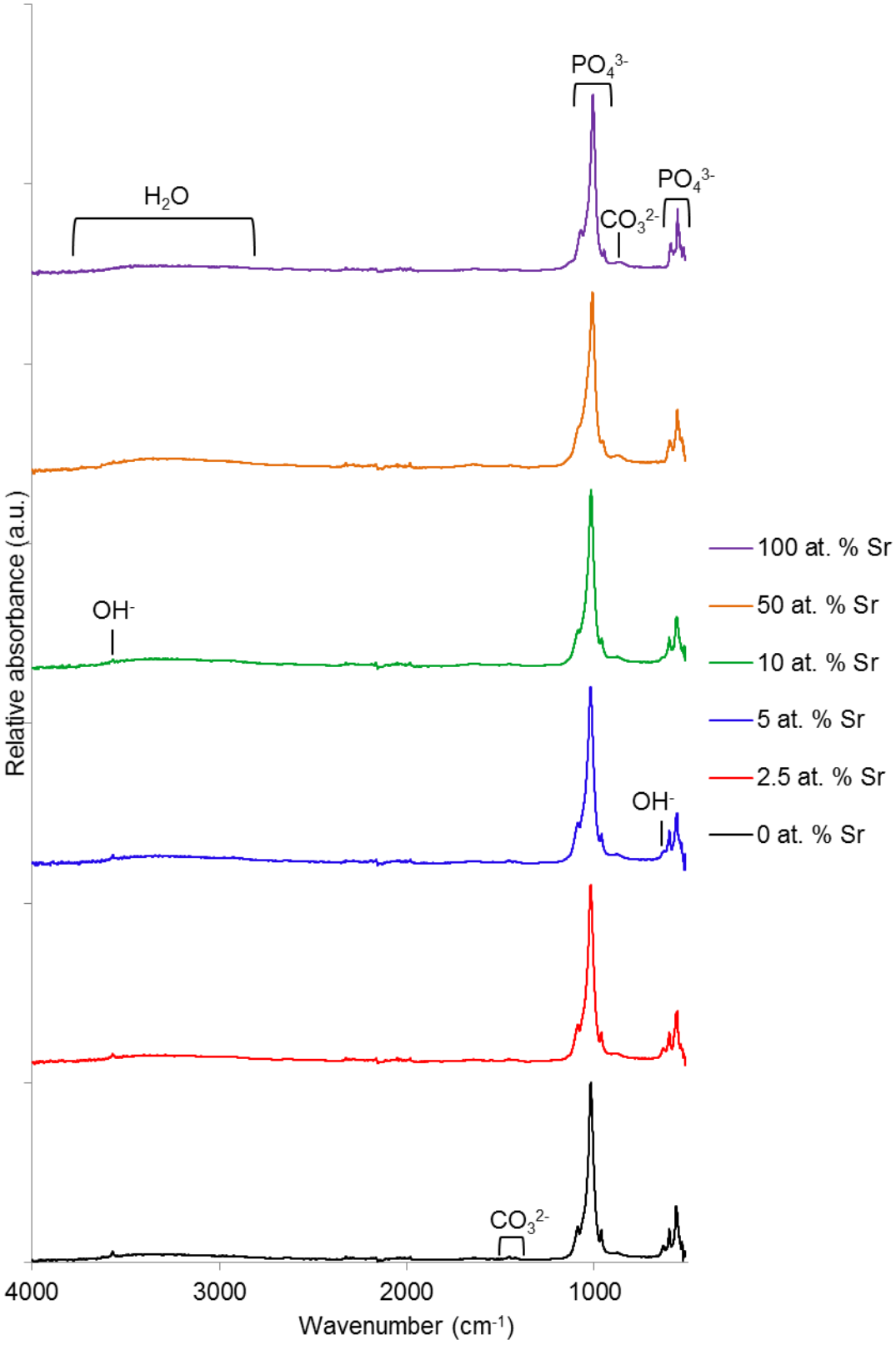

Figure 5.24. FTIR-ATR spectra of unsintered strontium-substituted nHA powders (0, 2.5, 5, 10, 50 and 100 at. % Sr) produced using optimised method 3.

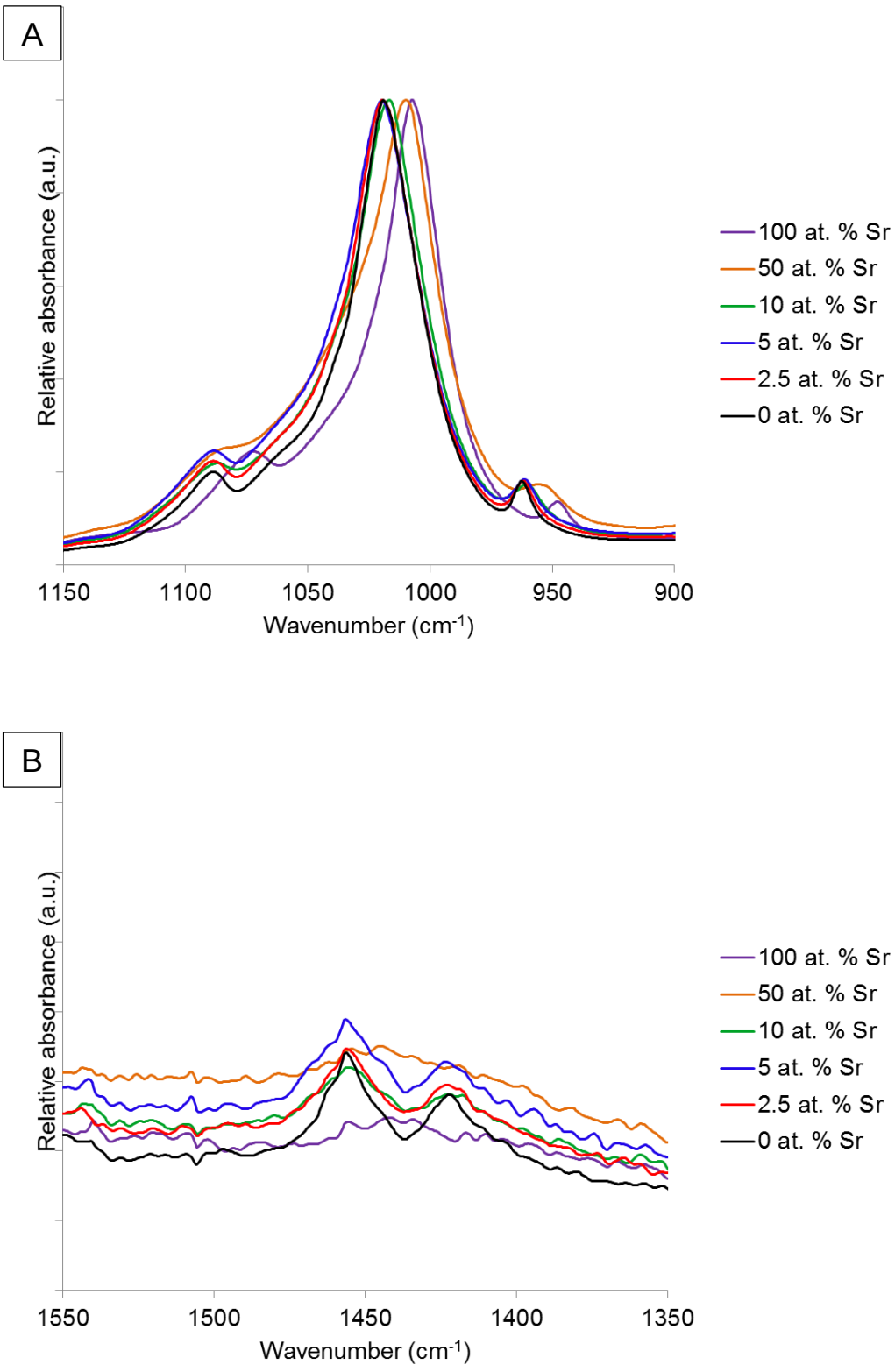

Figure 5.25. FTIR-ATR spectra of unsintered strontium-substituted nHA powders (0, 2.5, 5, 10, 50 and 100 at. % Sr) produced using optimised method 3. (A) 1150 – 900 cm^{-1}: phosphate group bands. (B) 1550 - 1350 cm^{-1}: carbonate group bands.

The radiopacity of the strontium-substituted nHA powders increased in a non-linear manner (Figure 5.27) as seen for the powders produced using optimised method 1. The radiopacity values recorded were slightly higher than those found for the powders produced using optimised method 1. For instance, the radiopacity values recorded for the samples produced using optimised method 1 ranged from 2.0 to 6.6 mm of Al, whereas the powders produced using optimised method 3 ranged from 3.4 to 7.7 mm of Al.

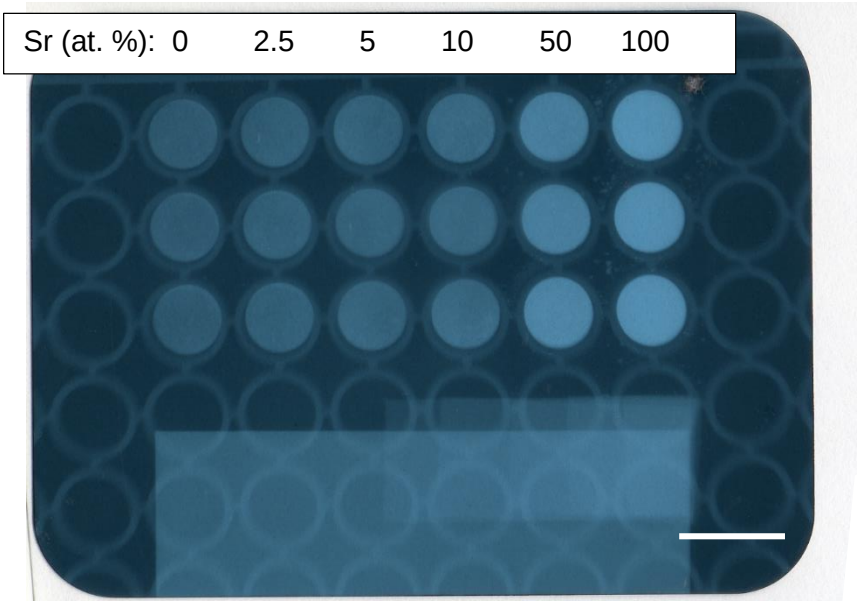

Figure 5.26. Radiograph of strontium-substituted nHA powders (0, 2.5, 5, 10, 50 and 100 at. % Sr) produced using optimised method 3, n=3, with aluminium step wedge used for quantification. Scale bar = 1 cm.

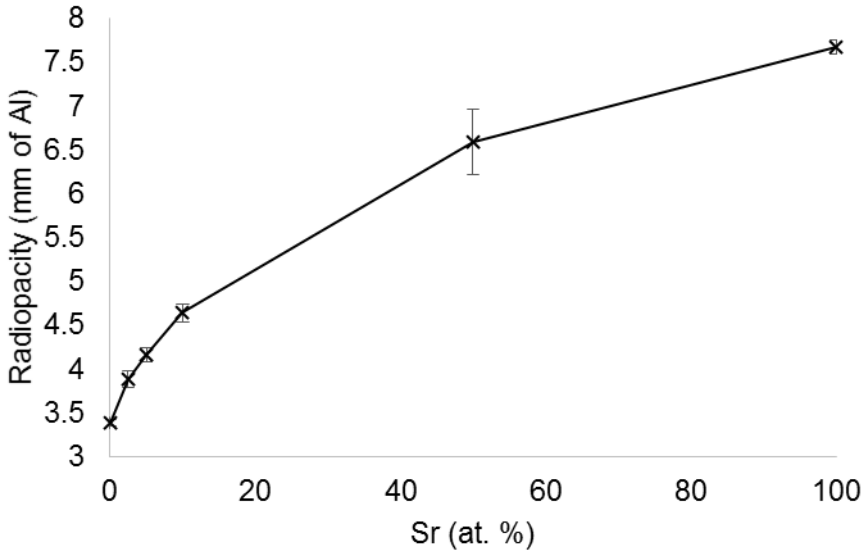

Figure 5.27. Quantification of radiopacity of strontium-substituted nHA powders (0, 2.5, 5, 10, 50 and 100 at. % Sr) produced using optimised method 3, n=3. Error bars: ± S.D.

5.4 Synthesis of Silver-doped Nanoscale Hydroxyapatite (Altered Method 1)

XRD patterns showed the precipitation of a HA phase for the 0, 2 and 5 at. % silver-doped samples (Figure 5.28). However, when the level of silver-doping was increased to 10 at. %, silver phosphate was detected alongside the HA phase. Furthermore, an increase in the relative intensity at around 10 degrees 2θ indicated an increase amorphous residue, with a higher degree of amorphous residue observed with increasing silver content. After high temperature treatment, increasing amounts of β-TCP were detected as the amount of silver-doping was increased (Figure 5.29). For the 5 and 10 at. % silver-doped samples, metallic silver was detected after sintering.

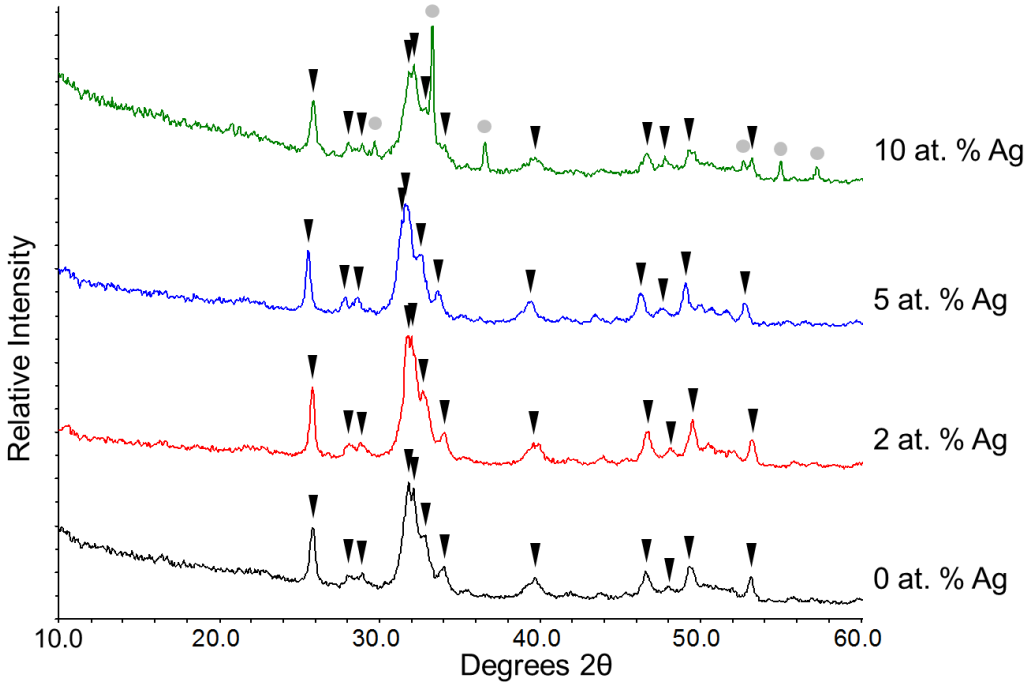

Figure 5.28. XRD patterns of unsintered silver-doped nHA powders (0, 2, 5 and 10 at. % Ag) produced using altered method 1. Peak labels: ▼ hydroxyapatite; ● silver phosphate.

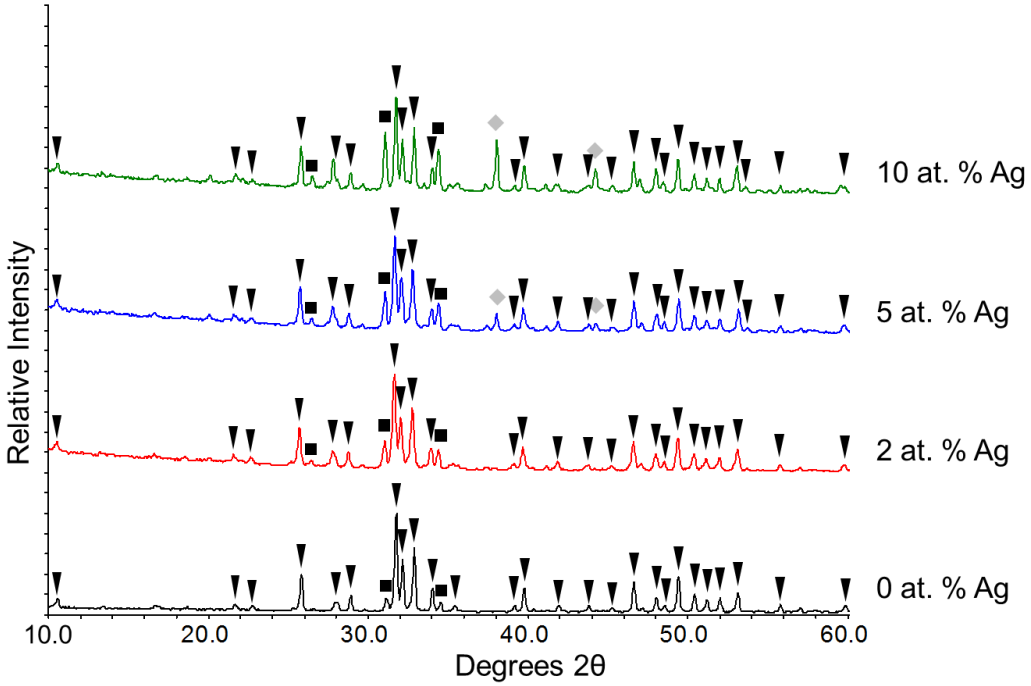

Figure 5.29. XRD patterns of silver-doped nHA powders (0, 2, 5 and 10 at. % Ag) produced using altered method 1 sintered at 1000 °C for 2 h. Peak labels: ▼ hydroxyapatite; ■ β-tricalcium phosphate; ◆ silver.

The full width half maximum of the (002) XRD peak for the sintered silver-doped nHA samples were consistently lower than for the unsintered samples (Table 5.8). As stated previously, based on the Scherrer equation the reduction in the FWHM corresponds with an increase in the crystallite size after sintering.

Table 5.8. Full width half maximum (FWHM) values for the (002) XRD peak located at approximately 26 degrees 2θ of silver-doped nHA produced using altered method 1.

Ag (at. %)	FWHM of (002) XRD peak (Degrees 2θ)	
	Unsintered	Sintered
0	0.32	0.23
2	0.30	0.20
5	0.32	0.22
10	0.31	0.21

TEM micrographs (Figure 5.30) showed no major morphological changes in the nHA particles when different levels of silver-doping were introduced. However, dark spots were observed on some particles in the 5 and 10 at. % silver-doped samples.

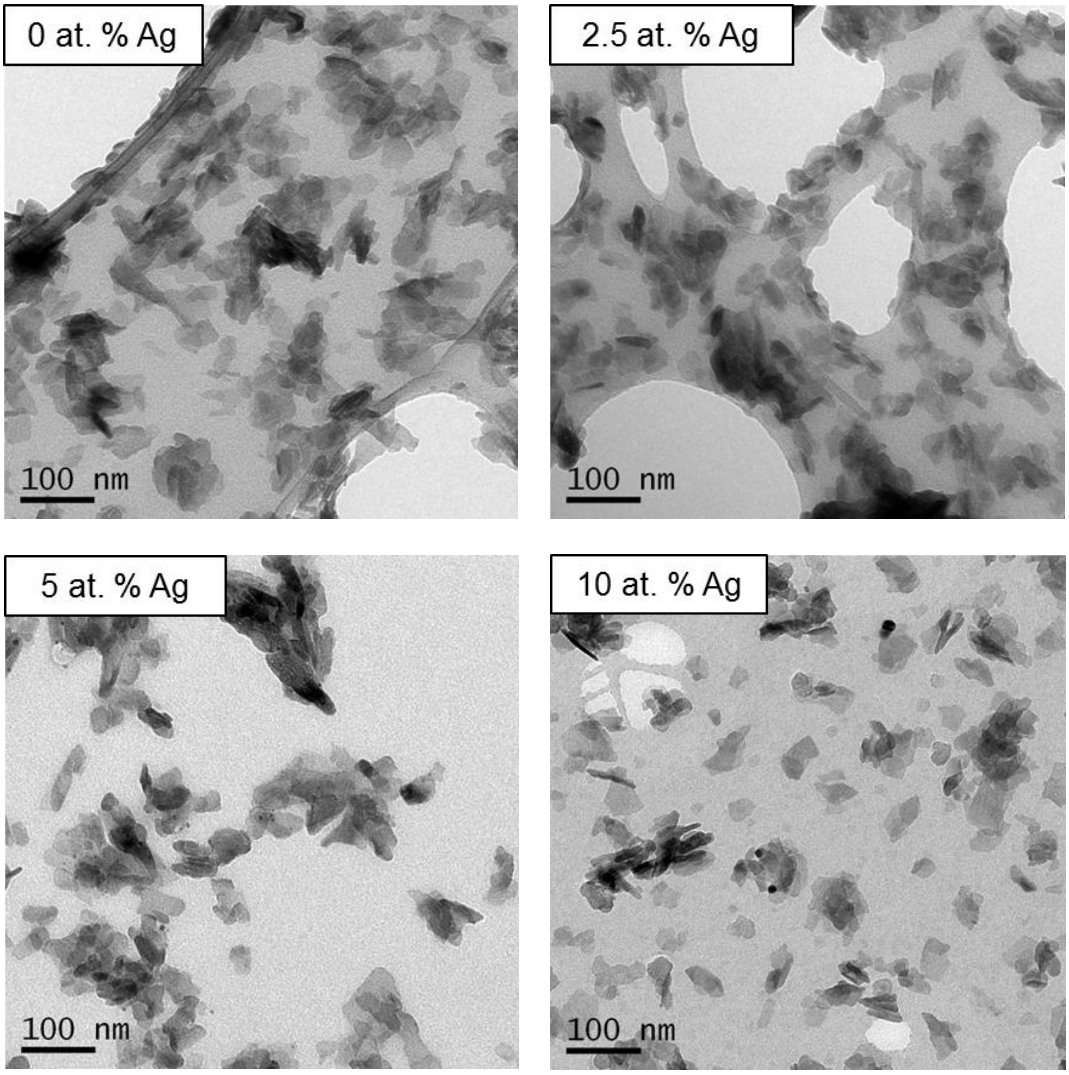

Figure 5.30. TEM micrographs of unsintered silver-doped nHA powders (0, 2, 5 and 10 at. % Ag) produced using altered method 1.

XRF data showed that the silver to calcium molar ratio of the products were lower than the amount of silver used in the method (Table 5.9). However, the relative silver to calcium molar ratio increased as more silver was used in the method.

Table 5.9. XRF results for unsintered 0, 2, 5 and 10 at. % silver-doped nHA samples produced using altered method 1.

Experimental Ag:Ca molar ratio (mol. %)	**Ag:Ca molar ratio from XRF (mol. %)**
0	0
2	1.69
5	3.34
10	6.72

All FTIR-ATR spectra for the unsintered silver-doped powders displayed the characteristic bands of phosphate and hydroxyl groups associated with hydroxyapatite (Figure 5.31) (as listed in section 5.3.1 *Optimised Method 1: Synthesis of Strontium-substituted Nanoscale Hydroxyapatite*). Unsintered samples displayed the bands of absorbed water and carbonate groups (Figure 5.32). The high temperature sintering process removed the water and carbonate groups and also resolved the spectral hydroxyl group bands (Figure 5.33 and Figure 5.34). A peak shift to a higher wave number was observed only for the 10 at. % silver-doped sample for the unsintered and sintered samples (Figure 5.32 and Figure 5.34). It can also be seen that the phosphate group bands were poorly defined for the 10 at. % silver-doped sample compared to the other formulations. Shoulders were observed in the phosphate group activity (1150 – 900 cm^{-1}) for the sintered samples indicating the presence of β-TCP [211], particularly for 2, 5 and 10 at. % Ag; approximate positions 1126, 990 and 945 cm^{-1}.

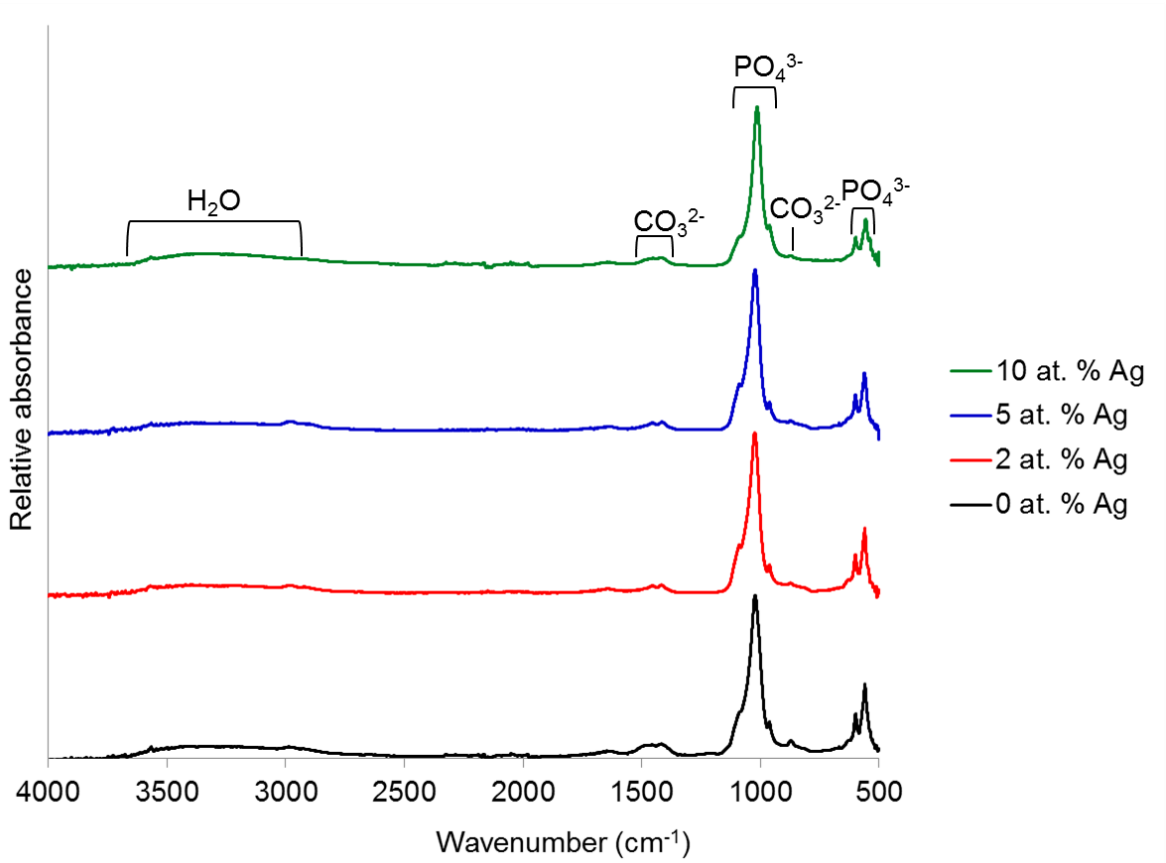

Figure 5.31. FTIR-ATR spectra of unsintered silver-doped nHA powders (0, 2, 5 and 10 at. % Ag) produced using altered method 1.

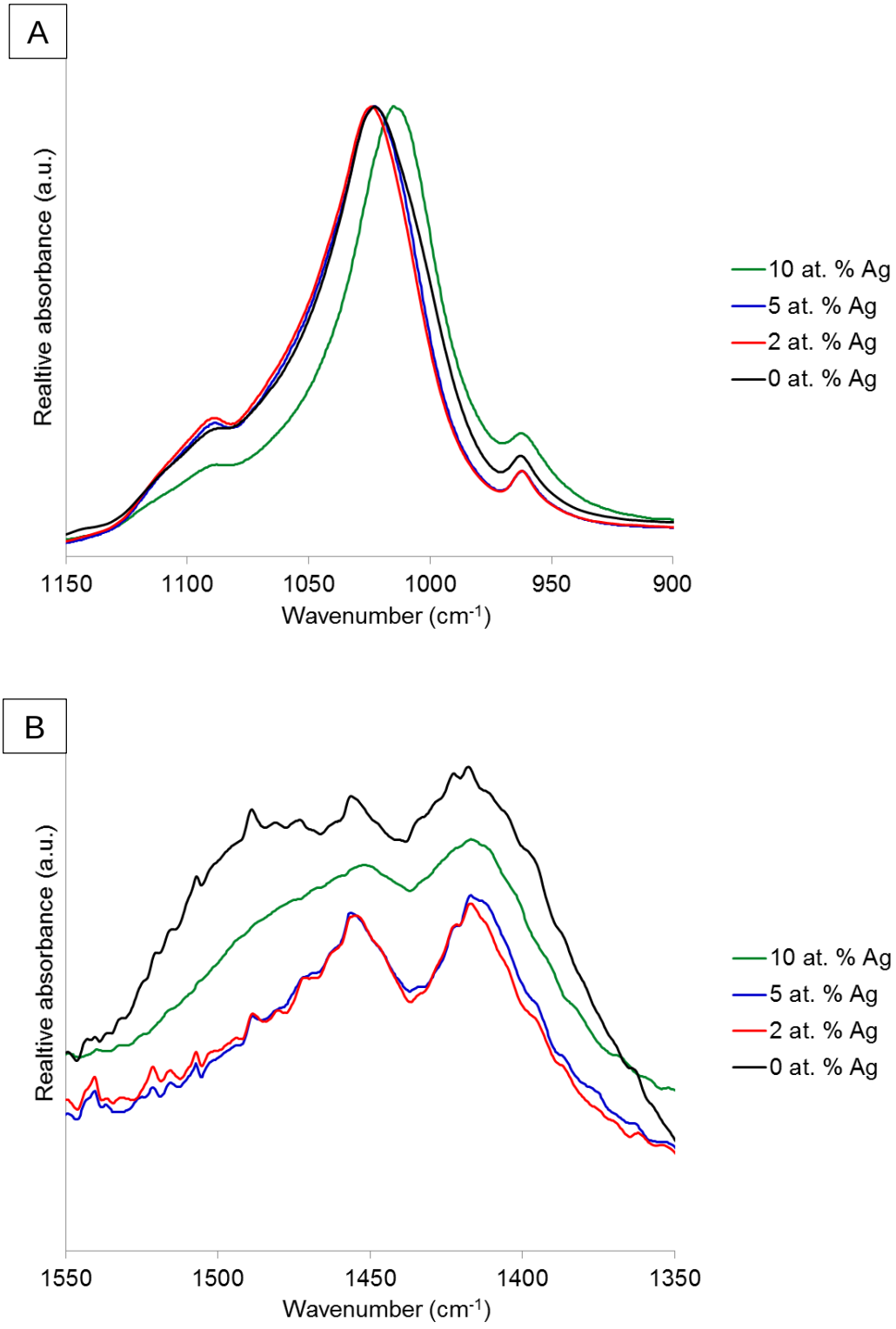

Figure 5.32. FTIR-ATR spectra of unsintered silver-doped nHA powders (0, 2, 5 and 10 at. % Ag) produced using altered method 1. (A) 1150 – 900 cm^{-1}: phosphate group bands. (B) 1550 - 1350 cm^{-1}: carbonate group bands.

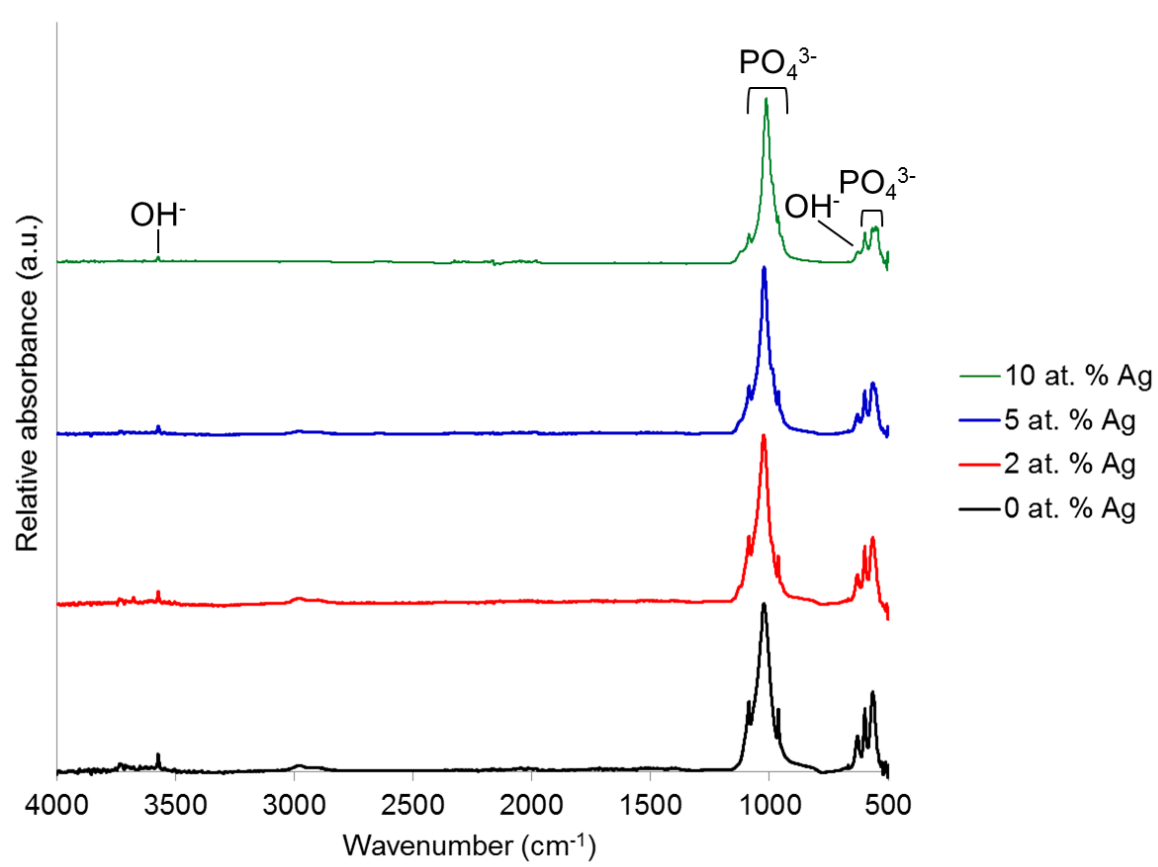

Figure 5.33. FTIR-ATR spectra of silver-doped nHA powders (0, 2, 5 and 10 at. % Ag) sintered at 1000 °C for 2 h produced using altered method 1.

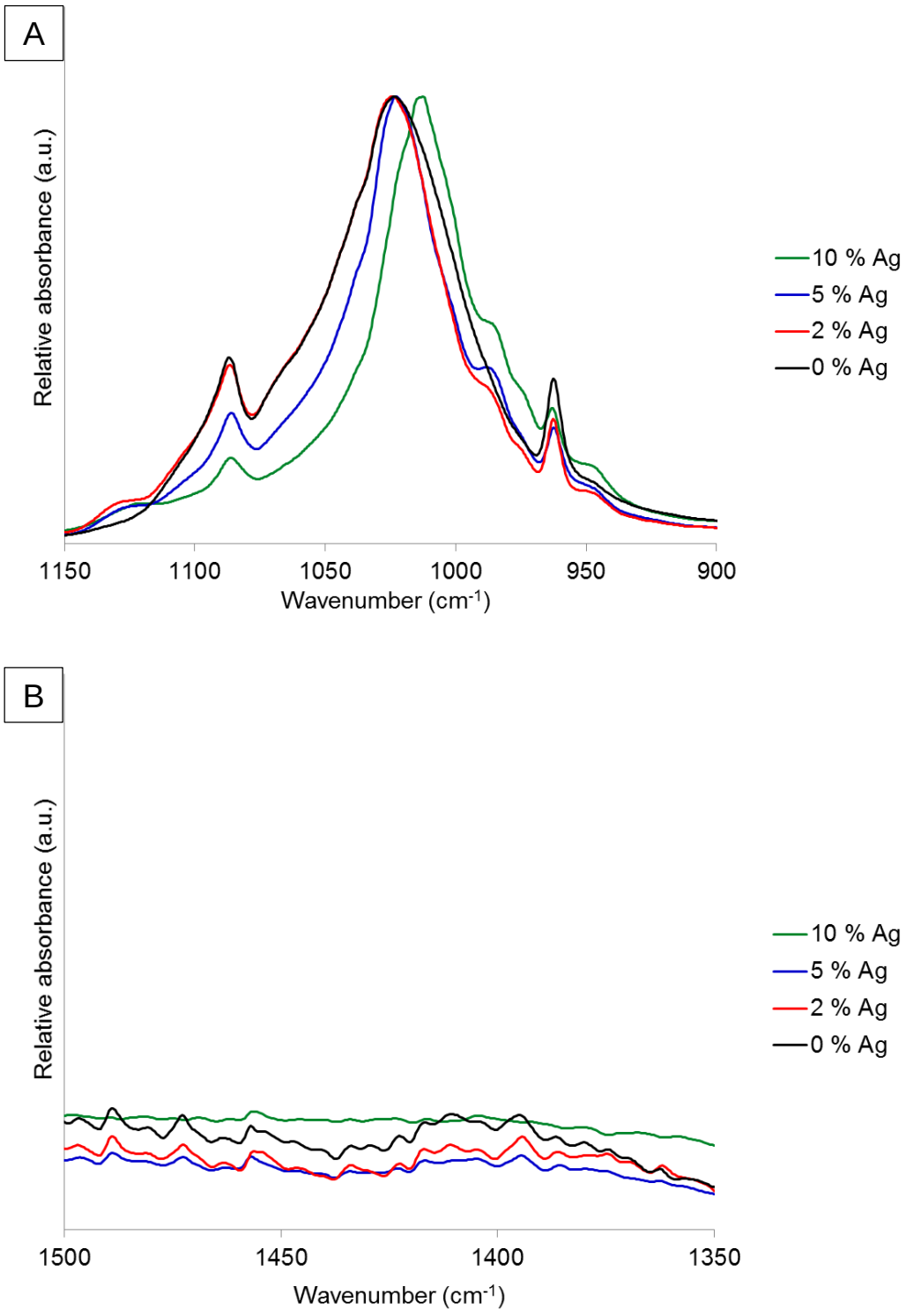

Figure 5.34. FTIR-ATR spectra of silver-doped nHA powders (0, 2, 5 and 10 at. % Ag) sintered at 1000 °C for 2 h produced using altered method 1. (A) 1150 – 900 cm^{-1}: phosphate group bands. (B) 1550 - 1350 cm^{-1}: carbonate group bands.

5.5 Nanoscale Hydroxyapatite Paste and Gel Characterisation

5.5.1 *In Vitro* Biocompatibility of Strontium-substituted Nanoscale Hydroxyapatite Pastes and Gels Produced by Optimised Methods 1 and 3

In vitro evaluation using cultured cells has the potential to predict the behaviour of materials prior to clinical use, or can be used to investigate some specific cell-mediated interactions. Indirect and direct assays were carried out on the strontium-substituted pastes and gels to evaluate the potential biocompatibility of the materials as described in section 4.2.7.1 *In Vitro Evaluation of Strontium-substituted Nanoscale Hydroxyapatite Paste and Gel Produced using Optimised Methods 1 and 3*.

For the indirect assays, the 2.5, 5 and 10 at. % Sr nHA paste showed a significantly lower viability than the cells cultured with 0 and 100 at. % Sr nHA pastes (Figure 5.35). Moreover, the 0 and 100 at. % Sr nHA pastes showed the same viability as the cells cultured on tissue culture plastic. Variable amount of nHA particles were observed in the preconditioned media between different materials tested despite all media undergoing centrifugation prior to application. Live/Dead fluorescence images showed that the majority of cells were alive, with few dead cells observed (Figure 5.36).

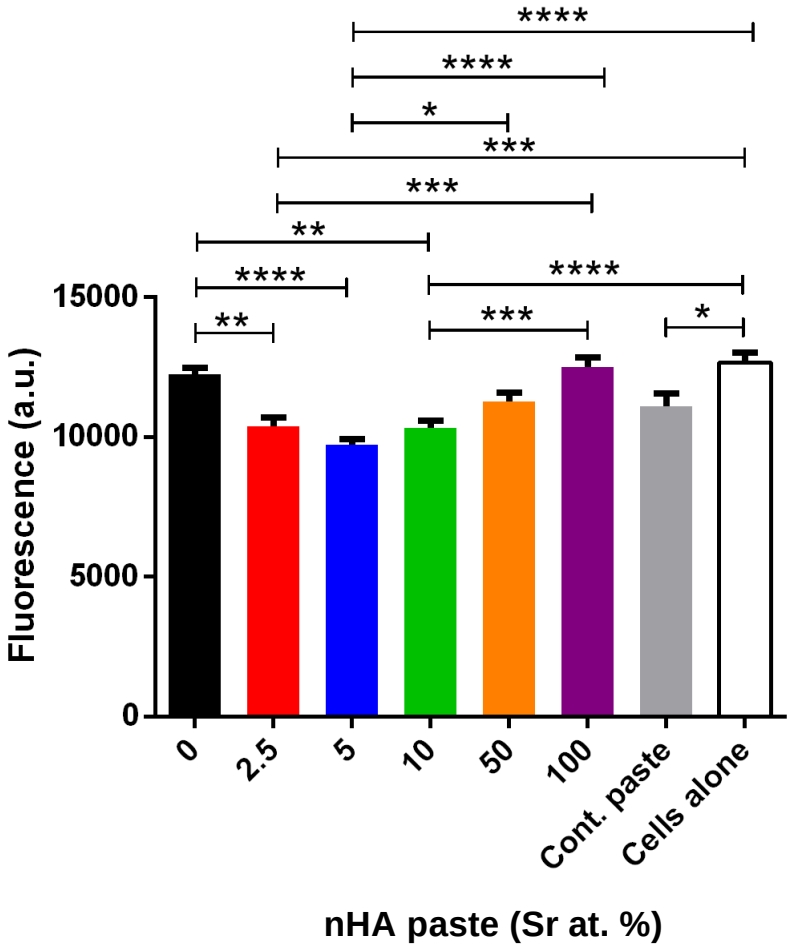

Figure 5.35. PrestoBlue® viability assay results at 24 h for MG63 cells cultured indirectly with strontium-substituted nHA pastes produced using optimised method 1 (0, 2.5, 5, 10, 50 and 100 at. % Sr), control paste (ReproBone *novo*™) and with no material present (n = 9). Error bars ± standard error of the mean. Significance level: *: p< 0.05, **: p< 0.01, ***: p< 0.001, ****: p< 0.0001.

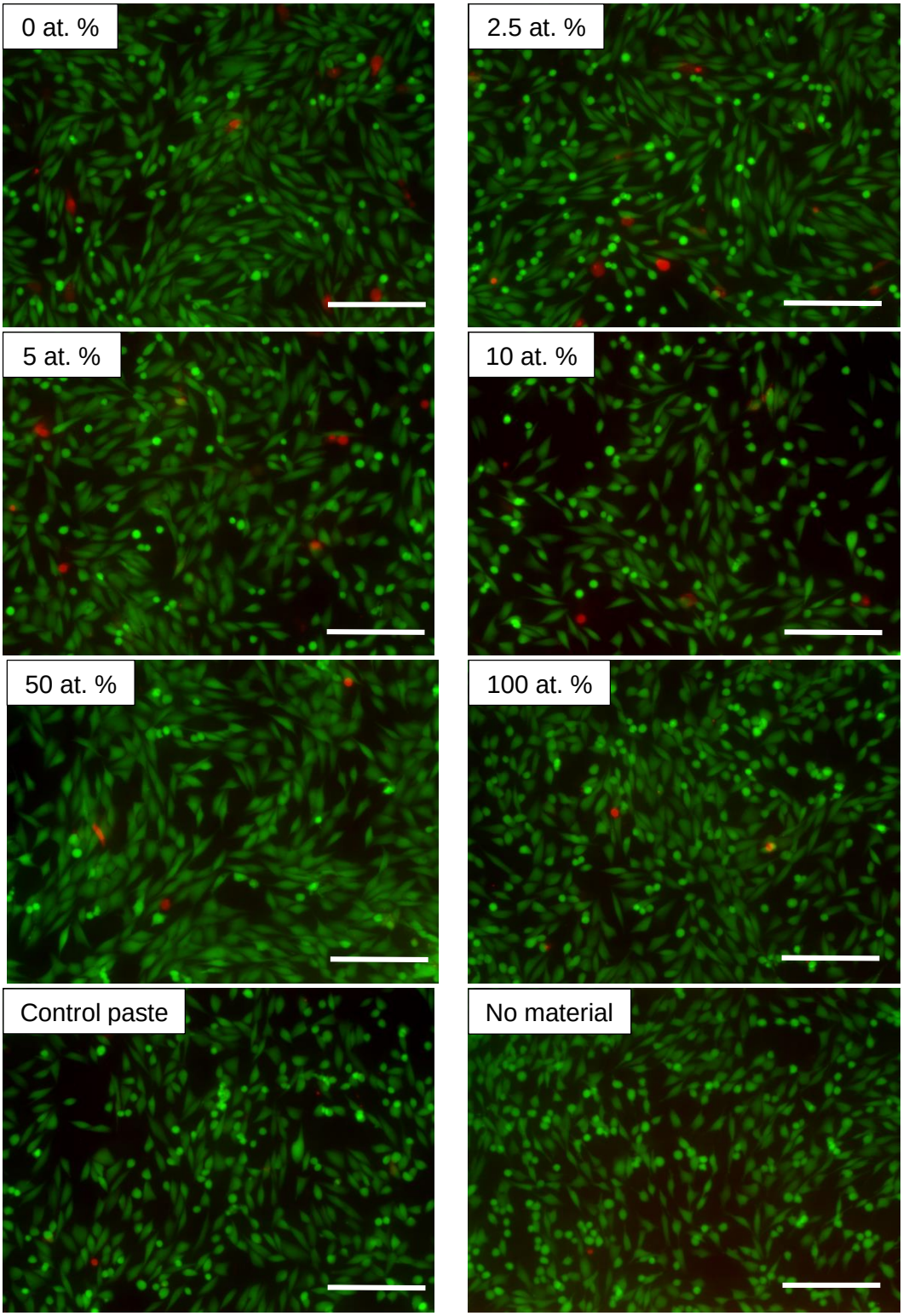

Figure 5.36. Live/Dead fluorescence imaging for MG63 cells cultured indirectly with strontium-substituted nHA pastes produced using optimised method 1 (0, 2.5, 5, 10, 50 and 100 at. % Sr), control paste (ReproBone *novo*^{TM}) and with no material present. Scale bar = 200 µm.

The cells cultured alongside the nHA paste with 5 at. % Sr content had a significantly lower viability than the 0, 2.5, 10 and 50 at. % Sr nHA pastes (Figure 5.37). It was also observed that the 5 at. % Sr nHA pastes had a greater tendency to fragment during the 48 h incubation than the pastes with other Sr contents (Figure 5.38). The cells cultured directly with the 0 at. % Sr nHA paste had statistically greater viability than the cells cultured with the 100 at. % Sr nHA paste. This was in contrast to the indirect viability assays where the cells cultured with preconditioned media from the 0 and 100 at. % Sr nHA pastes had the same viability (Figure 5.35). Light microscopy and fluorescence microscopy showed the survival and morphology of the cells in direct contact with the paste (Figure 5.39 and Figure 5.40). For the fluorescence microscopy images, some cells close to the paste had a rounded morphology which may have displayed the growth of cells inside the pastes (Figure 5.40).

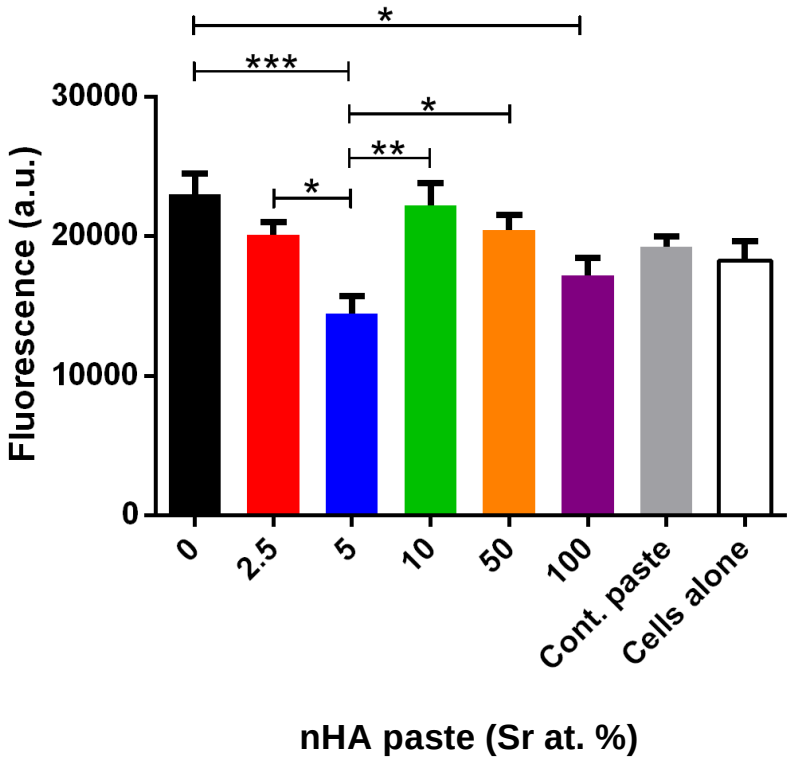

Figure 5.37. PrestoBlue® viability assay results at 48 h for MG63 cells cultured directly with strontium-substituted nHA pastes produced using optimised method 1 (0, 2.5, 5, 10, 50 and 100 at. % Sr), control paste (ReproBone *novo*™) and with no material (n = 9). Error bars ± standard error of the mean. Significance level: *: p< 0.05, **: p< 0.01, ***: p< 0.001.

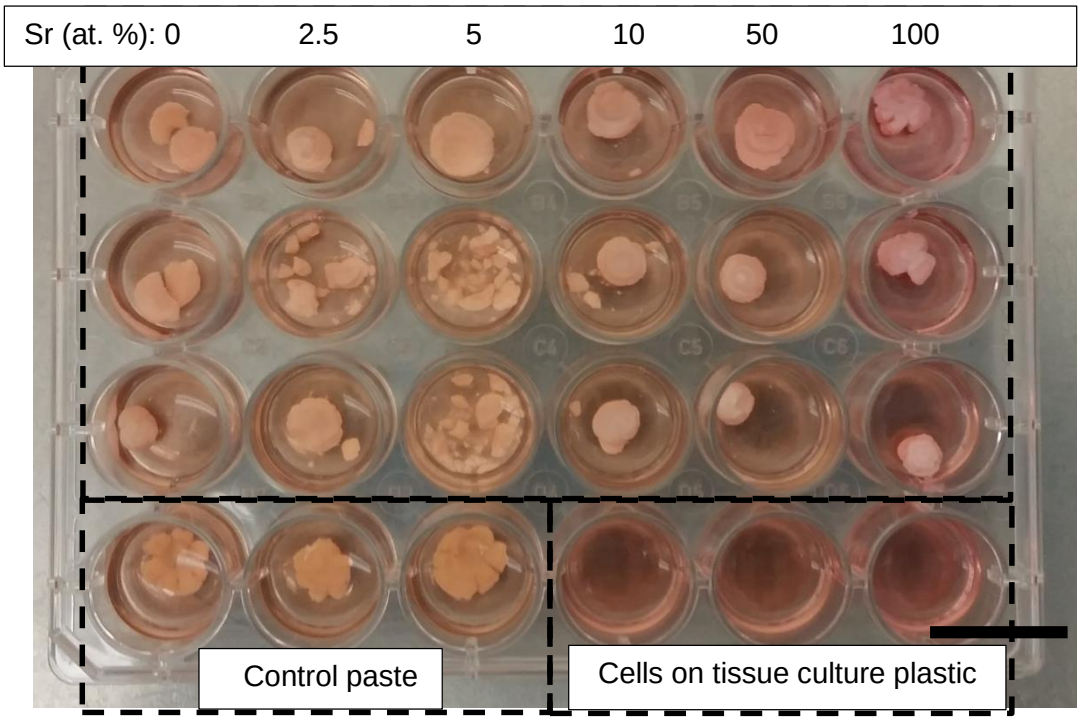

Figure 5.38. Image of 24 well plate after 48 h incubation of MG63 cells with strontium-substituted nHA pastes produced using optimised method 1 (0, 2.5, 5, 10, 50 and 100 at. % Sr), control paste (ReproBone *novo*^{TM}) and with no material present after 48 h incubation with MG63 cells. All samples in triplicate. Scale bar = 2 cm.

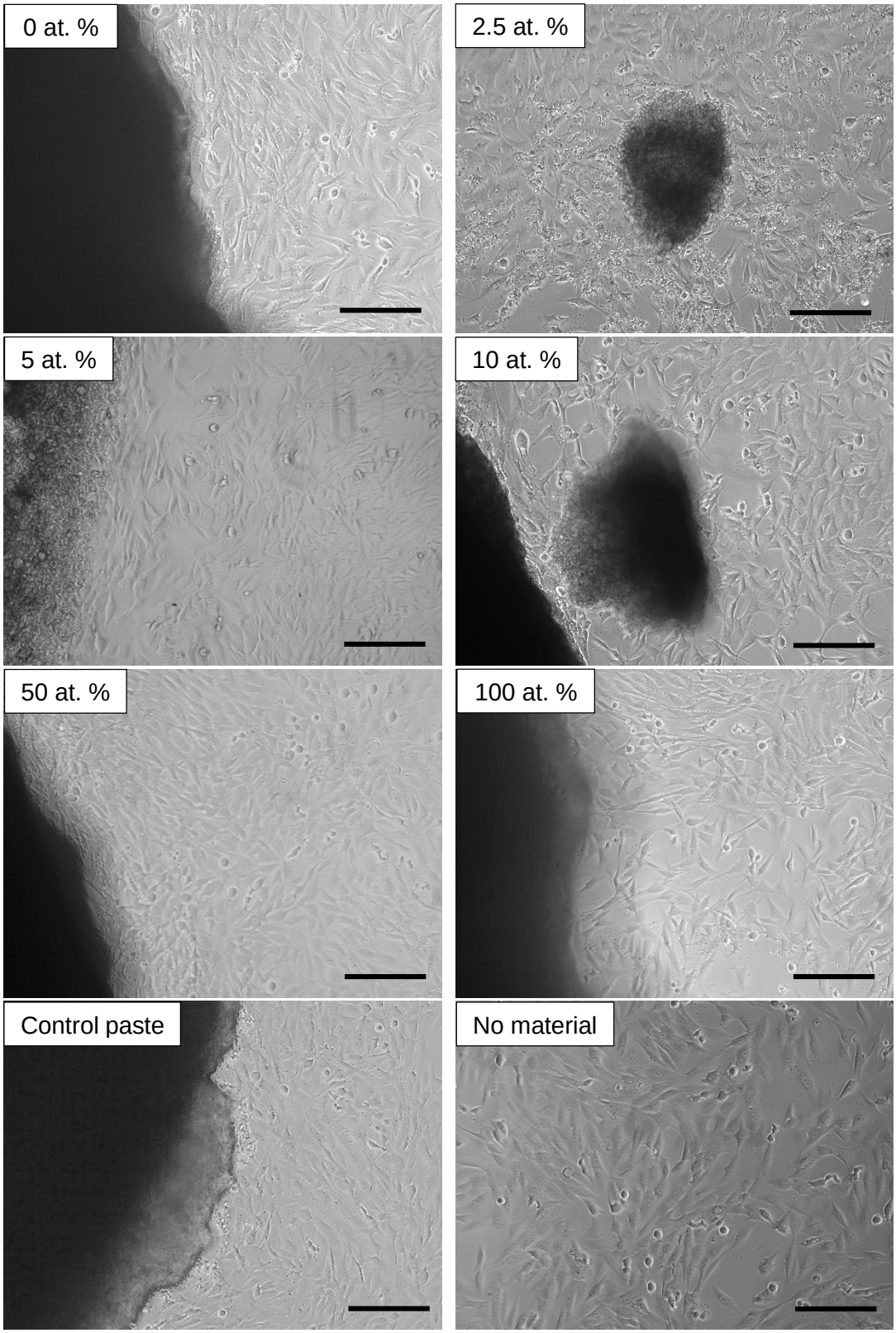

Figure 5.39. Light microscopy images for MG63 cells cultured directly with strontium-substituted nHA pastes produced using optimised method 1 (0, 2.5, 5, 10, 50 and 100 at. % Sr), control paste (ReproBone *novo*™) and with no material present. Scale bar = 200 µm.

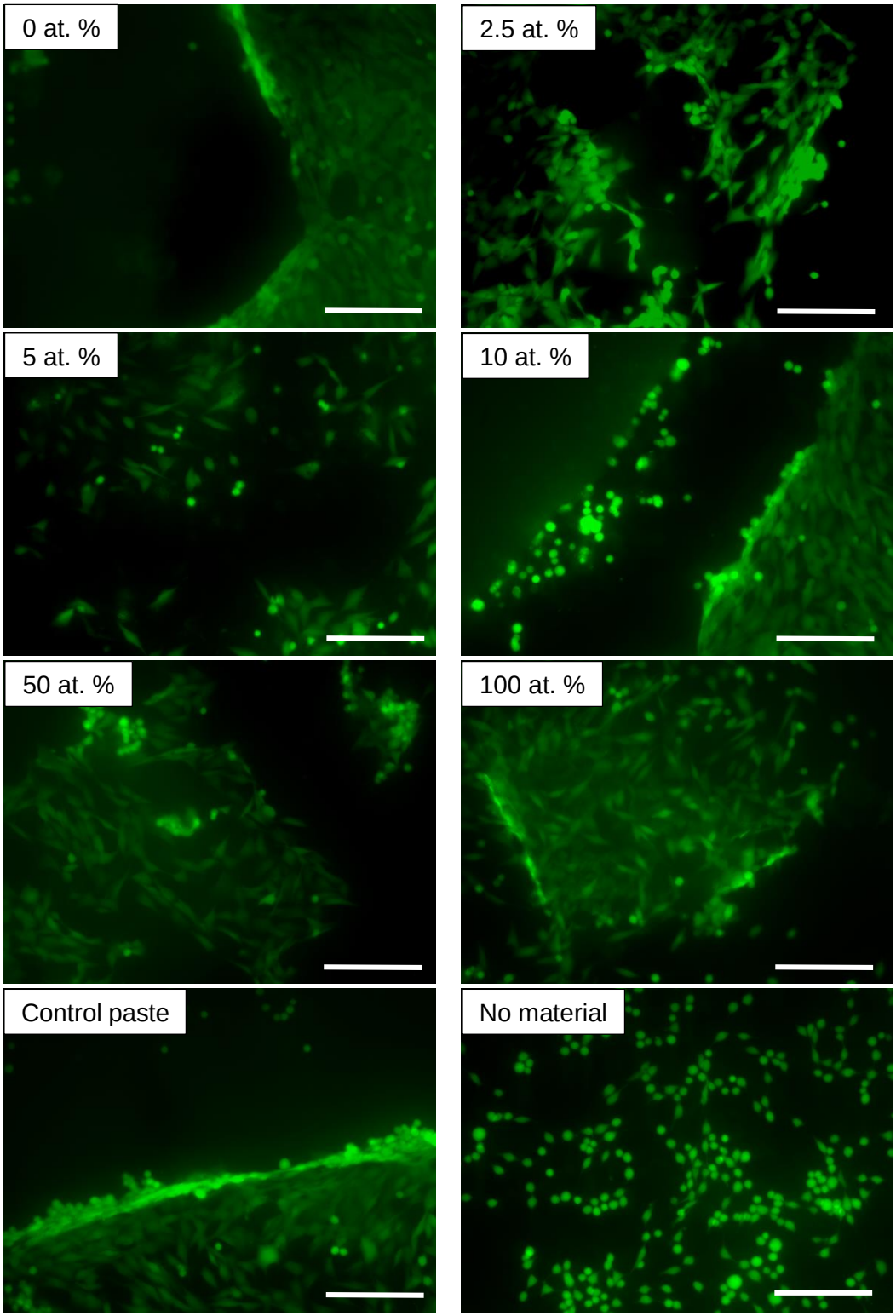

Figure 5.40. Live/Dead fluorescence imaging for MG63 cells cultured directly with strontium-substituted nHA pastes produced using optimised method 1 (0, 2.5, 5, 10, 50 and 100 at. % Sr), control paste (ReproBone *novo*™) and with no material present. Only green channel shown. Scale bar = 200 µm.

Preconditioned media produced by incubation with the strontium gels had no detrimental effect on the viability of the cells (Figure 5.41). nHA particles were also observed in the preconditioned media after centrifugation, as observed for the paste preconditioned media. Live/Dead fluorescence images showed good cell survival, with few dead cells observed (Figure 5.42).

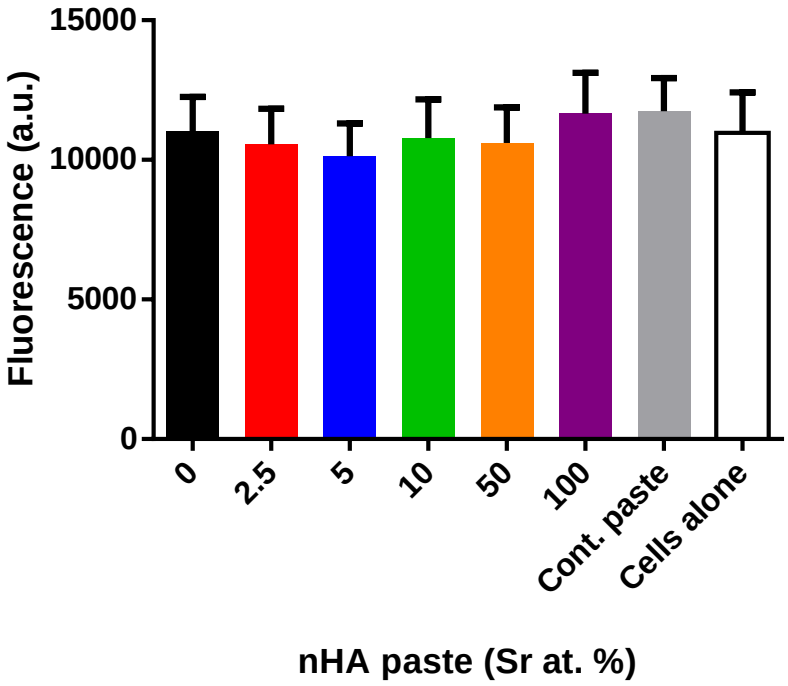

Figure 5.41. PrestoBlue® viability assay results at 24 h for MG63 cells cultured indirectly with strontium-substituted nHA gels produced using optimised method 3 (0, 2.5, 5, 10, 50 and 100 at. % Sr), control paste (ReproBone *novo*™) and with no material (n = 9). Error bars ± standard error of the mean. No significant difference was observed between the materials tested.

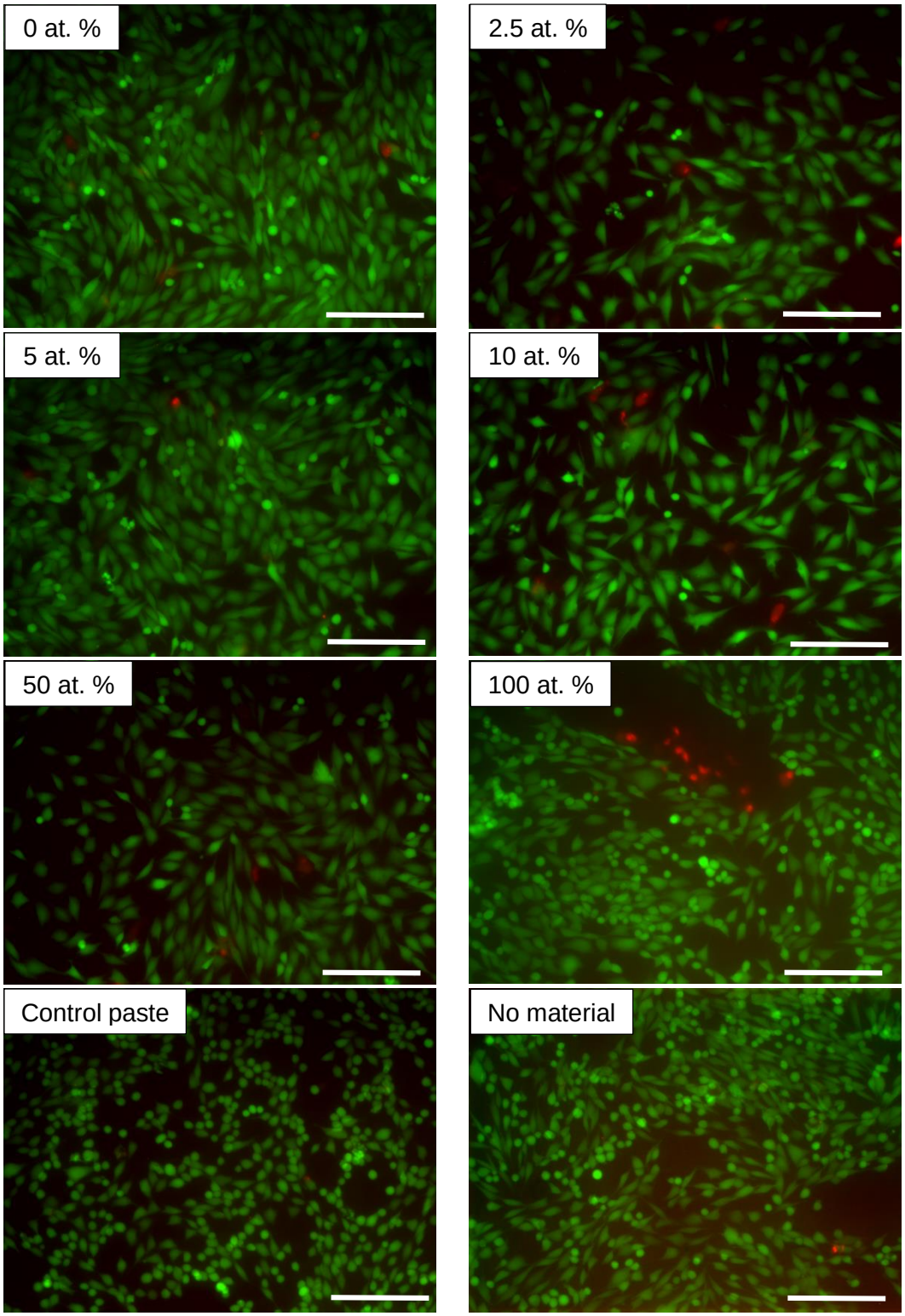

Figure 5.42. Live/Dead fluorescence imaging for MG63 cells cultured indirectly with strontium-substituted nHA gels produced using optimised method 3 (0, 2.5, 5, 10, 50 and 100 at. % Sr), control paste (ReproBone *novo*™) and with no material present. Scale bar = 200 µm.

Cells grown with 0 and 100 at. % Sr nHA gels had significantly reduced viability compared with 50 at. % Sr nHA gel, the control paste and cells on tissue culture plastic (Figure 5.43). Furthermore, cells cultured with 2.5 at. % Sr nHA gel had a lower viability than those cultured with 50 at. % Sr nHA gel and the control paste. The nHA gels were observed to fragment considerably during the 48 h incubation period (Figure 5.44). Microscopy images displayed the growth of cells in direct contact with paste (Figure 5.45). Similarly to the Live/Dead fluorescence images for the nHA pastes, cells with a rounded morphology were observed at the edges of the gels, which may have been evidence of cells growing within the gels (Figure 5.46).

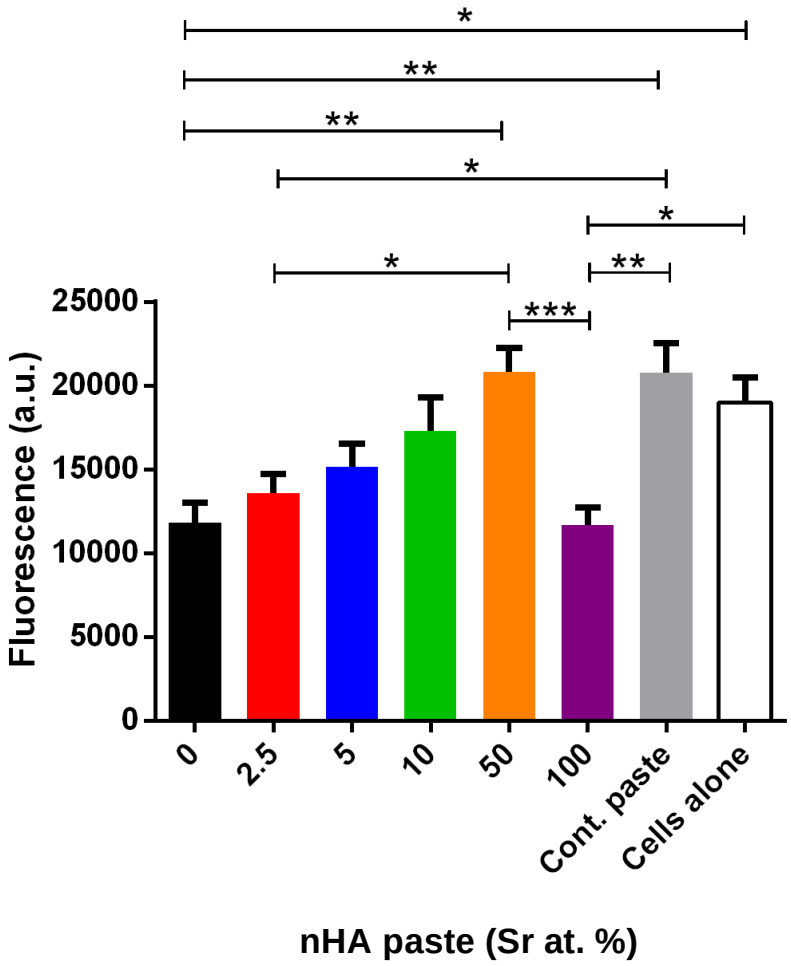

Figure 5.43. PrestoBlue® viability assay results at 48 h for MG63 cells cultured directly with strontium-substituted nHA gels produced using optimised method 3 (0, 2.5, 5, 10, 50 and 100 at. % Sr), control paste (ReproBone *novo*™) and with no material (n = 9). Error bars ± standard error of the mean. Significance level: *: p< 0.05, **: p< 0.01, ***: p< 0.001.

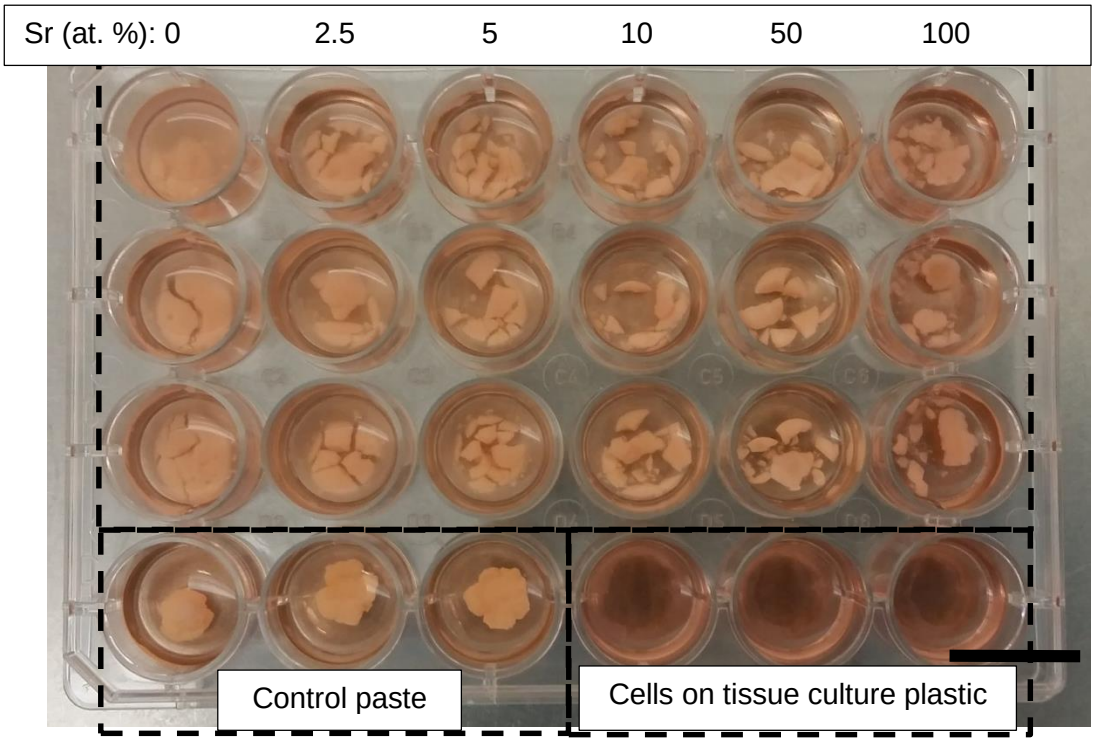

Figure 5.44. Image of 24 well plate after 48 h incubation of MG63 cells with strontium-substituted nHA gels produced using optimised method 3 (0, 2.5, 5, 10, 50 and 100 at. % Sr), control paste (ReproBone *novo*^{TM}) and with no material present. All samples in triplicate. Scale bar = 2 cm.

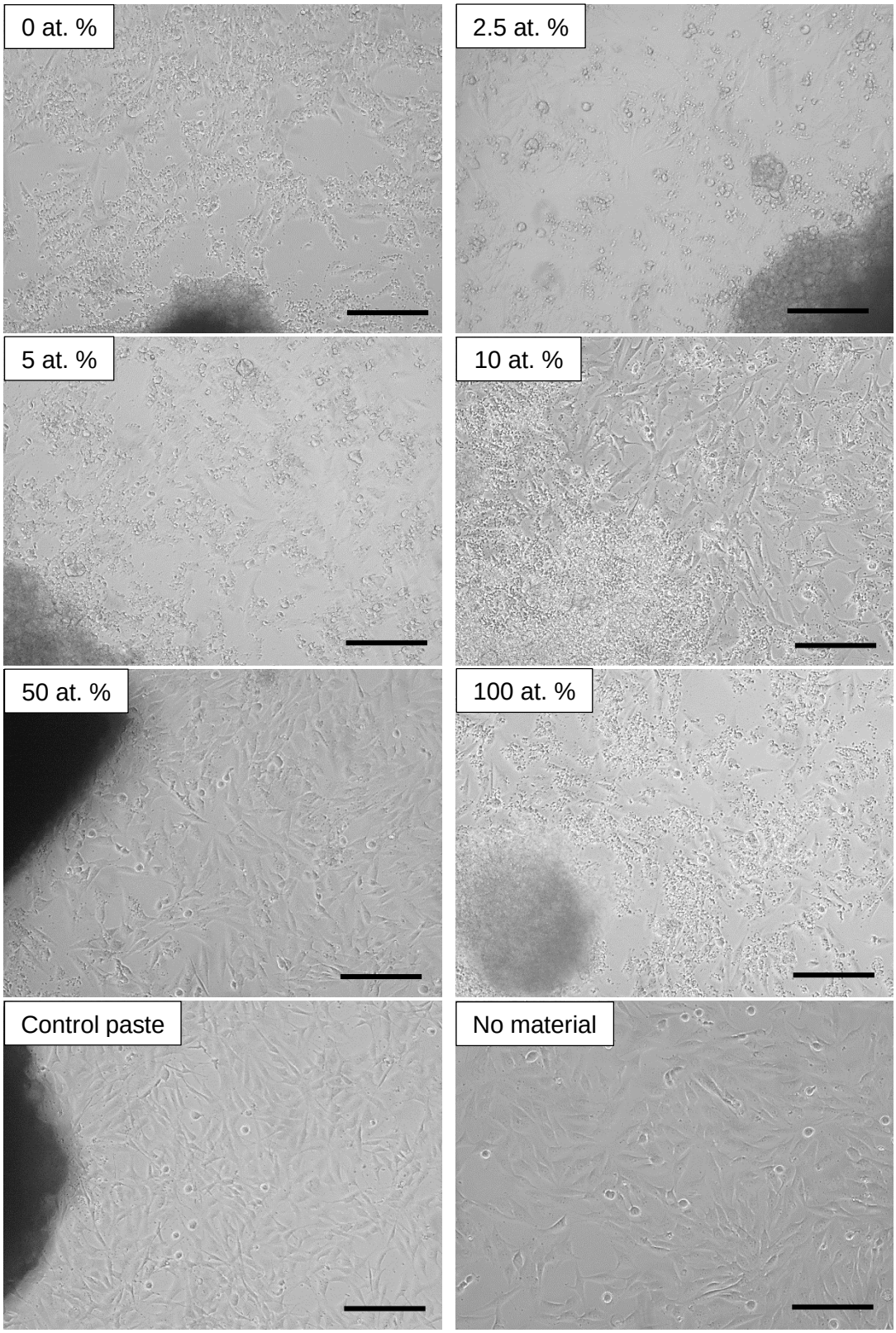

Figure 5.45. Light microscopy images for MG63 cells cultured directly with strontium-substituted nHA gels produced using optimised method 1 (0, 2.5, 5, 10, 50 and 100 at. % Sr), control paste (ReproBone *novo*™) and with no material present. Scale bar = 200 µm.

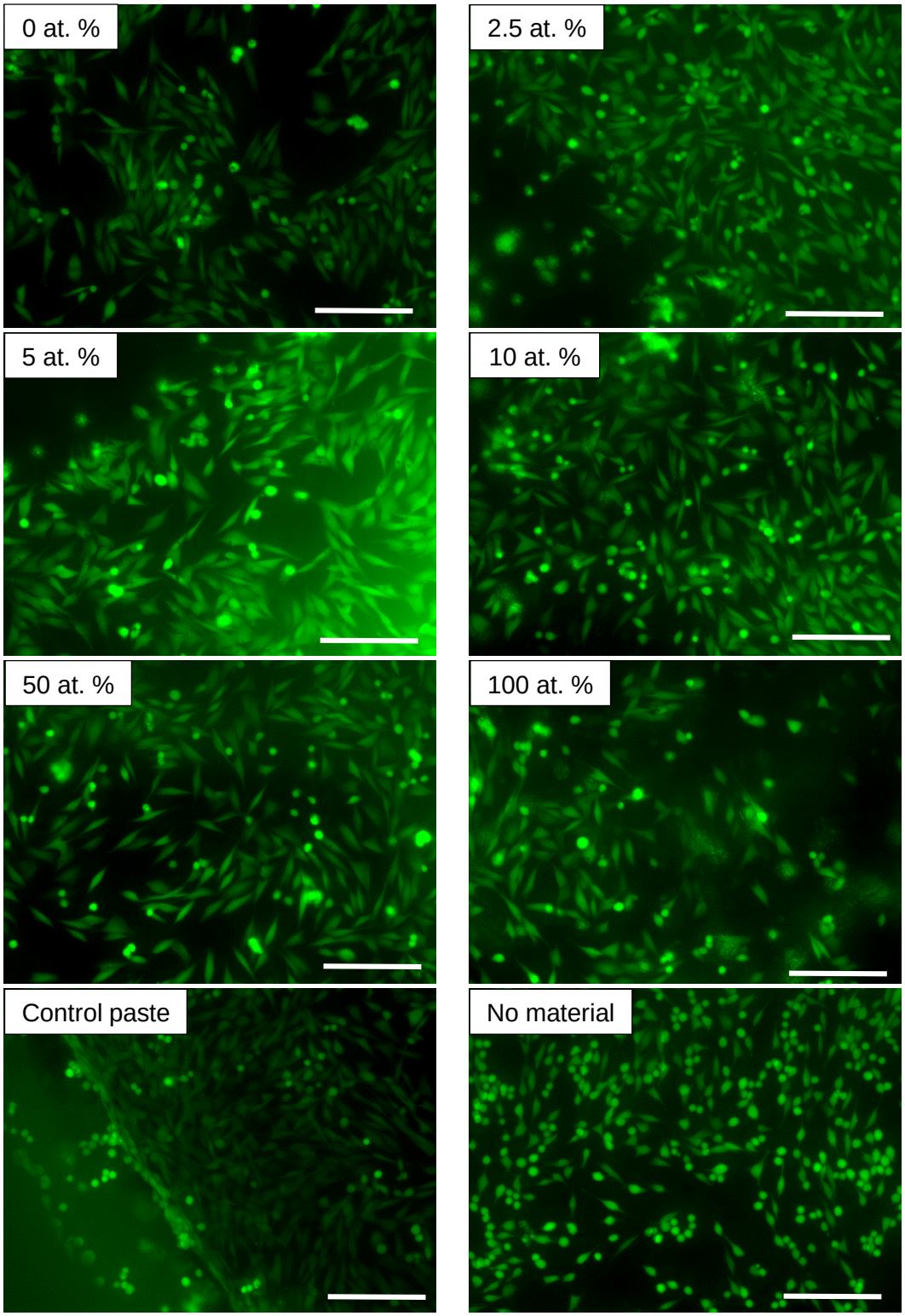

Figure 5.46. Live/Dead fluorescence imaging for MG63 cells cultured directly with strontium-substituted nHA gels produced using optimised method 3 (0, 2.5, 5, 10, 50 and 100 at. % Sr), control paste (ReproBone *novo*^{TM}) and with no material present. Only green channel shown. Scale bar = 200 µm.

The comparison of the indirect and direct biocompatibility results for the strontium-substituted nHA pastes and gels (Figure 5.47) showed that the viability data for the indirect paste and gel cultures followed the same pattern, with a reduction in viability observed from 0 at. % to 5 at. % Sr nHA. The viability then increased for the cells cultured indirectly with the 5 at. % to 100 at. % Sr nHA pastes and gels. Direct viability results showed a reduction in viability for 100 % at. Sr nHA paste and gel compared with the highest direct viability results for the pastes (0 at. % Sr) and gels (50 at. % Sr) respectively. Similarly to the indirect assays, the direct paste assays showed a reduction in viability for the 5 at. % Sr paste.

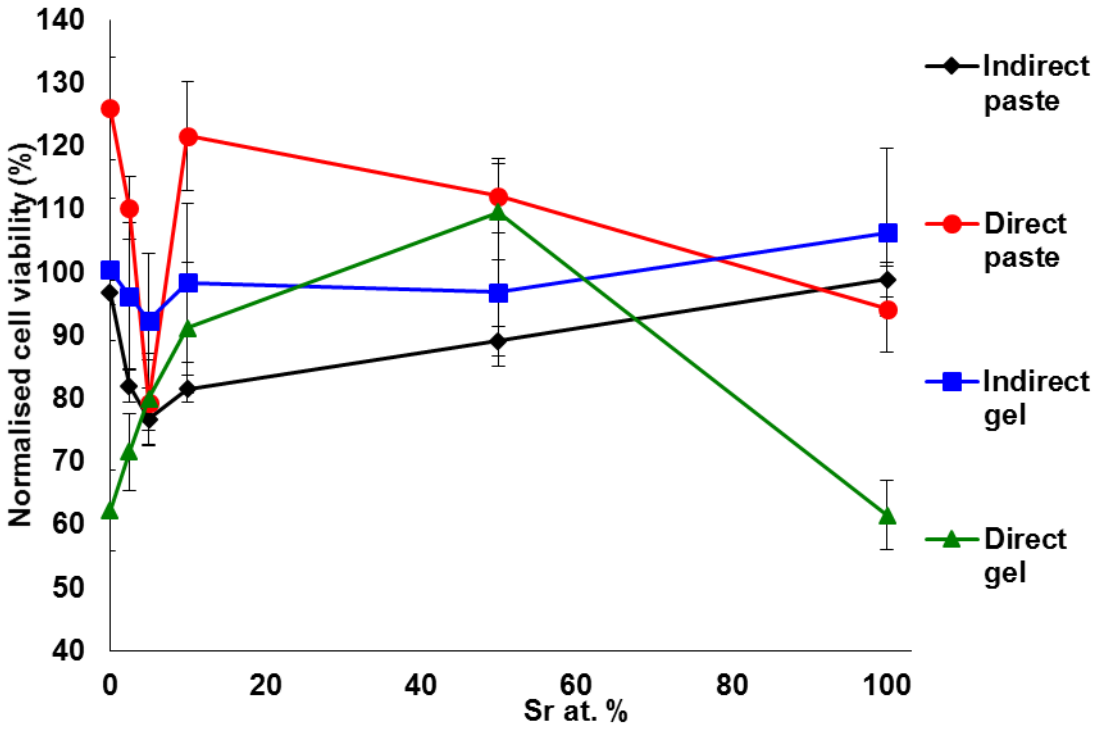

Figure 5.47. PrestoBlue® viability assay results at 48 h for MG63 cells cultured directly and indirectly with strontium-substituted (0, 2.5, 5, 10, 50 and 100 at. % Sr) nHA pastes produced using optimised method 1 and gels produced using optimised method 3. All data was normalised to the experimental cell control with no material present. Error bars ± standard error of the mean.

5.5.2 Antibacterial Activity of Silver-doped Nanoscale Hydroxyapatite Pastes Produced by Altered Method 1

Agar diffusion assays to investigate the antibacterial activity of the silver-doped nHA pastes against *S. aureus* and *P. aeruginosa* displayed a clear growth inhibition zone surrounding the silver-doped materials (Figure 5.48). There was no zone of inhibition observed around the nHA paste that was not silver-doped. For the agar diffusion assay involving *S. aureus,* silver was observed to have chemically reduced on the surface of the silver-doped pastes whilst no chemically reduced silver was observed on the surface of the pastes for the *P. aeruginosa* agar diffusion assay. ICP results confirmed the presence of silver ions in the agar adjacent to the paste materials with the higher silver-doped materials allowing greater diffusion of silver ions into the agar gel (Figure 5.49). The amount of silver detected in the agar when the paste were incubated with *S. aureus* was consistently lower than when the pastes were incubated with *P. aeruginosa*.

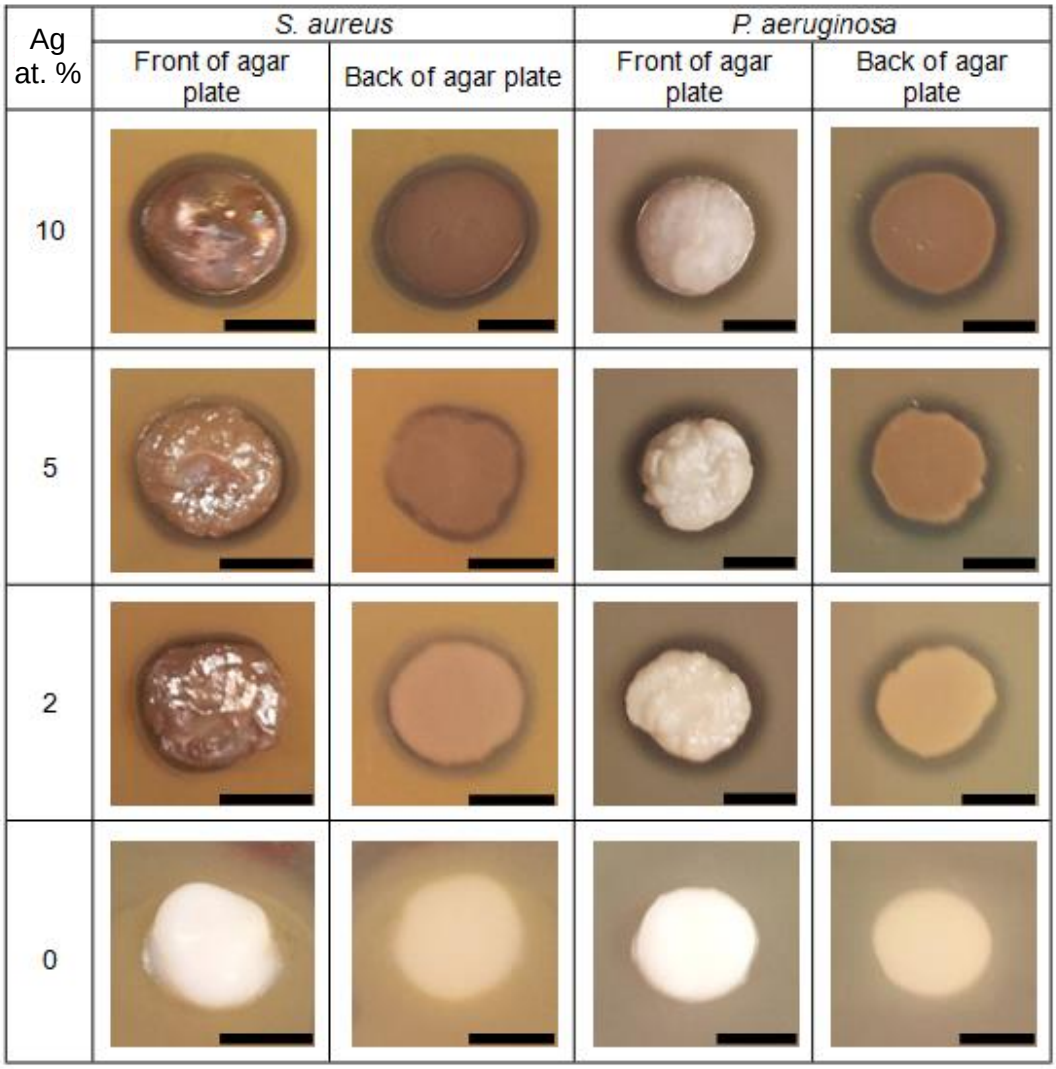

Figure 5.48. Agar diffusion assay of 0, 2, 5 and 10 at. % silver-doped nHA paste incubated overnight with *S. aureus* and *P. aeruginosa,* scale bars = 0.5 cm.

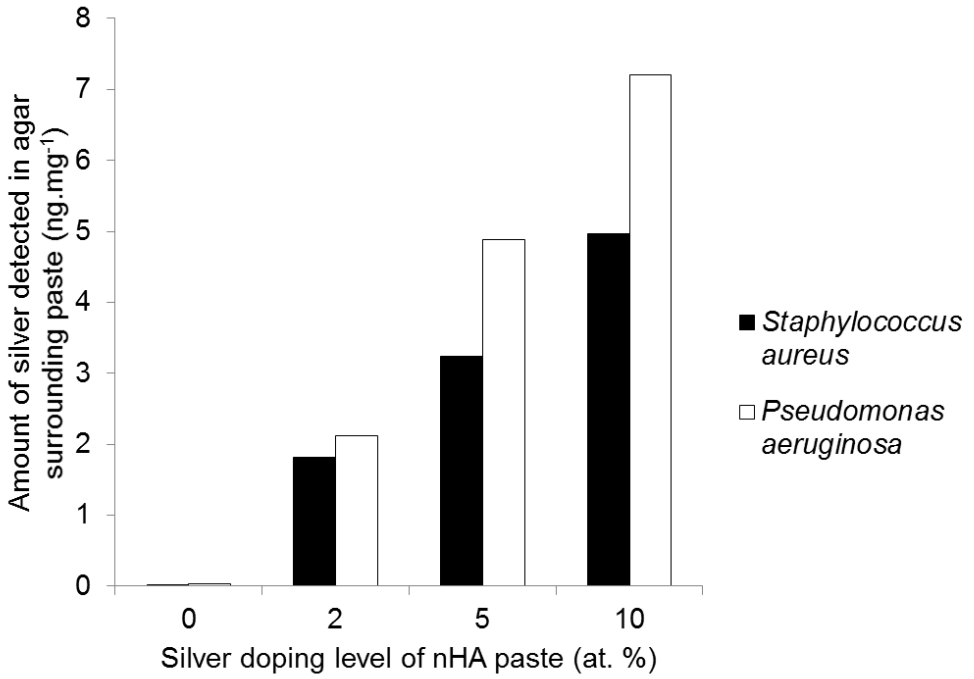

Figure 5.49. ICP-MS quantification of silver concentration in agar plugs surrounding the silver-doped nHA paste materials for agar diffusion assays with *S. aureus* and *P. aeruginosa,* n=2, difference between experiments did not exceed 1.5 $ng.mg^{-1}$.

When the bacteria were cultured in suspension with the pastes there was a reduction in bacterial growth observed for the paste with no silver-doping as the concentration of the paste was increased (Figure 5.50). However, the silver-doped pastes showed a greater level of growth inhibition in a dose dependent manner with the 10 at. % silver-doped paste inhibiting bacterial growth the most followed by the 5 and the 2 at. % silver-doped nHA pastes respectively. This was clearly shown by the increasing MIC for the silver-doped pastes with a higher silver-doping level (Table 5.10). There was also an increase in the optical density for the highest concentrations of the 10 at. % silver-doped paste when investigated in suspension culture against *S. aureus,* which was not observed as clearly when *P. aeruginosa* was cultured with the 10 at. % silver-doped material.

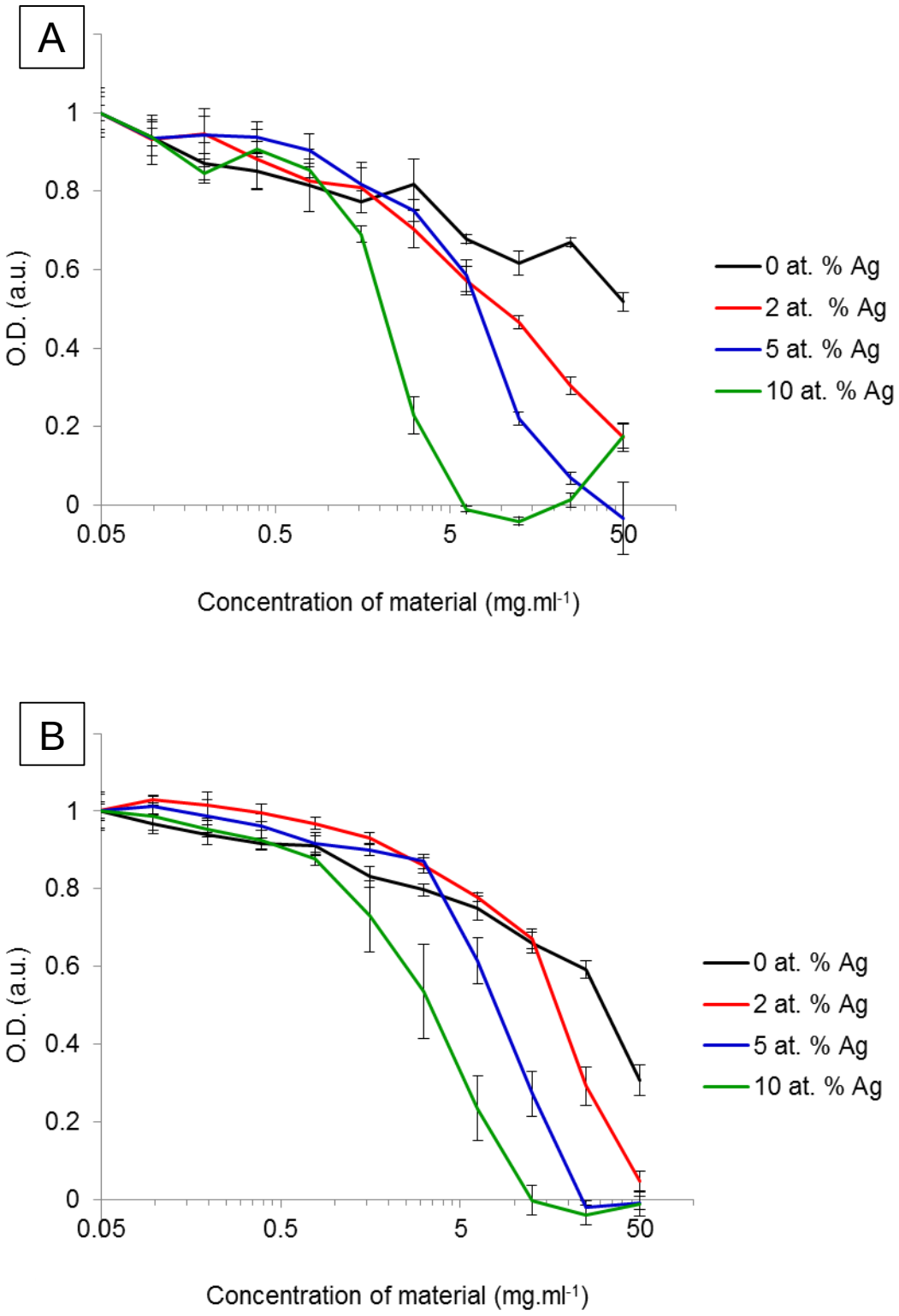

Figure 5.50. Optical density of *S. aureus* (A) and *P. aeruginosa* (B) in suspension culture at 20 h incubated with 0, 2, 5 and 10 at. % silver-doped nHA paste (paste material control subtracted) (n = 9). Error bars ± standard error of the mean.

Table 5.10. Minimum inhibition concentration (MIC) of silver-doped nHA pastes in $mg.mL^{-1}$.

Organism	**Level of silver-doping in nHA paste (at. %)**			
	0	2	5	10
S. aureus	>50	12	9	2.5
P. aeruginosa	35	29	8	3.5

6. Discussion

6.1 Evaluation of Wet Precipitation and Sol-gel Methods of Nanoscale Hydroxyapatite Synthesis (Methods 1 - 4)

During the evaluation of the nHA synthesis methods, the wet precipitation method proved to be a reliable and convenient method for the production of nHA particles with a high aspect ratio (i.e. needle shaped). Method 1, involving the reaction of calcium hydroxide and phosphoric acid, was particularly advantageous due to the simple acid-base nature of the reaction which avoided the formation of chemical by-products. Indeed, the high alkalinity of calcium hydroxide allowed for the reaction pH to be 'self-controlled' [127], thereby simplifying the preparation by removing the need for additional pH control. However, the major concern with this method was the presence of residual calcium hydroxide which was expected to have a detrimental effect on the pH when the product was placed in an aqueous environment. This, in turn, could compromise the biocompatibility of the material. XRF data (Table 5.1) suggested that the presence of calcium hydroxide was minor, with the Ca:P ratio only increasing by 1.8 % from the stoichiometric HA value of 1.67.

For the wet precipitation method 2 (reaction of calcium chloride and potassium phosphate), the complete thermal decomposition and the low Ca:P ratio (1.38) suggested that the precipitated nHA was particularly calcium-deficient (Figure 5.3 and Table 5.1). For this reaction, the main factor in the production of calcium-deficient HA was likely to be too low a pH which led to the incorporation of HPO_4 groups. However, since the pH had already been adjusted to 11 and 12 prior to the titration for the calcium and phosphorus solutions respectively, this method was deemed to be difficult for the large scale production of nHA due to the strong basic pH that would be required to produce a stoichiometric nHA and ensure that no other calcium phosphate phases were produced. The thermal decomposition of nHA below 1000

°C, prepared using the wet precipitation method, has been reported elsewhere [86, 175]. It is recognised that the decomposition temperature of HA is strongly dependent on the synthesis conditions [86, 88] such as the amount of solution ageing time and the solution pH. It has been well documented that the main cause for low temperature thermal decomposition is the formation of calcium-deficient HA. For instance, Gibson *et al.* reported decomposition temperatures between 710-740 °C for calcium-deficient HA [213]. The XRD reference cards of calcium-deficient HA and stoichiometric HA are remarkable similar and this makes phase identification extremely difficult particularly especially on unsintered samples with low crystallinity.

Sol-gel method 3, involving the reaction of calcium nitrate and ammonium phosphate, was found to successfully produce low aspect ratio nanoscale HA particles with good thermal stability; only minor decomposition was observed when the product was sintered at 1000 °C (Figure 5.5 and Figure 5.6). The low stoichiometric Ca:P ratio (1.51) was again likely to contribute to the lower thermal stability of this calcium-deficient sample. The thermal decomposition of HA synthesised using the sol-gel method has been widely reported [88, 184, 214]. Indeed, sol-gel nanoscale HA sintered at temperatures as low as 600 °C has been found to contain β-TCP [190]. In the literature, the reaction between calcium nitrate and ammonium phosphate to produce hydroxyapatite has been referred to both as a sol-gel [184-186, 215] and a precipitation method [90, 180, 181, 216, 217]. The sol-gel classification was adopted for this thesis due to the formation of a gel during the drying process.

In contrast to all of the other nHA preparation methods, there were no detectable crystalline phases prior to sintering for sol-gel method 4 (reaction of calcium nitrate and triethyl phosphite) (Figure 5.7). The presence of β-TCP when the product was sintered demonstrated a deviation from stoichiometry. These XRD results displayed that a sintering temperature of 600 °C was required to achieve a detectable level of β-TCP in the XRD patterns (Figure 5.8). Sol-gel powders with a high thermal

sensitivity were also reported by Fathi *et al*. [88]; hydroxyapatite was the only phase present when the sample was sintered at 600 °C, whereas β-TCP and CaO were present after sintering at 700 °C. For hydroxyapatite prepared using sol-gel methods, lower sintering temperature are required to densify the ceramics compared to powders produced using wet precipitation. The lower sintering temperature required has been attributed to the higher reactivity of the sol-gel powders [218] and the smaller particle size formed by the sol-gel method [190]. The XRF results for these samples were varied suggesting that the chemical homogeneity of the sample was poor, which was surprising since the sol-gel method is said to promote molecular level mixing resulting in high chemical homogeneity [184]. The detection of ammonium nitrate in the sintered samples showed that the washing stages were inadequate to remove this by-product from the reaction. Furthermore, it can be seen that a sintering temperature above 600 °C is necessary to thermally decompose all of the residual ammonium nitrate.

The nHA particles produced using method 4 were the largest obtained from all the methods due to the high temperature treatment which causes particle growth by diffusion (sintering) (Figure 5.8). The additional steps of washing with centrifugation were also time consuming and a considerable disadvantage of the method, when compared to the previous methods. Furthermore, the requirement to sinter the material prior to obtaining a HA phase was considered unsuitable for the production of an injectable nHA paste or gel. Instead it was deemed preferable not to dry the nHA suspension fully to prevent agglomeration. Therefore, to produce the paste and gel materials the drying of the nHA suspensions was stopped when an appropriate water content was obtained. For the evaluation of the initial methods, FTIR analysis would have been useful in determining how the presence of carbonate and hydrogen phosphate groups may have affected the thermal stability of the nHA prepared.

From these initial methods, 1 and 3 were selected for further development due to their favourable properties. The major advantages associated with each method were the relative ease of nHA production and the absence of by-products for method 1. The good chemical stoichiometry and small nanoscale dimensions of the products were also favourable, as well as the possible production of a nHA gel using method 3. The major difference between methods 1 and 3 was the solubility of the calcium reagent which may have contributed to the different particle morphologies obtained.

Calcium hydroxide has a very low solubility and therefore only a limited amount of calcium is available for conversion into hydroxyapatite at any one time. In contrast, the high solubility of calcium nitrate allows for a high availability of calcium which greatly affects the precipitation kinetics. As discussed by Prakash *et al*. [176], the effect of temperature on nHA particle morphology is completely opposite for systems involving calcium hydroxide and more soluble calcium salts such as calcium nitrate or calcium chloride. It was reported that, during nHA synthesis with calcium hydroxide and phosphoric acid, an increased reaction temperature was found to yield particles with a lower aspect ratio (i.e. more rounded). Conversely, an increase in reaction temperature increased the particle aspect ratio (i.e. became more needle-like) when investigated for calcium chloride and sodium phosphate. Since a higher precipitation rate results in particles with a high aspect ratio, the final crystal morphology can highlight the differences in the precipitation kinetics. Indeed, the difference in the Gibbs free energy is the stimulating factor for precipitation which depends upon the concentration of the ions and the temperature of the reaction among other thermodynamic factors. The simple control of particle morphology by temperature is an advantage due to the ability to yield different nHA morphologies and in turn behaviours. As well as physicochemical, rheological and mechanical differences, the bioactivity of nHA is likely to be affected by its particle morphology. Therefore, the

production of different nHA morphology may provide optimised particles for different applications.

6.2 Development of Selected Synthesis Methods (Methods 1 and 3)

6.2.1 Development of Method 1

The rate of the phosphoric acid addition was found to have the greatest effect of all the synthesis parameters investigated, in terms of chemical composition and particle morphology of the product (Table 5.2 and Figure 5.10). When the phosphoric acid was poured into the calcium hydroxide suspension, the rapid decrease in the pH of the solution was likely to have contributed to the successful conversion of the poorly soluble calcium hydroxide into hydroxyapatite by encouraging the dissolution of calcium hydroxide. Since the main intensity XRD peak of calcium hydroxide overlaps with the (202) HA peak at 34.1° degrees 2θ, it is only in the sintered sample that the presence of calcium hydroxide in the precipitated product can be inferred from the detection of its thermal decomposition product, calcium oxide [174]. The elimination of the calcium hydroxide residue by the increase in addition rate can clearly be seen from the XRD results, with no calcium oxide residue in the rapidly mixed sintered product (method 1-B) as opposed to its presence in the product prepared using slow titration (method 1-A). These results were in contrast to those reported by Bouyer *et al*. [174]; in their study, calcium oxide was detected in the XRD pattern at the highest phosphoric acid addition rate (2.4 $L.min^{-1}$) which indicated the presence of calcium hydroxide in the precipitated product. It is possible that the calcium hydroxide used by Bouyer *et al.* was composed of larger particles than that used in this project, which could explain the increased solubility of calcium hydroxide observed in the current investigations. Several other strategies have been suggested to eliminate the calcium hydroxide residue including increased stirring, using a lower minimum adjusted pH level and adding extra acid [177].

It is likely that the low pH caused by the rapid addition of phosphoric acid contributed to the incorporation of HPO_4 groups into the HA, which caused the precipitation of a calcium-deficient product with a lower thermal stability. This hypothesis is supported by the lower than stoichiometric Ca:P ratio (1.63) obtained for the nHA prepared using the optimised route 1 method. It has been suggested that the hydroxyl ions in the calcium hydroxide suspension are rapidly neutralised when the phosphoric acid solution is added quickly, which lowers the pH in the majority of the suspension but not at the surface of the calcium hydroxide particles [177]. A similar effect was also reported by Osaka [219] where a high phosphoric acid addition rate caused the precipitation of HA with a lower thermal stability. As mentioned previously, it is well established that calcium-deficient HA (CDHA) has a lower thermal decomposition temperature than stoichiometric HA [213, 220-222]. In detail, it is believed that the increased thermal instability of calcium-deficient HA is due to the condensation of the HPO_4^{2-} ions and the subsequent reaction of $P_2O_7^{4-}$ ion with the OH^- ion [221]. Using a combination of XRD and FTIR, Gibson *et al.* were able to identify structural changes between 500 and 1100 °C during the thermal decomposition of CDHA [213]. In this study, CDHA with a Ca:P ratio of 1.5 was found to decompose over 710 – 740 °C. The thermal stability of CDHA is likely to be dependent on the degree of calcium deficiency, however it is difficult to make comparison between different studies due to the different processing parameters used. As discussed by Gibson *et al*., the different decomposition temperatures reported by various researchers may be due to the different sintering times used [213].

The noticeable effect of the phosphoric acid addition rate on the nHA particle morphology could clearly been seen in TEM images (Figure 5.10). The changes in particle morphology can be attributed to the difference in the precipitation rate [175, 176]. Interestingly, the rapid addition of phosphoric acid caused a reduction in the precipitation rate resulting in particles with a decreased aspect ratio, whereas the

particles with a higher aspect ratio correspond with a faster precipitation rate. This can also be explained by considering the energy of particle growth verses the energy of new particle nucleation. As discussed by Bouyer *et al.,* when the rate of crystal nucleation becomes higher than the rate of crystal growth, the specific surface area increases typically resulting in a larger number of smaller particles [174]. Similar results were reported by Afshar *et al.* with a slower acid addition rate contributing to the growth of larger particles [177].

The lower solubility of calcium hydroxide at an increased temperature was likely to have contributed to the presence of residual calcium hydroxide in the titrated nHA product when the calcium hydroxide suspension was heated (method 1-A). However, it was observed that no residual calcium hydroxide was present after the rapid phosphoric acid addition rate was employed even at an elevated temperature (method 1-B). Despite this, the increased conductivity of the nHA suspension when the reaction was carried out at a higher temperature (Table 5.3) may be due to the presence of trace amounts of residual calcium hydroxide. Although not detectable on the XRD pattern, this is an important parameter to consider for obtaining a product with optimal biocompatibility as even the presence of trace amounts of basic calcium hydroxide may detrimentally alter the *in vivo* response through a lowering of pH.

It was difficult to compare the precise effects of temperature change on particle morphology with those reported by other researchers due to the difference in phosphoric acid solution addition rates. Despite the reported effect that temperature has been found to have on nHA morphology, for this project the effect was clearly overshadowed by the notable change caused by the rate of phosphoric acid addition. As described elsewhere for titration reactions, the aspect ratio of the nHA particles increases with increasing temperature. Bouyer *et al.* reported a maximum in crystallite size at 60 °C due to the balance of two thermodynamic effects. It was discussed that although the temperature rise increases the crystallinity of the HA, it also limits the

growth along the c axis due to the nanoscale crystals tending to a monocrystalline phase [174]. For the development of the paste it was decided that a platelet shaped nHA would have superior rheological properties to promote high injectability. There is evidence to suggest that nHA particles with a high aspect ratio have a poorer flowability and pronounced shear thinning effects due to the alignment of the needles under conditions of flow [223, 224]. As this is an important factor for the preparation of injectable nHA systems, it has been highlighted as an area for future work in Chapter 8.

When the concentration of the reactants was increased there were no noticeable changes in the chemical composition or morphology of the nHA (method 1-D compared with method 1-C). Presumably, there exists a maximum concentration at which the chemical diffusion is limited which prevents the successful conversion of the reagents into the products. At certain levels, the precipitation of nHA is likely to be heavily influenced by the reactant concentration due the thermodynamic alterations to the system. For example, the change in the Gibbs free energy, which is the driving force for precipitation, is directly proportional to the ionic concentrations in the solution. The precipitation of nHA is a relatively complex due to the many factors which govern the process. Although relationships on the effect of a particular variable on particle morphology can be made, under different conditions the reverse can be true. This is clearly demonstrated by the effect of temperature which has the opposite effect on aspect ratio for systems with low and high solubility calcium reagents.

In terms of scaling up the method for industrial application, the main consideration should be the effective mixing of the suspension to ensure that the product has good chemical homogeneity. Indeed, it was concluded by Afshar *et al.* that powerful high speed stirring is beneficial in maintaining a homogenous media for the precipitation of a consistent HA product [177].

6.2.2 Development of Method 3

The product formed using method 3 and the thermal stability of the nHA was found to be highly dependent on the pH of the initial calcium and phosphorous solutions (Table 5.4). When the pH was too low, the state of the orthophosphate ions was not suitable for stoichiometric HA preparation. This was due to the incorporation of HPO_4^{2-} ions into the HA crystal structure which caused the formation of calcium-deficient HA [219]. This theory was supported by the reduced Ca:P ratio (1.59) obtained using XRF on the optimised method 3 product. As described for method 1, the preparation of a calcium-deficient nHA decreased the thermal stability of the product. For method 3 there was a clear increase in β-TCP in the sintered product when the pH was lowered (methods 3-B, 3-C and 3-D), thereby demonstrating the thermal stability dependence on the preparation pH. Furthermore, brushite was formed when the pH of the calcium and phosphorus solutions was 9 prior to titration. Brushite is known to form at a lower pH than hydroxyapatite, and has a reported pH stability range of 2.0 – 6.0 compared to 9.5 – 12 reported for hydroxyapatite [225].

No considerable differences were found between the nHA produced when the phosphate solution addition rate was increased (Table 5.4 and Figure 5.11, method 3-A compared with method 3-E), which was in complete contrast to method 1 where chemical and morphological changes were detected. This may be due to the highly soluble nature of the reactants used in method 3, which differs significantly from the sparingly soluble calcium hydroxide used in method 1. The difference in solubility has understandably had an effect on nHA crystal morphology. The presence of small platelet shaped crystals suggests that the precipitation rate was relatively slow and the rate of new particle nucleation was faster than the rate of particle growth. When the concentration of reactants was increased, slightly larger particles were obtained (method 3-F), which suggests that the crystal growth rate was increased by the higher concentration of reactants. As described by Liu *et al*. the precipitation of HA from

solutions of calcium nitrate and ammonium phosphate is a fairly complex multistage process. Initially, octacalcium phosphate is formed which rapidly converts to amorphous calcium phosphate. This is followed by the formation of calcium-deficient HA which then converts to HA. The speed of this process was reported to be temperature dependent, with an increased rate found at higher temperatures [216].

No ammonium nitrate was detected in the dried products demonstrating that the by-product of the reaction had successfully been removed during the washing stages. This was an important factor to consider since the presence of ammonium nitrate may detrimentally affect the biocompatibility of the synthesised gel [226]. Other approaches have included sintering the product to remove the ammonium nitrate [215]. However, this was unsuitable for the production of a nHA gel due to the increase in particle size obtained during high temperature treatment and the agglomeration of nHA particles when the product is dried completely.

The pH was also observed to have an effect on the settling of the nHA suspension. The lower the pH, the lower the settling level of the nHA which in turn affected its' ability to form a stable gel. This was likely to be due to the change in pH affecting the colloidal nature of the settled suspension. In general, the sol-gel method produces a colloidal solution which has been hypothesised to have an oligometric structure. The nHA particles are suspended in the gel phase by the presence of metal hydroxide bonds. During the drying process the particles consolidate through van der Waals attractions [183]. The surface charge of the particles is a key factor in the stability of the solution. Indeed, the decreasing surface charge of the particles characterises the change from a solution into a gel [14]. The pH is likely to affect the nHA particle surface charge and in turn the agglomeration of the particles in the colloidal suspension. The use of a high pH therefore allowed the formation of a stable nHA gel composed of 90 wt. % water.

Considering injectable nHA systems, there is a very limited amount of publications regarding nHA gels. The majority of published work has been focussed on nHA poly(vinyl alcohol) (PVA) hydrogels, which contain molecular chains of PVA cross linked by irradiation. These gels are generally developed with the view to use for articular cartilage repair [227-229]. Other nHA gels have been based on collagen and alginate [230], or collagen and chitosan [231] gel networks. The polymer gel networks add extra complexity to the production and processing of these materials for use as medical devices. However, providing the product has been washed of by-products which may be detrimental to the biocompatibility, the 'gel' stage of the sol-gel process may provide a simple nHA gel material composed of nHA particles suspended in water suitable for bone tissue augmentation. Although not formally defined, it could be suggested that paste and gels differ in their water content and appearance with translucent gels possessing a higher water content than the corresponding opaque paste materials.

6.3 Production and Characterisation of Strontium-substituted Nanoscale Hydroxyapatite (Optimised Methods 1 and 3)

The substitution of strontium for calcium in the HA crystal lattice had a variety of physicochemical effects which were detected using a range of materials characterisation techniques. Firstly, the increase in the unit cell parameters for the strontium-substituted nHA was evident in the peak shift to lower degrees 2θ displayed in the XRD patterns (Figure 5.12, Figure 5.13 and Figure 5.21). Indeed, increased peak shift was observed for a higher amount of strontium substitution for both optimised methods. The larger ionic radius of strontium when compared to calcium was responsible for the increase in lattice parameters. As reported by O'Donnell *et al.*, the increase in the lattice parameters, unit cell volume and density were linear over the whole range of strontium substitution (0 – 100 at. %) [124]. It was observed that the XRD pattern for the 100 at. % strontium HA had the highest intensity peaks.

This effect may be due to the greater electron density of strontium which allows for the efficient scattering of X-rays [124].

It has been reported that strontium is able to substitute into both calcium sites within the HA crystal lattice, with some reports suggesting a preference for strontium substitution into the M(II) site [124]. It has also been found that at very low strontium content (at. %) a slight preference for the M(I) site exists. In detail, for strontium incorporation below 1 at. % a preference for the M(I) site was observed. Since HA contains six M(II) sites and four M(I) sites, the ideal statistical occupancy can be described as M(II)/M(I) equating to 1.5. This ratio was achieved for compositions around 5 at. %. At higher strontium substitutions the preference for the M(II) site was confirmed [232]. Similar results were reported by Bigi *et al*. with a preference for the M(I) site found for 5 at. % compared to a preference for the M(II) site for 10 and 50 at. % [125]. Theoretical analysis suggested that strontium substitution caused a strong local distortion on the HA crystal lattice, with more distortion encountered at the M(II) site. Specifically the metal oxygen bond structures at the metal sites cause lattice disorder [232]. The M(II) site has been described as 'larger' than M(I) to signify the increased preference for the larger strontium ion to occupy this site. This is due to the ability of the M(II) atoms to form staggered equilateral triangles, compared to the constrained columns of the M(I) sites aligned parallel to the c-axis. The preference for the M(I) site at lower concentrations may be explained by the longer M(I)-O distances when few strontium atoms are present [125].

Sr nHA produced using optimised method 1 displayed greater thermal instability with the co-presence of strontium and calcium in the crystal, since the lowest intensity breakdown product peaks were observed for 100 at. % calcium nHA and 100 at. % strontium nHA (Figure 5.13). This is likely to be due to strain exerted on the crystal lattice due to the size difference between the two atoms. For instance, it was reported that 50 at. % strontium-substituted nHA had the smallest crystallite size over the

range of 0 – 100 at. % strontium substitution due to the greater amount of disorder in the crystals [124]. A similar effect was reported elsewhere with a low content of strontium decreasing the crystallite size whilst a higher content of strontium significantly increased the crystallinity of the product [125]. The decrease in crystallinity was reported to be caused by the incorporation of strontium increasing the length of the metal hydroxyl bond which also decreased the lattice energy [128]. The decrease in the crystallite size can be observed by the broadening of the XRD peaks, with the unsintered 50 at. % Sr samples produced using both methods having the broadest peaks (Figure 5.12 and Figure 5.21). Further evidence for the reduced crystallite size of the strontium and calcium mixed apatite was observed in the FTIR-ATR spectra (Figure 5.16, Figure 5.18 and Figure 5.25), where the phosphate group bands were broader for the 50 at. % strontium hydroxyapatite compared with all the other compositions (0, 2.5, 5, 10 and 100 Sr at. %) produced using both optimised methods. Other researchers have correlated the reduction in phosphate group band definition with a decreased product crystallinity [208, 233]. The measurement of the FWHM (Table 5.5) of the (002) XRD peak showed the increase in crystallite size as the products were sintered. However, no measureable change in the FWHM for the 100 at. % Sr sample was detected. This may be due to the high intensity diffraction pattern already observed for the unsintered 100 at. % Sr nHA material.

The noticeable difference between the thermal stability of the strontium-substituted nHA produced by the different optimised methods suggested that the optimised method 3 product had a greater degree of calcium / strontium deficiency (Figure 5.13 and Figure 5.22). However, it is interesting to note that the 100 at. % strontium-substituted sample produced using optimised method 3 ((Ca+Sr)/P of 1.52) had a much lower thermal stability than the 100 at. % strontium-substituted sample produced using optimised method 1 ((Ca+Sr)/P of 1.50) (Table 5.6).

It has been reported that the presence of B-type carbonate substitution stabilises the apatitic structure due to the presence of water in two types of vacancies [234]. The vacancies are present due to the negative charge deficiency when the CO_3^{2-} ion substitutes for the PO_4^{3-} ion [235]. Therefore B-type carbonate substitution may have contributed to the increased thermal stability for the 100 at. % strontium hydroxyapatite produced using the optimised method 1. However, it should be noted that B-type carbonate substitution bands were less defined for the 50 and 100 at. % Sr nHA produced using both optimised methods. Therefore it is difficult to conclude whether this effect could have contributed to the increased thermal stability observed for the 100 at. % Sr nHA produced using optimised method 1. From the TEM micrographs it can be seen that the 100 at. % strontium nHA produced using optimised method 3 (Figure 5.23) has much straighter edges and sharper vertices than the 100 at. % Sr nHA produced using optimised method 1 (Figure 5.14). This could suggest a higher surface energy of the 100 at. % Sr nHA produced using optimised method 3, which in turn could contribute to its lower thermal stability.

The XRF results showed a general decrease in (Ca+Sr)/P ratio as the strontium content was increased, which was unexpected due to the high thermal stability of the 100 at. % strontium-substituted produced using optimised method 1 (Table 5.6). This raised concerns over the reliability of the XRF data, and it may be that the accuracy limitations of the technique have provided conflicting data.

TEM images clearly displayed the noticeable effect strontium had on the crystal growth of the nHA particles. Although much more pronounced in optimised method 3 (Figure 5.23), it was still clear in optimised method 1 that the 100 at. % strontium-substituted nHA was composed of particles with a higher aspect ratio than the 100 at. % calcium nHA (Figure 5.14). This provided insights to the effect that strontium has on the precipitation of the nHA. In detail, the change in particle aspect ratio suggested that the presence of strontium instead of calcium caused a change in the precipitation

rate, due to the energy of crystal growth being lower than energy required for new crystal nucleation. These effects promoted growth along the c axis [174] which resulted in the large aspect ratio particles for the 100 at. % strontium nHA particles. It can be seen that the nHA particles for the mixed calcium-strontium nHA particles are generally composed of smaller sub particles with ill-defined edges, particularly for the optimised method 1 products. Similar effects were reported elsewhere and corresponded with a lower degree of crystallinity [125]. It could be proposed that the co-presence of calcium and strontium slowed down the crystal growth rate resulting in a larger number of smaller particles, probably due to the increased difficulty to accommodate both atoms in the crystal lattice. Furthermore, an increase in particle aspect ratio for increased strontium content has also been reported for strontium-substituted nHA produced using the same reagents as optimised method 3 [125].

XRF results demonstrated that the level of incorporation of strontium into the products was generally very close to the attempted substitution level, albeit in a calcium / strontium deficient product (Table 5.6 and Table 5.7). This showed the readiness of strontium to substitute into the nHA crystal lattice and was probably aided by the isoelectric nature of the substitution of divalent calcium ions for divalent strontium ions.

The presence of strontium in the nHA had a clear effect on the phosphate group bands as showed by the peak shift to a lower wavenumber, observed in the FTIR-ATR spectra (Figure 5.16, Figure 5.18 and Figure 5.25). This change in the chemical environment is likely to be due to the larger strontium atom creating a modified crystal lattice which in turn allows for different vibrational and stretching energies for the chemical groups. As described for Raman spectroscopy by O'Donnell *et al*. the frequency of the bands are dependent on the lattice vibrational energies; this is the same case for FTIR spectroscopy. Therefore, the position of the vibration is defined by the masses of the atoms present and the strength of the forces between them

[124]. As discussed in detail for strontium substitution in HA by Bigi *et al.,* the FTIR phosphate peaks shifts can be attributed to the increased size of strontium compared to calcium. The presence of a larger atom caused a decrease in the anionic repulsion of the PO_4^{3-} groups and, in combination with an increased anionic separation, caused the change in energies observed in the spectra [125].

The FTIR-ATR spectra showed modest levels of carbonate substitution for the strontium-substituted nHA produced using both optimised methods (Figure 5.16 and Figure 5.25). The bands at around 1450 and 1420 cm^{-1} can be attributed to the B-type substitution of carbonate groups for phosphate groups. In contrast, no bands for the A-type substitution of carbonate for hydroxyl groups were observed, which are generally present at around 1550 cm^{-1} [86, 236, 237]. A possible explanation for the carbonate substitution may be that the alkalinity of the precipitation solutions allowed for dissolution of atmospheric carbon dioxide. The carbonate groups observed for the unsintered optimised method 1 product are removed during the sintering treatment at 1000 °C (Figure 5.18). As described by Rau *et al.* the loss of carbonate groups from HA can begin at relatively low temperatures e.g. 400 °C. However it was found that the preparation conditions had a significant effect on the loss of carbonate during thermal treatment, with different carbonated HA displaying vastly different carbonate loss regimes [238].

Based on the evidence of the characterisation results, the strontium-substituted nHA prepared during these investigations may have the following chemical formula (i.e. calcium / strontium deficient and carbonate substituted):

$$Ca_{10-x-\frac{y}{2}-\frac{z}{2}}\ Sr_{x-\frac{y}{2}-\frac{z}{2}}\ (HPO_4)_y\ (PO_4)_{6-y-z}\ (CO_3)_z(OH)_{2-y-z}$$

$$x = \text{Sr at. \% / 10}$$

$$0 \leq x \leq 10$$

$$0 \leq y \leq 1$$

$$0 \leq z \leq 1$$

Since the natural form of nHA is carbonated and calcium-deficient, the production of non-stoichiometric HA actually presents a more biomimetic approach which may possess greater bioactivity. For example, research on biomimetic calcium-deficient carbonated nHA has shown it is able to stimulate proliferation and the alkaline phosphatase activity of murine preosteoblast cells to a greater degree than conventional nHA [239].

The increase in radiopacity with increasing strontium content was expected due to the higher atomic mass of strontium compared to calcium. This allows strontium to absorb more X-ray energy [240]. Therefore, for the same mass of dried powder an increase of radiopacity was clearly observed with increasing strontium content (Figure 5.20 and Figure 5.27). The density of the different powders may have contributed to the difference seen between powders produced by the different methods, as for the same strontium content, a higher radiopacity was observed for the powders produced using optimised method 3. The difference in density may be linked to the amount of absorbed water present in the powders. No published studies have been found on the radiopacity of strontium hydroxyapatite powder alone and therefore more investigations are required to better understand an optimal strontium content for the effective detection of strontium-substituted HA *in vivo*. However, the increased

radiopacity of strontium hydroxyapatite bone cements have also been reported [122, 123].

The *in vitro* biocompatibility results highlighted the sensitivity of cultured cells to different forms of substituted nHA. Indeed, any significant differences in cellular viability observed in these experiments (Figure 5.47) may have been due to a change in chemistry or particle morphology or a combination of the two effects.

For the indirect assays, variable amounts of particles were observed in the preconditioned media prepared using pastes or gels with different strontium contents, despite identical media preparation. However, it was interesting to note that the indirect paste assays showed significant variances in viability (Figure 5.35) whereas no significant differences were observed for the indirect gel assays (Figure 5.41). The gels were observed to consistently fragment (Figure 5.44) which may have allowed for similar particle content during the preparation of the preconditioned media for the indirect assays. Since the 5 at. % Sr nHA paste displayed the greatest fragmentation when cultured directly with the cells (Figure 5.38), this may have allowed for a greater surface area for the release of nHA particles during the preparation of the preconditioned media. This effect might have contributed to the decreased viability of the cells cultured with preconditioned media prepared using the 5 at. % Sr nHA paste. The cells cultured indirectly with the 0 and 100 at. % Sr nHA pastes showed the greatest viability, which implied that the strontium-substituted nHA pastes containing calcium and strontium had a detrimental effect on cellular viability. It could be suggested that the increased solubility, expected for the strontium-substituted samples containing strontium and calcium, caused a high concentration of dissolved ions which may have reduced the viability of the cells through osmotic effects or other mechanisms. The presence of the larger strontium ion has been proposed to contribute to the increased solubility of strontium-substituted nHA samples due to a destabilising effect on the crystal structure [241].

For the direct assays, the fragmentation of the 5 at. % Sr nHA paste was likely to have reduced the surface area of the well plate where cells could grow in an unconstrained manner, thereby reducing the overall viability. No significant differences in viability were observed for the 0, 2.5, 10 and 50 at. % Sr nHA pastes (Figure 5.41) suggesting that for these samples, the increased amount of strontium was not detrimental to the cells. The fragmentation of the gels may have also contributed to the variable viability observed between gels of different strontium contents (Figure 5.43). The reduced viability of cells cultured with 0 and 100 at. % Sr nHA gels suggested that for these experiments, the co-presence of strontium and calcium were beneficial for cellular viability, with the 50 at. % Sr nHA gel showing the highest level of viability. This was in contrast to the results for the indirect paste assay where the 0 and 100 at. % Sr nHA samples had a beneficial effect on cellular viability compared to the strontium-substituted samples (Figure 5.35).

The difference between biocompatibility investigations observed for the pastes and gels may have been affected by the different water contents of the two materials, since the gel was composed of 90 wt. % water and the paste had an 80 wt. % water content. Therefore, the paste culture samples would have been subjected to a higher dose of nHA particles and presumably a higher dose of any ions released from the materials. Furthermore, the gel material may have released more water into the media which may have affected the cellular response.

The greatest difference in particle morphology was observed for the 100 at. % strontium-substituted nHA prepared by both methods (Figure 5.14 and Figure 5.23). For the pastes prepared using optimised method 1, the 0 at. % Sr nHA paste had a significantly higher viability level than the 100 at. % strontium nHA paste when the direct biocompatibility was compared. However, for the gels prepared using optimised method 3 there was no significant difference in the direct viability between 0 and 100 at. % Sr nHA. This makes it difficult to conclude whether particle morphology has a

distinct effect on cell viability. As mentioned previously, the combination of chemical and morphological changes can make it difficult to ascertain which changes have the greatest effect of cellular viability.

The strontium-substituted nHA particles produced by the two different methods had a similar morphology when samples containing the same Sr content were compared. For the direct biocompatibility assays, the co-presence of strontium and calcium in the gel had a beneficial effect on cellular viability; for the paste investigations the samples with strontium and calcium generally did not have a detrimental effect on the cells. These results suggest that the materials are not cytotoxic and are therefore promising biomaterials.

As discussed in section 2.5.1.1 *Substitutions Intended to Enhance the Bioactivity of Hydroxyapatite,* few detailed reports are published regarding the biocompatibility of strontium-substituted nHA. However, those which have been published have concluded a variety of optimal strontium concentrations. It must be noted that different strontium content ranges are often considered which makes it difficult to compare between studies. Furthermore, the investigations of different forms of material and different particle morphologies can further complicate the results due to their distinct effects on cellular behaviour.

Several experiments with MG63 cells tested on Sr nHA have reported that the presence of Sr has a positive effects on cellular viability [115, 132, 242]. In contrast, other investigations have found that SrHA has no significant effect on cellular viability for MSCs [134] or for L929 fibroblasts [243]. These results highlight the limitations of *in vitro* biocompatibility testing, as different results may be obtained using different cells types. For instance, Crawford *et al.* have reported that nHA particles have a cytotoxic effect for a range of cell types, with two dimensional cultures showing increased sensitivity compared to three dimensional systems [244]. It was found that

some nHA particles had been internalised by the cells which may have contributed to the toxicity.

The investigation of the full compositional range of strontium-substituted nHA produced by different preparation methods in this thesis has highlighted the sensitivity of *in vitro* biocompatibility testing; similar materials produced using different methods have significantly different results. Without the presence of the complex *in vivo* processes it is not possible to fully conclude which materials may be more beneficial to encourage bone healing. Due to the limitations of *in vitro* testing it is necessary to investigate the biocompatibility of the materials in an *in vivo* model as outlined in Chapter 8 *Future Work*.

This report has demonstrated the successful production of strontium-substituted nHA pastes and gels using relatively simple, low cost methodologies. The current evidence suggests that these materials are likely to have a beneficial biological response. Therefore, these investigations are of great interest for the development of the next generation of nHA pastes. Few reports in the literature investigate the production of injectable strontium-substituted nHA systems and therefore these studies considerably add to the prior knowledge, which can be used to develop superior biomaterials with enhanced functionality.

6.4 Production and Characterisation of Silver-doped Nanoscale Hydroxyapatite (Altered Method 1)

The successful formation of nHA in all the silver-doped samples was displayed by X-ray diffraction (Figure 5.28) and confirmed by FTIR-ATR analysis (Figure 5.31). The presence of silver phosphate when 10 at. % silver doping was attempted highlighted the sensitive balance of the precipitation system; when present in high levels the formation of silver phosphate effectively removed phosphorous from the solution which should ensure that any precipitated HA is not calcium-deficient. This is due to

the effective increase in the calcium: phosphorus ratio. The greater amount of β-TCP observed for the higher silver-doped samples demonstrated that increased amounts of silver had a destabilising effect on the HA crystal lattice (Figure 5.29). Indeed, the increased thermal decomposition of the silver-doped samples suggested that either the presence of silver aided the thermal decomposition of the samples or that a more unstable nHA was precipitated.

The majority of investigations reported in the literature used a substitution approach where the amount of calcium in the method was reduced in order to allow silver to substitute readily into the crystal lattice. However, this approach makes it difficult to conclude whether the decreased thermal stability was due to silver substitution or the precipitation of a calcium-deficient apatite which has been reported to have a lower thermal stability [89, 213]. In this study, since a constant amount of calcium hydroxide was used regardless of the level of silver nitrate addition, it was unlikely that an excessively calcium-deficient HA was precipitated, especially considering the effective increase in calcium: phosphorous ratio caused by the silver phosphate formation for the 10 at. % silver-doped sample. It is possible that trace amounts of silver phosphate were formed in the 2 and 5 at. % samples, which were undetectable by XRD due to their small quantities.

The decreased thermal stability of the silver-doped samples may be due to the partial substitution of silver for calcium atoms in the HA structure as suggested by other researchers [152, 157, 161]. Specifically, the hydroxyl vacancy was reported to contribute to the increased thermal decomposition caused by the difference in charge between Ag^{+} and Ca^{2+} [157]. The increased ionic radius of Ag^{+} (0.128 nm) when compared to Ca^{2+} (0.099 nm) was also reported to increase the unit cell parameters of the silver substituted nHA. Alternatively, silver may be present on the surface of the nHA crystal or may be in the form of free ions in the aqueous paste. The presence of a metallic silver phase in the sintered silver-doped samples demonstrated that the

high temperature treatment may have caused the dissociation of silver from the nHA. Otherwise, the silver may be present due to the decomposition of silver phosphate or residual silver nitrate.

The peak shift observed in the phosphate group bands in the FTIR-ATR spectra for the unsintered and sintered 10 at. % silver-doped sample may indicate that silver substitution has taken place (Figure 5.32 A and Figure 5.34 A). As seen for the strontium-substituted samples, a peak shift indicates a change in the phosphate environment, which may potentially be due to the incorporation of the larger silver ion. However, no significant peak shift was observed for the XRD patterns suggesting that the substitution of silver had a minor effect on the unit cell parameters, perhaps due to a very low level of incorporation into the unit cell.

The precipitated nHA had a small crystallite size as demonstrated by the broad XRD peaks and quantified by the relatively large FWHM of the (002) XRD peak (Table 5.9). The decrease in FWHM after high temperature sintering corresponded with an increase in the sample crystallite size. It was reported elsewhere that HA samples with an increased silver content had a lower crystallinity, which in turn increased the solubility [154]. In this project, although the XRD patterns of the nHA samples with different amount of silver doping were similar, the hydroxyl and phosphate peaks of the FTIR-ATR spectra were less defined for the higher silver-doped samples. Other reports have correlated these changes in FTIR spectra with a lower HA crystallinity [208, 233].

XRF results demonstrated the incorporation of silver into the product albeit with a decreased silver: calcium molar ratio than that was used in the method (Table 5.9). The lower levels were potentially due to silver being washed away during the washing of the silver-doped nHA suspensions. The difficulty of silver incorporation was also demonstrated by the precipitation of a silver phosphate phase. Other reports have

also reported lower levels of silver incorporation than attempted. For instance, the highest incorporation level of 10 wt. % silver attempted by Lim *et al.* only resulted in 1.1 wt. % silver content in the product when analysed using XRF [161]. However, it should also be noted that the sublimation of nanometer-sized has been reported at 950 K (677 °C) [245] which could also have affected the silver: calcium molar ratios during the XRF analysis.

TEM analysis displayed no noticeable changes in the size or shape of the nHA particles obtained from the wet precipitation with different amounts of silver doping (Figure 5.30). Several papers also reported no significant changes in nHA morphology with the addition of silver [149, 152, 154]. However, small dark particles were observed on the 5 and 10 at. % samples in this project. This observation corresponded with the TEM carried out by other researchers who had attempted the addition of silver nanoparticles to nHA [155, 156]. These reports clearly showed the presence of small silver particles which were noticeably darker that the nHA particles when observed using TEM. This may demonstrate that part of the silver content is not substituted in the lattice; instead the silver is present on the surface of the particles. However, this may be in the form of silver phosphate which was detected in the XRD analysis (Figure 5.28).

The clear zones of inhibition surrounding the silver-doped nHA pastes in the agar diffusion assay displayed the diffusion limited nature of the antibacterial activity (Figure 5.48). Furthermore, ICP-MS analysis of the agar surrounding the pastes demonstrated that the antibacterial activity of the pastes was at least partially due to the action of diffusible silver ions (Figure 5.49). The diffusion limited mobility of the silver ions is likely to be beneficial for the *in vivo* activity of the pastes. Indeed, it was reported by Peetsch *et al.* that the cytotoxic effects of silver-doped calcium phosphates observed *in vitro* were due to the rapid release of silver ions [246]. In this study it was also suggested that *in vivo*, the diffusion limited nature of the silver

release combined with the rapid dilution of silver ions would reduce the cytotoxic effects to the host cells; it was believed that this approach would maintain a potent antibacterial effect at the site of implantation for antibacterial nanoparticle coatings on calcium phosphate [247]. Therefore in our studies, the low levels of silver detected in the agar, with the maximum reading of 7 $ng.mg^{-1}$, showed that the silver beneficially remained in close association with the nHA phase during incubation at 37 °C.

The reduction of metallic silver on the surface of the silver-doped nHA pastes during incubation with *S. aureus,* whilst no reduction was observed when the pastes was incubated with *P. aeruginosa,* demonstrated the unusual behaviour of the pastes in the presence of different bacteria (Figure 5.48). It was noted that the reduction of the silver may have limited the diffusion potential of the silver ions into the agar (Figure 5.49), thereby maintaining a high level of antibacterial effectiveness at the paste site. Whilst there is no definite explanation for the surface reduction of the silver, this effect may have been caused by a reaction with intracellular contents or metabolites.

When investigated in suspension culture, the apparent antibacterial activity of the nHA with no silver-doping was attributed to the probable adhesion of bacteria to the nHA, causing agglomeration and aggregation, thus reducing the optical density of the suspension (Figure 5.50). This effect was likely to be aided by the high surface area to volume ratio of the nHA particles with a similar effect being reported by Ciobanu *et al.* [149]. In detail, Ciobanu *et al.* found statistically lower levels of adherence of *S. aureus* on the silver-doped nHA powders investigated when compared to undoped nHA powders. This demonstrated the strong affinity of bacteria to adhere to nHA and therefore the need for antibacterial consideration when designing implantable nHA materials. The antibacterial activity of the silver-doped samples was noticeably higher and therefore was evidently an effect of silver incorporation, with an increased growth reduction effect observed for the nHA pastes with a higher silver content. This was clearly shown by the decreasing MIC with increasing silver content (Table 5.10). The

unexpected increase in optical density observed for the highest concentrations of the 10 at. % silver-doped nHA paste may have been due to the reduction of silver by the bacteria as observed in the agar diffusion assays.

Potent antibacterial activity of silver HA powders and coatings have been reported by other researchers. Typically, dose dependent antibacterial activity was observed with higher levels of silver incorporation contributing to a more effective bactericidal response [154, 161]. In a study by Stanic *et al.* the antimicrobial properties of silver-doped nHA powders were studied using *E.coli, S. aureus* and *C. albicans*. Using atomic force microscopy, it was found that incubation with the silver-doped materials had caused changes in cellular morphology for all organisms investigated which may have contributed to cell death. Low levels of haemolysis demonstrated good blood compatibility suggesting that these materials have promising biocompatibility [154].

Silver is a particularly potent antibacterial agent due to its multiple modes of action on the bacterial cell, and acts primarily with exposed sulfhydryl complexes to form S-Ag groups [165]. This reaction has extensive toxic effects including membrane potential disruption and the inhibition of adenosine triphosphate production [165, 166]. Furthermore, the membrane integrity of the cells is compromised, and the action of silver causes the denaturation of key metabolic enzymes. The production of free-radicals and the interaction of silver with DNA further compound the toxicity of silver. In detail, pyrimidine dimerization disrupts DNA replication, which prevents bacterial reproduction [165]. Indeed it is these multiple modes of action that makes silver a promising element to combat the rise of antibiotic resistant bacteria. For instance, it was reported by Samani *et al*. that silver-doped HA coatings had effective antibacterial activity against methicillin-resistant *S. aureus* (MRSA) in terms of reducing the proliferation rate [157].

The potent antibacterial activity of the silver-doped nHA pastes produced in this thesis support the antibacterial effectiveness of silver reported elsewhere. Therefore, these materials are very promising for reducing the incidence of implant associated infections whilst maintaining an injectable form which can allow for minimally invasive surgery to be performed.

7. Conclusions

Although hydroxyapatite has been used extensively for bone augmentation, relatively little research has been directed at the development of nHA for use as a medical device. As well as having injectable properties to allow for minimally invasive surgical intervention, a combination of inorganically modified nHA and water has the potential to offer enhanced biofunctionality. As outlined in Chapter 3, the aim of this project was therefore to develop methods to produce modified nHA pastes and gels, and to characterise the resulting materials to better understand the chemical processes underpinning their preparation and properties. The conclusions of this research may be summarised as:

1. Of the nHA production methods investigated, the reaction of calcium hydroxide and phosphoric acid (method 1) was identified as the most promising route for the wet precipitation of nHA with a close chemical similarity to stoichiometric HA. Further advantages included the lack of noxious chemical by-products, obviously attractive in the preparation of a biomaterial. The nHA sol-gel production method based on the reaction of calcium nitrate and ammonium phosphate (method 3) was also selected for further development due to its ability to form a stable gel during the drying process.

2. Development of these two selected methods showed that the alteration of synthesis parameters had a marked effect on nHA chemistry and morphology. These investigations demonstrated that rapid mixing methods may be implemented which allowed for the preparation of nHA with biomimetic features, specifically carbonate-substituted and calcium-deficient nHA. For method 1, the rapid addition of phosphoric acid into the calcium hydroxide suspension eliminated the calcium hydroxide residue that was observed with a slower addition rate. The increase in phosphoric acid solution addition rate also decreased the aspect ratio of the nHA particles. For method

3, a high pH was critical for the formation of nHA with a high thermal stability and also for the formation of a stable gel product.

3. A range of strontium-substituted nHA (0, 2.5, 5, 10, 50 and 100 at. % Sr) was successfully produced using optimised methods 1 and 3. Both methods allowed for an accurate incorporation of strontium into the product, with the synthesised nHA containing an amount of strontium close to attempted substitution level. When fully substituted (i.e. 100 at. %) strontium hydroxyapatite was prepared, the particle aspect ratio was increased. This was thought to be most likely due to changes in the precipitation rate during production. The strontium-substituted nHA had a higher radiopacity that was proportional to its strontium content. Initial *in vitro* biocompatibility tests suggested that the majority of the Sr nHA pastes and gels supported the growth of osteoblastic-like cells in direct and indirect contact.

4. Silver-doped nHA (0, 2, 5 and 10 at. %) pastes were also produced using a modified method 1. The detection of a silver phosphate phase when 10 at. % silver-doped nHA was attempted, highlighted the sensitivity of the reaction and suggested that the maximum level of silver-doping had been exceeded. Although the amount of silver incorporated in the product was lower than the attempted level, all the silver-doped pastes had potent antibacterial properties. The antibacterial activity of the silver-doped nHA paste was found to be dependent on the silver content of the paste, with higher levels of silver doping having a greater antibacterial response. Diffusible silver ions were at least partially responsible for the antibacterial activity of the pastes, and the low level of diffusion suggested that the materials could beneficially maintain a high level of antibacterial activity at the site of implantation.

The investigations reported in this thesis are the first detailed reports of methods that have successfully produced strontium-substituted nHA pastes and gels, and silver-doped nHA pastes which are promising materials with enhanced functionality for bone

augmentation. These materials are expected to be particularly useful due to the enhanced bioactivity and potent antibacterial activity of strontium-substituted and silver-doped nHA respectively. Therefore, this work has great potential to aid the development of novel biomaterials with improved functionality. The further work required for future clinical product development is detailed in the next chapter.

8. Future Work

Several aspects of this project should be considered for future development of injectable bone augmentation materials:

1. Firstly the scale up of the optimised production methods are likely to affect the material properties and therefore the biological properties of the synthesised materials. This is due to the sensitive nature of the precipitated nHA with the chemical nature and morphology particularly affected by solution pH and reactant addition rate. Therefore, in order to commercialise these materials it would be necessary to carefully consider how the scale up of such methods may affect the physicochemical properties of the materials. For example, effective mixing would be required to achieve an appropriate reactant distribution which in turn should ensure the successful conversion of the reactants into nHA.

2. In these investigations, variable results were obtained regarding the *in vitro* biocompatibility of the strontium-substituted nHA pastes and gels. In combination with scale up methods, an optimal strontium content should be investigated in order to fully optimise the biomaterial biological behaviour. Specifically, this could be initially investigated using quantitative PCR in order to better understand the effect of strontium-substituted nHA on the gene expression and in turn the biological behaviour of the material on the differentiation and activity of bone cells. Furthermore, the *in vivo* response of the strontium-substituted nHA materials should be investigated due to the limitations of *in vitro* experiments when analysing nHA paste and gel materials. In detail, the early bone regeneration response should be monitored in order to better understand the bone regeneration capacity of these materials.

3. The promising antibacterial activity of the silver-doped nHA paste suggested that this material might be useful for the prevention and treatment of deep bone infections. However, investigations must be carried out in order to ascertain the potential

cytotoxic effects of the silver-doped material. Firstly, the silver-doped paste materials should be screened *in vitro* in order to balance the antibacterial response with acceptable levels of cellular viability. Once determined, optimal silver concentrations should be screened *in vivo* in order to ensure the safety of these materials. The potent antibacterial activity of the silver-doped pastes suggested that perhaps a low level of silver-doping could be utilised in order to reduce potential mammalian cytotoxicity effects whilst maintaining antibacterial properties.

4. As well as enhancing the chemical composition, the paste and gels should be optimised in terms of water content as this parameter is likely to have an effect on the biological response. Furthermore, the water content has a direct effect on the rheological properties and in turn the injectability of the pastes and gels which must be optimised for clinical use. Greater injectability is required to treat deep bone voids and the surgeon must be able to easily deliver the materials to the required site. For example, excessive shear thinning behaviour would be undesirable for the controlled delivery of the paste or gel. This is due to the requirement of a large force to commence delivery, but once the material starts to flow, the force required for continued injection decreases. The shear thinning rheological behaviour of the materials should therefore be investigated and optimised.

5. Further developments could be to combine strontium and silver in order to synthesise a material with bioactive and antibacterial properties. Alternatively, biomimetic multi-substitutions such as carbonate, magnesium and strontium could be employed in order to promote *in vivo* resorption which in turn may promote optimal tissue regeneration.

6. Other interesting designs to consider could be the development of different products to suit different groups of patients. By considering the needs of individual patients, bone tissue regeneration may be truly optimised by matching the specific

requirements of the patient with a particular optimised product. This stratified design approach may be the most effective option to fulfil the needs of the patient whilst satisfying socio-economic demands.

Bibliography

[1] Giannoudis PV, Dinopoulos H, Tsiridis E. Bone substitutes: an update. Injury. 2005;36:S20-7.

[2] Busenlechner D, Huber CD, Vasak C, Dobsak A, Gruber R, Watzek G. Sinus augmentation analysis revised: the gradient of graft consolidation. Bone. 2009;44:1078-83.

[3] Huber FX, Berger I, McArthur N, Huber C, Kock HP, Hillmeier J*, et al.* Evaluation of a novel nanocrystalline hydroxyapatite paste and a solid hydroxyapatite ceramic for the treatment of critical size bone defects (CSD) in rabbits. Journal of Materials Science-Materials in Medicine. 2008;19:33-8.

[4] Marieb EN, Hoehn K. Human Anatomy and Physiology. 7 ed. San Francisco, California: Pearson Benjamin Cummings; 2007.p.178-193.

[5] Wang Y, Von Euw S, Fernandes FM, Cassaignon S, Selmane M, Laurent G*, et al.* Water-mediated structuring of bone apatite. Nature Materials. 2013;12:1144-53.

[6] Pasteris JD, Wopenka B, Valsami-Jones E. Bone and tooth mineralization: why apatite? Elements. 2008;4:97-104.

[7] Carter DH, Hatton PV, Aaron JE. The ultrastructure of slam-frozen bone mineral. Histochemical Journal. 1997;29:783-93.

[8] Rho JY, Kuhn-Spearing L, Zioupos P. Mechanical properties and the hierarchical structure of bone. Medical Engineering & Physics. 1998;20:92-102.

[9] Boanini E, Gazzano M, Bigi A. Ionic substitutions in calcium phosphates synthesized at low temperature. Acta Biomaterialia. 2010;6:1882-94.

[10] Tampieri A, Celotti G, Landi E. From biomimetic apatites to biologically inspired composites. Analytical and Bioanalytical Chemistry. 2005;381:568-76.

[11] Gibson IR, Bonfield W. Novel synthesis and characterization of an AB-type carbonate-substituted hydroxyapatite. Journal of Biomedical Materials Research. 2002;59:697-708.

[12] Wopenka B, Pasteris JD. A mineralogical perspective on the apatite in bone. Materials Science & Engineering C-Biomimetic and Supramolecular Systems. 2005;25:131-43.

[13] Elliott JC. Structure and chemistry of the apatites and other calcium orthophosphates. 2 ed. Amsterdam: Elsevier; 1994.p.260.

[14] Fox K, Tran PA, Nhiem T. Recent advances in research applications of nanophase hydroxyapatite. ChemPhysChem. 2012;13:2495-506.

[15] Hannink G, Arts JJC. Bioresorbability, porosity and mechanical strength of bone substitutes: what is optimal for bone regeneration? Injury. 2011;42:S22-5.

[16] Ten Cate AR. Oral histology: development, structure, and function. 5 ed. St. Louis, Missouri: Mosby Inc.; 1998.p.69-77.
[17] Boivin G. The hydroxyapatite crystal: a closer look. Medicographia. 2007;29:126-32.
[18] Lewandrowski KU, Gresser JD, Wise DL, Trantolo DJ. Bioresorbable bone graft substitutes of different osteoconductivities: a histologic evaluation of osteointegration of poly(propylene glycol-co-fumaric acid)-based cement implants in rats. Biomaterials. 2000;21:757-64.
[19] Kaveh K, Ibrahim R, Bakar MZA, Ibrahim TA. Bone grafting and bone graft substitutes. Journal of Animal and Veterinary Advances. 2010;9:1055-67.
[20] Van der Stok J, Van Lieshout EMM, El-Massoudi Y, Van Kralingen GH, Patka P. Bone substitutes in the Netherlands - A systematic literature review. Acta Biomaterialia. 2011;7:739-50.
[21] Kanakaris NK, Giannoudis PV. The health economics of the treatment of long-bone non-unions. Injury. 2007;38:S77-84.
[22] Coleman RE. Metastatic bone disease: clinical features, pathophysiology and treatment strategies. Cancer Treatment Reviews. 2001;27:165-76.
[23] Mundy GR. Metastasis: metastasis to bone: causes, consequences and therapeutic opportunities. Nature Reviews Cancer. 2002;2:584-93.
[24] Weilbaecher KN, Guise TA, McCauley LK. Cancer to bone: a fatal attraction. Nature Reviews Cancer. 2011;11:411-25.
[25] Cai Y, Liu Y, Yan W, Hu Q, Tao J, Zhang M*, et al.* Role of hydroxyapatite nanoparticle size in bone cell proliferation. Journal of Materials Chemistry. 2007;17:3780-7.
[26] Cowan JA, Dimick JB, Wainess R, Upchurch GR, Chandler WF, La Marca F. Changes in the utilization of spinal fusion in the United States. Neurosurgery. 2006;59:15-8.
[27] Miyazaki M, Tsumura H, Wang JC, Alanay A. An update on bone substitutes for spinal fusion. European Spine Journal. 2009;18:783-99.
[28] Myeroff C, Archdeacon M. Autogenous bone graft: donor sites and techniques. Journal of Bone and Joint Surgery-American Volume. 2011;93A:2227-36.
[29] Kolk A, Handschel J, Drescher W, Rothamel D, Kloss F, Blessmann M*, et al.* Current trends and future perspectives of bone substitute materials - from space holders to innovative biomaterials. Journal of Cranio-Maxillofacial Surgery. 2012;40:706-18.

[30] Campana V, Milano G, Pagano E, Barba M, Cicione C, Salonna G*, et al.* Bone substitutes in orthopaedic surgery: from basic science to clinical practice. Journal of Materials Science-Materials in Medicine. 2014;25:2445-61.

[31] Finkemeier CG. Bone-grafting and bone-graft substitutes. Journal of Bone and Joint Surgery-American Volume. 2002;84A:454-64.

[32] Jones JR. Review of bioactive glass: from Hench to hybrids. Acta Biomaterialia. 2013;9:4457-86.

[33] Thomas MV, Puleo DA. Calcium sulfate: properties and clinical applications. Journal of Biomedical Materials Research Part B-Applied Biomaterials. 2009;88B:597-610.

[34] Sidambe AT. Biocompatibility of advanced manufactured titanium implants - a review. Materials. 2014;7:8168-88.

[35] Peltier LF. The use of plaster of Paris to fill defects in bone. Clinical Orthopaedics. 1961;21:1-31.

[36] Moore WR, Graves SE, Bain GI. Synthetic bone graft substitutes. Australian and New Zealand Journal of Surgery. 2001;71:354-61.

[37] Low KL, Tan SH, Zein SHS, Roether JA, Mourino V, Boccaccini AR. Calcium phosphate-based composites as injectable bone substitute materials. Journal of Biomedical Materials Research Part B-Applied Biomaterials. 2010;94B:273-86.

[38] Tavakoli M, Davey P, Clift BA, Davies HTO. Diagnosis and management of osteomyelitis - decision analytic and pharmacoeconomic considerations. Pharmacoeconomics. 1999;16:627-47.

[39] Gomes D, Pereira M, Bettencourt AF. Osteomyelitis: an overview of antimicrobial therapy. Brazilian Journal of Pharmaceutical Sciences. 2013;49:13-27.

[40] Zimmerli W. Clinical presentation and treatment of orthopaedic implant-associated infection. Journal of Internal Medicine. 2014;276:111-9.

[41] Ciampolini J, Harding KG. Pathophysiology of chronic bacterial osteomyelitis. Why do antibiotics fail so often? Postgraduate Medical Journal. 2000;76:479-83.

[42] Zimmerli W. Prosthetic-joint-associated infections. Best Practice & Research in Clinical Rheumatology. 2006;20:1045-63.

[43] Smith AW. Biofilms and antibiotic therapy: is there a role for combating bacterial resistance by the use of novel drug delivery systems? Advanced Drug Delivery Reviews. 2005;57:1539-50.

[44] Gogia JS, Meehan JP, Di Cesare PE, Jamali AA. Local antibiotic therapy in osteomyelitis. Seminars in Plastic Surgery. 2009;23:100-7.

[45] Simchi A, Tamjid E, Pishbin F, Boccaccini AR. Recent progress in inorganic and composite coatings with bactericidal capability for orthopaedic applications. Nanomedicine-Nanotechnology Biology and Medicine. 2011;7:22-39.

[46] Nandi SK, Mukherjee P, Roy S, Kundu B, De DK, Basu D. Local antibiotic delivery systems for the treatment of osteomyelitis - a review. Materials Science & Engineering C-Materials for Biological Applications. 2009;29:2478-85.

[47] Walenkamp GHIM. Self-mixed antibiotic bone cement: western countries learn from developing countries. Acta Orthopaedica. 2009;80:505-7.

[48] Itokazu M, Yang WY, Aoki T, Ohara A, Kato N. Synthesis of antibiotic-loaded interporous hydroxyapatite blocks by vacuum method and *in vitro* drug release testing. Biomaterials. 1998;19:817-9.

[49] Lambotte JC, Thomazeau H, Cathelineau G, Lancien G, Minet J, Langlais F. Tricalcium phosphate as an antibiotic vector: a study using a rabbit experimental osteomyelitis implant. Chirurgie. 1998;123:572-9.

[50] Blair JMA, Webber MA, Baylay AJ, Ogbolu DO, Piddock LJV. Molecular mechanisms of antibiotic resistance. Nature Reviews Microbiology. 2015;13:42-51.

[51] Laschke MW, Witt K, Pohlemann T, Menger MD. Injectable nanocrystalline hydroxyapatite paste for bone substitution: *in vivo* analysis of biocompatibility and vascularization. Journal of Biomedical Materials Research Part B-Applied Biomaterials. 2007;82B:494-505.

[52] Tadic D, Epple M. A thorough physicochemical characterisation of 14 calcium phosphate-based bone substitution materials in comparison to natural bone. Biomaterials. 2004;25:987-94.

[53] Huber FX, Belyaev O, Hillmeier J, Kock HJ, Huber C, Meeder PJ*, et al.* First histological observations on the incorporation of a novel nanocrystalline hydroxyapatite paste OSTIM® in human cancellous bone. BMC Musculoskeletal Disorders. 2006;7:50.

[54] Chitsazi MT, Shirmohammadi A, Faramarzie M, Pourabbas R, Rostamzadeh A. A clinical comparison of nano-crystalline hydroxyapatite (Ostim) and autogenous bone graft in the treatment of periodontal intrabony defects. Medicina Oral Patologia Oral Y Cirugia Bucal. 2011;16:E448-E53.

[55] Dallari D, Savarino L, Albisinni U, Fornasari P, Ferruzzi A, Baldini N*, et al.* A prospective, randomised, controlled trial using a Mg-hydroxyapatite - demineralized bone matrix nanocomposite in tibial osteotomy. Biomaterials. 2012;33:72-9.

[56] Bigi A, Falini G, Foresti E, Ripamonti A, Gazzano M, Roveri N. Magnesium influence on hydroxyapatite crystallization. Journal of Inorganic Biochemistry. 1993;49:69-78.

[57] Spies CKG, Schnuerer S, Gotterbarm T, Breusch S. The efficacy of Biobon™ and Ostim™ within metaphyseal defects using the Gottinger minipig. Archives of Orthopaedic and Trauma Surgery. 2009;129:979-88.

[58] Arts JJC, Verdonschot N, Schreurs BW, Buma P. The use of a bioresorbable nano-crystalline hydroxyapatite paste in acetabular bone impaction grafting. Biomaterials. 2006;27:1110-8.

[59] Brandt J, Henning S, Michler G, Hein W, Bernstein A, Schulz M. Nanocrystalline hydroxyapatite for bone repair: an animal study. Journal of Materials Science-Materials in Medicine. 2010;21:283-94.

[60] Spies CKG, Schnuerer S, Gotterbarm T, Breusch S. Animal study of the bone substitute material Ostim™ within osseous defects in Gottinger minipigs. Zeitschrift Fur Orthopadie Und Unfallchirurgie. 2008;146:64-9.

[61] Bullens PHJ, Hannink G, Verdonschot N, Buma P. No effect of dynamic loading on bone graft healing in femoral segmental defect reconstructions in the goat. Injury-International Journal of the Care of the Injured. 2010;41:1284-91.

[62] Thorwarth M, Schultze-Mosgau S, Kessler P, Wiltfang J, Schlegel KA. Bone regeneration in osseous defects using a resorbable nanoparticular hydroxyapatite. Journal of Oral and Maxillofacial Surgery. 2005;63:1626-33.

[63] Huber FX, McArthur N, Hillmeier J, Kock HJ, Baier M, Diwo M*, et al.* Void filling of tibia compression fracture zones using a novel resorbable nanocrystalline hydroxyapatite paste in combination with a hydroxyapatite ceramic core: first clinical results. Archives of Orthopaedic and Trauma Surgery. 2006;126:533-40.

[64] Huber FX, Hillmeler J, Kock HJ, McArthur N, Huber C, Diwo M*, et al.* Filling of metaphyseal defects with nanocrystalline hydroxyapatite (Ostim®) for fractures of the radius. Zentralblatt Fur Chirurgie. 2008;133:577-81.

[65] Huber FX, Hillmeier J, Herzog L, McArthur N, Kock HJ, Meeder PJ. Open reduction and palmar plate-osteosynthesis in combination with a nanocrystalline hydroxyapatite spacer in the treatment of comminuted fractures of the distal radius. Journal of Hand Surgery-British and European Volume. 2006;31B:298-303.

[66] Smeets R, Grosjean MB, Jelitte G, Heiland M, Kasaj A, Riediger D*, et al.* Hydroxyapatite bone substitute (Ostim) in sinus floor elevation. Maxillary sinus floor augmentation: bone regeneration by means of a nanocrystalline in-phase hydroxyapatite (Ostim). Schweizer Monatsschrift fur Zahnmedizin. 2008;118:203-12.

[67] Zaffe D, Traversa G, Mozzati M, Morelli F, D'Angeli G. Behavior of aqueous nanocrystalline hydroxyapatite in oral bone regeneration. Journal of Applied Biomaterials & Biomechanics. 2011;9:19-25.

[68] Schwarz F, Bieling K, Latz T, Nuesry E, Becker J. Healing of intrabony peri-implantitis defects following application of a nanocrystalline hydroxyapatite (Ostim™) or a bovine-derived xenograft (Bio-Oss™) in combination with a collagen membrane (Bio-Gide™). A case series. Journal of Clinical Periodontology. 2006;33:491-9.

[69] Al Machot E, Hoffmann T, Lorenz K, Khalili I, Noack B. Clinical outcomes after treatment of periodontal intrabony defects with nanocrystalline hydroxyapatite (Ostim) or enamel matrix derivatives (Emdogain): a randomized controlled clinical trial. Biomed Research International. 2014;2014:786353.

[70] Heinz B, Kasaj A, Teich M, Jepsen S. Clinical effects of nanocrystalline hydroxyapatite paste in the treatment of intrabony periodontal defects: a randomized controlled clinical study. Clinical Oral Investigations. 2010;14:525-31.

[71] Canuto RA, Pol R, Martinasso G, Muzio G, Gallesio G, Mozzati M. Hydroxyapatite paste Ostim®, without elevation of full-thickness flaps, improves alveolar healing stimulating BMP- and VEGF-mediated signal pathways: an experimental study in humans. Clinical Oral Implants Research. 2013;24:42-8.

[72] Strietzel FP, Reichart PA, Graf HL. Lateral alveolar ridge augmentation using a synthetic nano-crystalline hydroxyapatite bone substitution material (Ostim®). Preliminary clinical and histological results. Clinical Oral Implants Research. 2007;18:743-51.

[73] Rebaudi A, Alberghini A, Pretto M, Benedicenti S. Sinus grafting with magnesium-enriched bioceramic granules and autogenous bone: a microcomputed tomographic evaluation of 11 patients. International Journal of Periodontics & Restorative Dentistry. 2010;30:53-61.

[74] Ceramisys Ltd. ReproBone novo™ Product Information Accessed on http://www.ceramisys.com/bone_graft_substitute_paste_properties.html on 07.06.15.

[75] Bone regeneration following socket preservation using different bone substitute materials. A pilot study in dogs. . Accessed on www.botiss.dk/download/maxresorb_04.pdf on 19/12/12.

[76] Herten M, Rothamel D, Schwarz F, Friesen K, Koegler G, Becker J. Surface- and nonsurface-dependent *in vitro* effects of bone substitutes on cell viability. Clinical Oral Investigations. 2009;13:149-55.

[77] Sullivan MP, McHale KJ, Parvizi J, Mehta S. Nanotechnology. Bone & Joint Journal. 2014;96B:569-73.

[78] Wang Z, Tang Z, Qing F, Hong Y, Zhang X. Applications of calcium phosphate nanoparticles in porous hard tissue engineering scaffolds. Nano. 2012;7:1230004.

[79] Aoki H, Kutsuno T, Li W, Niwa M. An *in vivo* study on the reaction of hydroxyapatite-sol injected into blood. Journal of Materials Science-Materials in Medicine. 2000;11:67-72.

[80] Ma G, Liu XY. Hydroxyapatite: hexagonal or monoclinic? Crystal Growth & Design. 2009;9:2291-4.

[81] Kay MI, Young RA, Posner AS. Crystal structure of hydroxyapatite. Nature. 1964;204:1050-2.

[82] Eanes ED, Gillesse LH, Gosner AS. Intermediate states in precipitation of hydroxyapatite. Nature. 1965;208:365-7.

[83] Onuma K, Ito A. Cluster growth model for hydroxyapatite. Chemistry of Materials. 1998;10:3346-51.

[84] Johnsson MSA, Nancollas GH. The role of brushite and octacalcium phosphate in apatite formation. Critical Reviews in Oral Biology & Medicine. 1992;3:61-82.

[85] Cihlar J, Buchal A, Trunec M. Kinetics of thermal decomposition of hydroxyapatite bioceramics. Journal of Materials Science. 1999;34:6121-31.

[86] Kumta PN, Sfeir C, Lee DH, Olton D, Choi D. Nanostructured calcium phosphates for biomedical applications: novel synthesis and characterization. Acta Biomaterialia. 2005;1:65-83.

[87] Kivrak N, Tas AC. Synthesis of calcium hydroxyapatite-tricalcium phosphate (HA-TCP) composite bioceramic powders and their sintering behavior. Journal of the American Ceramic Society. 1998;81:2245-52.

[88] Fathi MH, Hanifi A. Evaluation and characterization of nanostructure hydroxyapatite powder prepared by simple sol-gel method. Materials Letters. 2007;61:3978-83.

[89] Mostafa NY. Characterization, thermal stability and sintering of hydroxyapatite powders prepared by different routes. Materials Chemistry and Physics. 2005;94:333-41.

[90] Bianco A, Cacciotti I, Lombardi M, Montanaro L, Gusmano G. Thermal stability and sintering behaviour of hydroxyapatite nanopowders. Journal of Thermal Analysis and Calorimetry. 2007;88:237-43.

[91] Bigi A, Foresti E, Gandolfi M, Gazzano M, Roveri N. Inhibiting effect of zinc on hydroxylapatite crystallization. Journal of Inorganic Biochemistry. 1995;58:49-58.

[92] Kanzaki N, Onuma K, Treboux G, Tsutsumi S, Ito A. Inhibitory effect of magnesium and zinc on crystallization kinetics of hydroxyapatite (0001) face. Journal of Physical Chemistry B. 2000;104:4189-94.

[93] Roveri N, Battistella E, Bianchi CL, Foltran I, Foresti E, Iafisco M*, et al.* Surface enamel remineralization: Biomimetic apatite nanocrystals and fluoride ions different effects. Journal of Nanomaterials. 2009;2009:746383.

[94] Chen YM, Miao XG. Thermal and chemical stability of fluorohydroxyapatite ceramics with different fluorine contents. Biomaterials. 2005;26:1205-10.

[95] Hench LL. Bioceramics. Journal of the American Ceramic Society. 1998;81:1705-28.

[96] Carlisle EM. Silicon - a requirement in bone-formation independent of vitamin D1. Calcified Tissue International. 1981;33:27-34.

[97] Vallet-Regi M, Arcos D. Silicon substituted hydroxyapatites. A method to upgrade calcium phosphate based implants. Journal of Materials Chemistry. 2005;15:1509-16.

[98] Arcos D, Rodriguez-Carvajal J, Vallet-Regi M. Silicon incorporation in hydroxylapatite obtained by controlled crystallization. Chemistry of Materials. 2004;16:2300-8.

[99] Gibson IR, Best SM, Bonfield W. Chemical characterization of silicon-substituted hydroxyapatite. Journal of Biomedical Materials Research. 1999;44:422-8.

[100] Balas F, Perez-Pariente J, Vallet-Regi M. *In vitro* bioactivity of silicon-substituted hydroxyapatites. Journal of Biomedical Materials Research Part A. 2003;66A:364-75.

[101] Bohner M. Silicon-substituted calcium phosphates - a critical view. Biomaterials. 2009;30:6403-6.

[102] Patel N, Best SM, Bonfield W, Gibson IR, Hing KA, Damien E*, et al.* A comparative study on the *in vivo* behavior of hydroxyapatite and silicon substituted hydroxyapatite granules. Journal of Materials Science-Materials in Medicine. 2002;13:1199-206.

[103] Coathup MJ, Samizadeh S, Fang YS, Buckland T, Hing KA, Blunn GW. The osteoinductivity of silicate-substituted calcium phosphate. Journal of Bone and Joint Surgery-American Volume. 2011;93A:2219-26.

[104] Bigi A, Foresti E, Gregorini R, Ripamonti A, Roveri N, Shah JS. The role of magnesium on the structure of biological apatites. Calcified Tissue International. 1992;50:439-44.

[105] Landi E, Logroscino G, Proietti L, Tampieri A, Sandri M, Sprio S. Biomimetic Mg-substituted hydroxyapatite: from synthesis to *in vivo* behaviour. Journal of Materials Science-Materials in Medicine. 2008;19:239-47.

[106] Crespi R, Mariani E, Benasciutti E, Cappare P, Cenci S, Gherlone E. Magnesium-enriched hydroxyapatite versus autologous bone in maxillary sinus

grafting: combining histomorphometry with osteoblast gene expression profiles ex vivo. Journal of Periodontology. 2009;80:586-93.

[107] Adams BR, Mostafa A, Schwartz Z, Boyan BD. Osteoblast response to nanocrystalline calcium hydroxyapatite depends on carbonate content. Journal of Biomedical Materials Research Part A. 2014;102:3237-42.

[108] Spence G, Patel N, Brooks R, Bonfield W, Rushton N. Osteoclastogenesis on hydroxyapatite ceramics: the effect of carbonate substitution. Journal of Biomedical Materials Research Part A. 2010;92A:1292-300.

[109] Spence G, Patel N, Brooks R, Rushton N. Carbonate substituted hydroxyapatite: resorption by osteoclasts modifies the osteoblastic response. Journal of Biomedical Materials Research Part A. 2009;90A:217-24.

[110] Porter A, Patel N, Brooks R, Best S, Rushton N, Bonfield W. Effect of carbonate substitution on the ultrastructural characteristics of hydroxyapatite implants. Journal of Materials Science-Materials in Medicine. 2005;16:899-907.

[111] Spence G, Phillips S, Campion C, Brooks R, Rushton N. Bone formation in a carbonate-substituted hydroxyapatite implant is inhibited by zoledronate: the importance of bioresorption to osteoconduction Journal of Bone and Joint Surgery-British Volume. 2008;90B:1635-40.

[112] Dahl SG, Allain P, Marie PJ, Mauras Y, Boivin G, Ammann P*, et al.* Incorporation and distribution of strontium in bone. Bone. 2001;28:446-53.

[113] Marie PJ, Ammann P, Boivin G, Rey C. Mechanisms of action and therapeutic potential of strontium in bone. Calcified Tissue International. 2001;69:121-9.

[114] Fonseca JE. Rebalancing bone turnover in favour of formation with strontium ranelate: implications for bone strength. Rheumatology. 2008;47:iv17-9.

[115] Capuccini C, Torricelli P, Boanini E, Gazzano M, Giardino R, Bigi A. Interaction of Sr-doped hydroxyapatite nanocrystals with osteoclast and osteoblast-like cells. Journal of Biomedical Materials Research Part A. 2009;89A:594-600.

[116] Saidak Z, Marie PJ. Strontium signaling: molecular mechanisms and therapeutic implications in osteoporosis. Pharmacology & Therapeutics. 2012;136:216-26.

[117] Bonnelye E, Chabadel A, Saltel F, Jurdic P. Dual effect of strontium ranelate: stimulation of osteoblast differentiation and inhibition of osteoclast formation and resorption *in vitro*. Bone. 2008;42:129-38.

[118] Saidak Z, Hay E, Marty C, Barbara A, Marie PJ. Strontium ranelate rebalances bone marrow adipogenesis and osteoblastogenesis in senescent osteopenic mice through NFATc/Maf and Wnt signaling. Aging Cell. 2012;11:467-74.

[119] Fromigue O, Hay E, Barbara A, Petrel C, Traiffort E, Ruat M*, et al.* Calcium sensing receptor-dependent and receptor-independent activation of osteoblast replication and survival by strontium ranelate. Journal of Cellular and Molecular Medicine. 2009;13:2189-99.

[120] Atkins GJ, Welldon KJ, Halbout P, Findlay DM. Strontium ranelate treatment of human primary osteoblasts promotes an osteocyte-like phenotype while eliciting an osteoprotegerin response. Osteoporosis International. 2009;20:653-64.

[121] Santocildes-Romero ME, Crawford A, Hatton PV, Goodchild RL, Reaney IM, Miller CA. The osteogenic response of mesenchymal stromal cells to strontium-substituted bioactive glasses. Journal of Tissue Engineering and Regenerative Medicine. 2015;9:619-31.

[122] Hernandez L, Parra J, Vazquez B, Lopez Bravo A, Collia F, Goni I*, et al.* Injectable acrylic bone cements for vertebroplasty based on a radiopaque hydroxyapatite. Bioactivity and biocompatibility. Journal of Biomedical Materials Research Part B-Applied Biomaterials. 2009;88B:103-14.

[123] Schumacher M, Henss A, Rohnke M, Gelinsky M. A novel and easy-to-prepare strontium(II) modified calcium phosphate bone cement with enhanced mechanical properties. Acta Biomaterialia. 2013;9:7536-44.

[124] O'Donnell MD, Fredholm Y, de Rouffignac A, Hill RG. Structural analysis of a series of strontium-substituted apatites. Acta Biomaterialia. 2008;4:1455-64.

[125] Bigi A, Boanini E, Capuccini C, Gazzano M. Strontium-substituted hydroxyapatite nanocrystals. Inorganica Chimica Acta. 2007;360:1009-16.

[126] Matsunaga K, Murata H. Strontium substitution in bioactive calcium phosphates: a first-principles study. Journal of Physical Chemistry B. 2009;113:3584-9.

[127] Landi E, Tampieri A, Celotti G, Sprio S, Sandri M, Logroscino G. Sr-substituted hydroxyapatites for osteoporotic bone replacement. Acta Biomaterialia. 2007;3:961-9.

[128] Hanifi A, Fathi MH, Sadeghi HMM. Effect of strontium ions substitution on gene delivery related properties of calcium phosphate nanoparticles. Journal of Materials Science-Materials in Medicine. 2010;21:2601-9.

[129] Renaudin G, Jallot E, Nedelec JM. Effect of strontium substitution on the composition and microstructure of sol-gel derived calcium phosphates. Journal of Sol-Gel Science and Technology. 2009;51:287-94.

[130] Boyd AR, Rutledge L, Randolph LD, Meenan BJ. Strontium-substituted hydroxyapatite coatings deposited via a co-deposition sputter technique. Materials Science & Engineering C-Materials for Biological Applications. 2015;46:290-300.

[131] Boyd AR, Rutledge L, Randolph LD, Mutreja I, Meenan BJ. The deposition of strontium-substituted hydroxyapatite coatings. Journal of Materials Science-Materials in Medicine. 2015;26:65.

[132] Zhang W, Shen Y, Pan H, Lin K, Liu X, Darvell BW*, et al.* Effects of strontium in modified biomaterials. Acta Biomaterialia. 2011;7:800-8.

[133] Aina V, Bergandi L, Lusvardi G, Malavasi G, Imrie FE, Gibson IR*, et al.* Sr-containing hydroxyapatite: morphologies of HA crystals and bioactivity on osteoblast cells. Materials Science & Engineering C-Materials for Biological Applications. 2013;33:1132-42.

[134] Raucci MG, Giugliano D, Alvarez-Perez MA, Ambrosio L. Effects on growth and osteogenic differentiation of mesenchymal stem cells by the strontium-added sol-gel hydroxyapatite gel materials. Journal of Materials Science-Materials in Medicine. 2015;26:90.

[135] Ni GX, Lu WW, Xu B, Chiu KY, Yang C, Li ZY*, et al.* Interfacial behaviour of strontium-containing hydroxyapatite cement with cancellous and cortical bone. Biomaterials. 2006;27:5127-33.

[136] Kolmas J, Groszyk E, Kwiatkowska-Rozycka D. Substituted hydroxyapatites with antibacterial properties. Biomed Research International. 2014;2014:178123.

[137] Yamaguchi M, Yamaguchi R. Action of zinc on bone metabolism in rate - increases in alkaline-phosphatase activity and DNA content. Biochemical Pharmacology. 1986;35:773-7.

[138] Moonga BS, Dempster DW. Zinc is a potent inhibitor of osteoclastic bone-resorption *in vitro*. Journal of Bone and Mineral Research. 1995;10:453-7.

[139] Yang F, Dong WJ, He FM, Wang XX, Zhao SF, Yang GL. Osteoblast response to porous titanium surfaces coated with zinc substituted hydroxyapatite. Oral Surgery Oral Medicine Oral Pathology Oral Radiology. 2012;113:313-8.

[140] de Lima IR, Alves GG, Fernandes GVD, Dias EP, Soares GD, Granjeiro JM. Evaluation of the *in vivo* biocompatibility of hydroxyapatite granules incorporated with zinc ions. Materials Research-Ibero-American Journal of Materials. 2010;13:563-8.

[141] Miyaji F, Kono Y, Suyama Y. Formation and structure of zinc-substituted calcium hydroxyapatite. Materials Research Bulletin. 2005;40:209-20.

[142] Stanic V, Dimitrijevic S, Antic-Stankovic J, Mitric M, Jokic B, Plecas IB*, et al.* Synthesis, characterization and antimicrobial activity of copper and zinc-doped hydroxyapatite nanopowders. Applied Surface Science. 2010;256:6083-9.

[143] Thian ES, Konishi T, Kawanobe Y, Lim PN, Choong C, Ho B*, et al.* Zinc-substituted hydroxyapatite: a biomaterial with enhanced bioactivity and antibacterial properties. Journal of Materials Science-Materials in Medicine. 2013;24:437-45.

[144] Ito A, Ojima K, Naito H, Ichinose N, Tateishi T. Preparation, solubility, and cytocompatibility of zinc-releasing calcium phosphate ceramics. Journal of Biomedical Materials Research. 2000;50:178-83.

[145] White C, Lee J, Kambe T, Fritsche K, Petris MJ. A role for the ATP7A copper-transporting ATPase in macrophage bactericidal activity. Journal of Biological Chemistry. 2009;284:33949-56.

[146] Radovanovic Z, Jokic B, Veljovic D, Dimitrijevic S, Kojic V, Petrovic R*, et al.* Antimicrobial activity and biocompatibility of Ag^{+} and Cu^{2+} doped biphasic hydroxyapatite/alpha-tricalcium phosphate obtained from hydrothermally synthesized Ag^{+}- and Cu^{2+} -doped hydroxyapatite. Applied Surface Science. 2014;307:513-9.

[147] Li Y, Ho J, Ooi CP. Antibacterial efficacy and cytotoxicity studies of copper (II) and titanium (IV) substituted hydroxyapatite nanoparticles. Materials Science & Engineering C-Materials for Biological Applications. 2010;30:1137-44.

[148] Kim TN, Feng QL, Kim JO, Wu J, Wang H, Chen GQ*, et al.* Antimicrobial effects of metal ions (Ag^{+}, Cu^{2+}, Zn^{2+}) in hydroxyapatite. Journal of Materials Science-Materials in Medicine. 1998;9:129-34.

[149] Ciobanu CS, Massuyeau F, Constantin LV, Predoi D. Structural and physical properties of antibacterial Ag-doped nano-hydroxyapatite synthesized at 100 degrees C. Nanoscale Research Letters. 2011;6:1-8.

[150] Ciobanu CS, Iconaru SL, Pasuk I, Vasile BS, Lupu AR, Hermenean A*, et al.* Structural properties of silver doped hydroxyapatite and their biocompatibility. Materials Science & Engineering C-Materials for Biological Applications. 2013;33:1395-402.

[151] Fadeeva IV, Bakunova NV, Komlev VS, Medvecky L, Fomin AS, Gurin AN*, et al.* Zinc- and silver-substituted hydroxyapatite: synthesis and properties. Doklady Chemistry. 2012;442:63-5.

[152] Rameshbabu N, Sampath Kumar TS, Prabhakar TG, Sastry VS, Murty KVGK, Prasad Rao K. Antibacterial nanosized silver substituted hydroxyapatite: synthesis and characterization. Journal of Biomedical Materials Research Part A. 2007;80A:581-91.

[153] Ramli R, Arawi AO, Mahat MM, Mohd AF, Yahya MFZR. Effect of silver (Ag) substitution nano-hydroxyapatite synthesis by microwave processing. International Conference on Business, Engineering and Industrial Applications (ICBEIA) Kuala Lumpur, Malaysia. 2011:180-3.

[154] Stanic V, Janackovic D, Dimitrijevic S, Tanaskovic SB, Mitric M, Pavlovic MS*, et al.* Synthesis of antimicrobial monophase silver-doped hydroxyapatite

nanopowders for bone tissue engineering. Applied Surface Science. 2011;257:4510-8.

[155] Guo C, Shao F, Zhang Y, Sheng X, Dong Y. Preparation of silver/hydroxyapatite nanoparticles using hydroxyapatite nanoparticles with different calcination temperatures. Micro & Nano Letters. 2012;7:904-6.

[156] Diaz M, Barba F, Miranda M, Guitian F, Torrecillas R, Moya JS. Synthesis and antimicrobial activity of a silver-hydroxyapatite nanocomposite. Journal of Nanomaterials. 2009;2009:498505.

[157] Samani S, Hossainalipour SM, Tamizifar M, Rezaie HR. *In vitro* antibacterial evaluation of sol-gel-derived Zn-, Ag-, and (Zn plus Ag)-doped hydroxyapatite coatings against methicillin-resistant *Staphylococcus aureus*. Journal of Biomedical Materials Research Part A. 2013;101A:222-30.

[158] Chung RJ, Hsieh MF, Huang KC, Perng LH, Chou FI, Chin TS. Anti-microbial hydroxyapatite particles synthesized by a sol-gel route. Journal of Sol-Gel Science and Technology. 2005;33:229-39.

[159] Lu Z, Sun K. Preparation and characterization of silver loaded hydroxyapatite. Rare Metal Materials and Engineering. 2009;38:56-60.

[160] Thompson ML, Kateley LJ. The Nernst equation: determination of equilibrium constants for complex ions of silver. Journal of Chemical Education. 1999;76:95-6.

[161] Lim PN, Teo EY, Ho B, Tay BY, Thian ES. Effect of silver content on the antibacterial and bioactive properties of silver-substituted hydroxyapatite. Journal of Biomedical Materials Research Part A. 2013;101:2456-64.

[162] Ipekoglu M, Altintas S. Silver substituted nanosized calcium deficient hydroxyapatite. Materials Technology. 2010;25:295-301.

[163] Sygnatowicz M, Keyshar K, Tiwari A. Antimicrobial properties of silver-doped hydroxyapatite nano-powders and thin films. Jom. 2010;62:65-70.

[164] Silver S. Bacterial silver resistance: molecular biology and uses and misuses of silver compounds. Fems Microbiology Reviews. 2003;27:341-53.

[165] Mijnendonckx K, Leys N, Mahillon J, Silver S, Van Houdt R. Antimicrobial silver: uses, toxicity and potential for resistance. Biometals. 2013;26:609-21.

[166] Marambio-Jones C, Hoek EMV. A review of the antibacterial effects of silver nanomaterials and potential implications for human health and the environment. Journal of Nanoparticle Research. 2010;12:1531-51.

[167] British Standards BS ISO 13779-3:2008 Implants for surgery - Hydroxyapatite. Part 3: Chemical analysis and characterisation of crystallinity and phase purity 2008.

[168] British Standards BS ISO 13779-1:2008 Implants for surgery - Hydroxyapatite. Part 1: Ceramic hydroxyapatite 2008.

[169] British Standards BS ISO 13175-3:2012 Implants for surgery - Calcium phosphates. Part 3: Hydroxyapatite and beta-tricalcium phosphate bone substitutes 2012.

[170] British Standards BS ISO 13779-6:2015 Implants for surgery - Hydroxyapatite. Part 6: Powders 2015.

[171] Kreyling WG, Semmler-Behnke M, Chaudhry Q. A complementary definition of nanomaterial. Nano Today. 2010;5:165-8.

[172] Luo P, Nieh TG. Synthesis of ultrafine hydroxyapatite particles by a spray dry method. Materials Science and Engineering: C. 1995;3:75-8.

[173] Dorozhkin SV. Nanosized and nanocrystalline calcium orthophosphates. Acta Biomaterialia. 2010;6:715-34.

[174] Bouyer E, Gitzhofer F, Boulos MI. Morphological study of hydroxyapatite nanocrystal suspension. Journal of Materials Science-Materials in Medicine. 2000;11:523-31.

[175] Kumar R, Prakash KH, Cheang P, Khor KA. Temperature driven morphological changes of chemically precipitated hydroxyapatite nanoparticles. Langmuir. 2004;20:5196-200.

[176] Prakash KH, Kumar R, Ooi CP, Cheang P, Khor KA. Apparent solubility of hydroxyapatite in aqueous medium and its influence on the morphology of nanocrystallites with precipitation temperature. Langmuir. 2006;22:11002-8.

[177] Afshar A, Ghorbani M, Ehsani N, Saeri MR, Sorrell CC. Some important factors in the wet precipitation process of hydroxyapatite. Materials & Design. 2003;24:197-202.

[178] Catros S, Guillemot F, Lebraud E, Chanseau C, Perez S, Bareille R*, et al.* Physico-chemical and biological properties of a nano-hydroxyapatite powder synthesized at room temperature. IRBM. 2010;31:226-33.

[179] Pang YX, Bao X. Influence of temperature, ripening time and calcination on the morphology and crystallinity of hydroxyapatite nanoparticles. Journal of the European Ceramic Society. 2003;23:1697-704.

[180] Liu H, Yazici H, Ergun C, Webster TJ, Bermek H. An *in vitro* evaluation of the Ca/P ratio for the cytocompatibility of nano-to-micron particulate calcium phosphates for bone regeneration. Acta Biomaterialia. 2008;4:1472-9.

[181] Safronova TV, Putlyaev VI, Shekhirev MA, Tretyakov YD, Kuznetsov AV, Belyakov AV. Densification additives for hydroxyapatite ceramics. Journal of the European Ceramic Society. 2009;29:1925-32.

[182] Kong LB, Ma J, Boey F. Nanosized hydroxyapatite powders derived from coprecipitation process. Journal of Materials Science. 2002;37:1131-4.

[183] Liu DM, Yang Q, Troczynski T, Tseng WJ. Structural evolution of sol–gel-derived hydroxyapatite. Biomaterials. 2002;23:1679-87.

[184] Liu DM, Troczynski T, Tseng WJ. Water-based sol-gel synthesis of hydroxyapatite: process development. Biomaterials. 2001;22:1721-30.

[185] Bigi A, Boanini E, Rubini K. Hydroxyapatite gels and nanocrystals prepared through a sol-gel process. Journal of Solid State Chemistry. 2004;177:3092-8.

[186] Kuriakose TA, Kalkura SN, Palanichamy M, Arivuoli D, Dierks K, Bocelli G*, et al.* Synthesis of stoichiometric nano crystalline hydroxyapatite by ethanol-based sol-gel technique at low temperature. Journal of Crystal Growth. 2004;263:517-23.

[187] Qaisar SA, Bilton M, Wallace R, Brydson R, Brown AP, Ward M*, et al.* Sol-gel synthesis and TEM-EDX characterisation of hydroxyapatite nanoscale powders modified by Mg, Sr or Ti. Journal of Physics: Conference Series, Sheffield, UK. 2010;241:012042.

[188] Natarajan UV, Rajeswari S. Influence of calcium precursors on the morphology and crystallinity of sol-gel-derived hydroxyapatite nanoparticles. Journal of Crystal Growth. 2008;310:4601-11.

[189] Wang J, Shaw LL. Synthesis of high purity hydroxyapatite nanopowder via sol-gel combustion process. Journal of Materials Science-Materials in Medicine. 2009;20:1223-7.

[190] Fathi MH, Hanifi A. Sol-gel derived nanostructure hydroxyapatite powder and coating: aging time optimisation. Advances in Applied Ceramics. 2009;108:363-8.

[191] Wang F, Li MS, Lu YP, Qi YX. A simple sol-gel technique for preparing hydroxyapatite nanopowders. Materials Letters. 2005;59:916-9.

[192] Sanosh KP, Chu MC, Balakrishnan A, Kim TN, Cho SJ. Preparation and characterization of nano-hydroxyapatite powder using sol-gel technique. Bulletin of Materials Science. 2009;32:465-70.

[193] Gentile P, Wilcock CJ, Miller CA, Moorehead R, Hatton PV. Process optimisation to control the physico-chemical characteristics of biomimetic nanoscale hydroxyapatites prepared using wet chemical precipitation. Materials. 2015;8:2297-310.

[194] Celotti G, Tampieri A, Sprio S, Landi E, Bertinetti L, Martra G*, et al.* Crystallinity in apatites: how can a truly disordered fraction be distinguished from nanosize crystalline domains? Journal of Materials Science-Materials in Medicine. 2006;17:1079-87.

[195] Dorozhkin SV. Amorphous calcium (ortho)phosphates. Acta Biomaterialia. 2010;6:4457-75.

[196] Antonakos A, Liarokapis E, Leventouri T. Micro-Raman and FTIR studies of synthetic and natural apatites. Biomaterials. 2007;28:3043-54.

[197] Hong Y, Fan H, Li B, Guo B, Liu M, Zhang X. Fabrication, biological effects, and medical applications of calcium phosphate nanoceramics. Materials Science & Engineering R-Reports. 2010;70:225-42.

[198] Webster TJ, Ergun C, Doremus RH, Siegel RW, Bizios R. Specific proteins mediate enhanced osteoblast adhesion on nanophase ceramics. Journal of Biomedical Materials Research. 2000;51:475-83.

[199] Guo X, Gough JE, Xiao P, Liu J, Shen Z. Fabrication of nanostructured hydroxyapatite and analysis of human osteoblastic cellular response. Journal of Biomedical Materials Research Part A. 2007;82A:1022-32.

[200] Huang Y, Zhou G, Zheng L, Liu H, Niu X, Fan Y. Micro-/nano-sized hydroxyapatite directs differentiation of rat bone marrow derived mesenchymal stem cells towards an osteoblast lineage. Nanoscale. 2012;4:2484-90.

[201] Aksakal B, Kom M, Tosun HB, Demirel M. Influence of micro- and nano-hydroxyapatite coatings on the osteointegration of metallic (Ti6Al4V) and bioabsorbable interference screws: an *in vivo* study. European Journal of Orthopaedic Surgery & Traumatology : Orthopedie Traumatologie. 2014;24:813-9.

[202] Cheng Z, Guo C, Dong W, He FM, Zhao Sf, Yang GL. Effect of thin nano-hydroxyapatite coating on implant osseointegration in ovariectomized rats. Oral Surgery Oral Medicine Oral Pathology Oral Radiology. 2012;113:E48-E53.

[203] Wang DX, He Y, Bi L, Qu ZH, Zou JW, Pan Z*, et al.* Enhancing the bioactivity of poly(lactic-co-glycolic acid) scaffold with a nano-hydroxyapatite coating for the treatment of segmental bone defect in a rabbit model. International Journal of Nanomedicine. 2013;8:1855-65.

[204] Xia L, Lin K, Jiang X, Xu Y, Zhang M, Chang J*, et al.* Enhanced osteogenesis through nano-structured surface design of macroporous hydroxyapatite bioceramic scaffolds via activation of ERK and p38 MAPK signaling pathways. Journal of Materials Chemistry B. 2013;1:5403-16.

[205] Tavakol S, Nikpour MR, Amani A, Soltani M, Rabiee SM, Rezayat SM*, et al.* Bone regeneration based on nano-hydroxyapatite and hydroxyapatite/chitosan nanocomposites: an *in vitro* and *in vivo* comparative study. Journal of Nanoparticle Research. 2013;15:1373.

[206] Ren J, Zhao P, Ren T, Gu S, Pan K. Poly (D,L-lactide)/nano-hydroxyapatite composite scaffolds for bone tissue engineering and biocompatibility evaluation. Journal of Materials Science-Materials in Medicine. 2008;19:1075-82.

[207] Brito Lopes JC, Gomes de Queiroz Dias MM, Tenedorio Matos da Silva VM, Quadros de Oliveira e Santos PA, Mendes Monteiro FJ, Da Cunha Gomes PJ*, et al.* Production method for calcium phosphate nano-particles with high purity and their use. Fluidinova, Engenharia de Fluidos, S.A., Instituto Nacional de Engenharia Biomedica. 2008;WO2008/007992A2.

[208] Khalid M, Mujahid M, Amin S, Rawat RS, Nusair A, Deen GR. Effect of surfactant and heat treatment on morphology, surface area and crystallinity in hydroxyapatite nanocrystals. Ceramics International. 2013;39:39-50.

[209] Miller CA, Herranz Diez C, Crawford A. Private communication: *in vitro* cytotoxicity assessment (IMCOSS project). 2014.

[210] British Standards BS ISO 10993-5:2009 Biological evaluation of medical devices Part 5: Test for in vitro cytotoxicity 2009.

[211] Koutsopoulos S. Synthesis and characterization of hydroxyapatite crystals: a review study on the analytical methods. Journal of Biomedical Materials Research. 2002;62:600-12.

[212] Rey C, Shimizu M, Collins B, Glimcher MJ. Resolution-enhanced Fourier-transform infrared-spectroscopy study of the environment of phosphate ions in the early deposits of a solid-phase of calcium-phosphate in bone and enamel, and their evolution with age. 1. Investigations in the v_4 PO_4 domain. Calcified Tissue International. 1990;46:384-94.

[213] Gibson IR, Rehman I, Best SM, Bonfield W. Characterization of the transformation from calcium-deficient apatite to beta-tricalcium phosphate. Journal of Materials Science-Materials in Medicine. 2000;11:533-9.

[214] Wang Y, Chen J, Wei K, Zhang S, Wang X. Surfactant-assisted synthesis of hydroxyapatite particles. Materials Letters. 2006;60:3227-31.

[215] Safronova TV, Shekhirev MA, Putlyaev VI, Tret'yakov YD. Hydroxyapatite-based ceramic materials prepared using solutions of different concentrations. Inorganic Materials. 2007;43:901-9.

[216] Liu CS, Huang Y, Shen W, Cui JH. Kinetics of hydroxyapatite precipitation at pH 10 to 11. Biomaterials. 2001;22:301-6.

[217] Ungureanu DN, Angelescu N, Bacinschi Z, Stoian EV, Rizescu CZ. Thermal stability of chemically precipitated hydroxyapatite nanopowders. International Journal of Biology and Biomedical Engineering. 2011;5:57-64.

[218] Bezzi G, Celotti G, Landi E, La Torretta TMG, Sopyan I, Tampieri A. A novel sol-gel technique for hydroxyapatite preparation. Materials Chemistry and Physics. 2003;78:816-24.

[219] Osaka A, Miura Y, Takeuchi K, Asada M, Takahashi K. Calcium apatite prepared from calcium hydroxide and orthophosphoric acid. Journal of Materials Science-Materials in Medicine. 1991;2:51-5.

[220] Siddharthan A, Seshadri SK, Kumar TSS. Microwave accelerated synthesis of nanosized calcium deficient hydroxyapatite. Journal of Materials Science-Materials in Medicine. 2004;15:1279-84.

[221] Yubao L, Klein C, Dewijn J, Vandemeer S, Degroot K. Shape change and phase-transition of needle-like nonstoichiometric apatite crystals. Journal of Materials Science-Materials in Medicine. 1994;5:263-8.

[222] Prieto Valdes JJ, Ortiz Lopez J, Rueda Morales G, Pacheco Malagon G, Prieto Gortcheva V. Fibrous growth of tricalcium phosphate ceramics. Journal of Materials Science-Materials in Medicine. 1997;8:297-301.

[223] Liu TY, Chen SY, Liu DM. Influence of the aspect ratio of bioactive nanofillers on rheological behavior of PMMA-based orthopedic materials. Journal of Biomedical Materials Research Part B-Applied Biomaterials. 2004;71B:116-22.

[224] Sun S-P, Wei M, Olson JR, Shaw MT. Rheological behavior of needle-like hydroxyapatite nano-particle suspensions. Rheologica Acta. 2011;50:65-74.

[225] Dorozhkin SV. Biphasic, triphasic and multiphasic calcium orthophosphates. Acta Biomaterialia. 2012;8:963-77.

[226] McGuigan CF. Effect of nitrate on human cell lines in culture. Saskatoon, Canada: University of Saskatchewan; 2007.

[227] Pan YS, Xiong DS. Preparation and characterization of nano-hydroxyapatite/polyvinyl alcohol gel composites. Journal of Wuhan University of Technology-Materials Science Edition. 2010;25:474-8.

[228] Xu FL, Li YB, Wang XJ, Wei J, Yang AP. Preparation and characterization of nano-hydroxyapatite/poly(vinyl alcohol) hydrogel biocomposite. Journal of Materials Science. 2004;39:5669-72.

[229] Pan Y, Xiong D, Gao F. Viscoelastic behavior of nano-hydroxyapatite reinforced poly(vinyl alcohol) gel biocomposites as an articular cartilage. Journal of Materials Science-Materials in Medicine. 2008;19:1963-9.

[230] Zheng L, Jiang X, Chen X, Fan H, Zhang X. Evaluation of novel in situ synthesized nano-hydroxyapatite/collagen/alginate hydrogels for osteochondral tissue engineering. Biomedical Materials. 2014;9:065004.

[231] Huang Z, Yu B, Feng Q, Li S, Chen Y, Luo L. In situ-forming chitosan/nano-hydroxyapatite/collagen gel for the delivery of bone marrow mesenchymal stem cells. Carbohydrate Polymers. 2011;85:261-7.

[232] Terra J, Dourado ER, Eon JG, Ellis DE, Gonzalez G, Rossi AM. The structure of strontium-doped hydroxyapatite: an experimental and theoretical study. Physical Chemistry Chemical Physics. 2009;11:568-77.

[233] Reyes-Gasga J, Martinez-Pineiro EL, Rodriguez-Alvarez G, Tiznado-Orozco GE, Garcia-Garcia R, Bres EF. XRD and FTIR crystallinity indices in sound human tooth enamel and synthetic hydroxyapatite. Materials Science & Engineering C-Materials for Biological Applications. 2013;33:4568-74.

[234] Tonsuaadu K, Gross KA, Pluduma L, Veiderma M. A review on the thermal stability of calcium apatites. Journal of Thermal Analysis and Calorimetry. 2012;110:647-59.

[235] Ivanova TI, Frank-Kamenetskaya OV, Kol'tsov AB, Ugolkov VL. Crystal structure of calcium-deficient carbonated hydroxyapatite. Thermal decomposition. Journal of Solid State Chemistry. 2001;160:340-9.

[236] Sofronia AM, Baies R, Anghel EM, Maritiescu CA, Tanasescu S. Thermal and structural characterization of synthetic and natural nanocrystalline hydroxyapatite. Materials Science & Engineering C-Materials for Biological Applications. 2014;43:153-63.

[237] Krajewski A, Mazzocchi M, Buldini PL, Ravaglioli A, Tinti A, Taddei P*, et al.* Synthesis of carbonated hydroxyapatites: efficiency of the substitution and critical evaluation of analytical methods. Journal of Molecular Structure. 2005;744:221-8.

[238] Rau JV, Cesaro SN, Ferro D, Barinov SM, Fadeeva IV. FTIR study of carbonate loss from carbonated apatites in the wide temperature range. Journal of Biomedical Materials Research Part B-Applied Biomaterials. 2004;71B:441-7.

[239] Deng Y, Sun Y, Chen X, Zhu P, Wei S. Biomimetic synthesis and biocompatibility evaluation of carbonated apatites template-mediated by heparin. Materials Science & Engineering C-Materials for Biological Applications. 2013;33:2905-13.

[240] Wang X, Ye J, Wang Y. Influence of a novel radiopacifier on the properties of an injectable calcium phosphate cement. Acta Biomaterialia. 2007;3:757-63.

[241] Pan HB, Li ZY, Lam WM, Wong JC, Darvell BW, Luk KDK*, et al.* Solubility of strontium-substituted apatite by solid titration. Acta Biomaterialia. 2009;5:1678-85.

[242] Bracci B, Torricelli P, Panzavolta S, Boanini E, Giardino R, Bigi A. Effect of Mg^{2+}, Sr^{2+}, and Mn^{2+} on the chemico-physical and *in vitro* biological properties of calcium phosphate biomimetic coatings. Journal of Inorganic Biochemistry. 2009;103:1666-74.

[243] Abert J, Bergmann C, Fischer H. Wet chemical synthesis of strontium-substituted hydroxyapatite and its influence on the mechanical and biological properties. Ceramics International. 2014;40:9195-203.

[244] Crawford A, Pinnock A, Hruschka V, Redl H, Hatton PV, Miller CA. Biocompatibility of nanohydroxyapatites in 2- and 3-dimensional culture systems. PER/International Association for Dental Research (IADR) Congress, Dubrovnik, Croatia. 2014.

[245] Lee JG, Lee J, Tanaka T, Mori H. In situ HREM observation of crystalline-to-gas transition in nanometer-sized Ag particles. Physical Review Letters. 2006;96:075504.

[246] Peetsch A, Greulich C, Braun D, Stroetges C, Rehage H, Siebers B*, et al.* Silver-doped calcium phosphate nanoparticles: Synthesis, characterization, and toxic effects toward mammalian and prokaryotic cells. Colloids and Surfaces B-Biointerfaces. 2013;102:724-9.

[247] Lee JS, Murphy WL. Functionalizing calcium phosphate biomaterials with antibacterial silver particles. Advanced Materials. 2013;25:1173-9.

Appendix

Conference Presentations

Poster presentation at Tissue Engineering and Regenerative Medicine (TERMIS) World Congress, 5th – 8th September 2012, Vienna, Austria.

Oral presentation at British Society of Oral and Dental Research (BSODR) Conference, 9th – 11th September 2013, Bath, UK.

Oral presentation at Materials in Medicine (MiMe) Conference, 8th – 11th October 2013, Faenza, Italy.

Poster presentation at Tissue Engineering and Regenerative Medicine (TERMIS) Conference, 10 – 13th June 2014, Genova, Italy.

Oral presentation at European Society for Biomaterials (ESB) Conference, 31st August – 3rd September 2014, Liverpool, UK.

Poster presentation at International Association for Dental Research (IADR) Conference, 10th- 13th September 2014, Dubrovnik, Croatia.

Manuscripts Prepared for Journal Submission

Preparation and Characterisation of a Novel Antibacterial Silver-doped Nanoscale Hydroxyapatite Paste.